Relaxation phenomena during non-equilibrium growth

Yen-Liang Chou

Dissertation submitted to the Faculty of the
Virginia Polytechnic Institute and State University
in partial fulfillment of the requirements for the degree of

Doctor of Philosophy
in
Physics

Michel J. Pleimling, Chair
Jean J. Heremans
Rahul V. Kulkarni
Uwe C. Täuber

August 1, 2011
Blacksburg, Virginia

Keywords: surface growth processes, kinetic roughening, dynamic scaling, correlation function, response function

Relaxation phenomena during non-equilibrium growth

Yen-Liang Chou

The surface width, a global quantity that depends on time, is used to characterize the temporal evolution of growing surfaces. One of the most successful concepts for describing the property of the surface width is the famous Family-Vicsek scaling relation. We discuss an extended scaling relation that yields a complete description for various growth models. For two linear Langevin equations, namely the Edwards-Wilkinson equation and the Mullins-Herring equation, we furthermore study analytically the behavior of global quantities related to the surface width or to a quantity which is conjugated to the diffusion constant. The global quantities depend in a non-trivial way on two different times. We discuss the dynamical scaling forms of global correlation and response functions.

For global functions related to the surface width, we show that the scaling behavior of the response can depend on how the system is perturbed. Different dynamic regimes, characterized by a power-law or by an exponential relaxation, are identified, and a dynamic phase diagram is constructed. We discuss global fluctuation-dissipation ratios and how to use them for the characterization of non-equilibrium growth processes. We also numerically study the same two-time quantities for the non-linear Kardar-Parisi-Zhang equation.

For global functions related to the quantity which is conjugated to the diffusion constant of the linear Langevin equations, we show that the integrated response is proportional to the correlation in the linear response regime. In the aging regime, the autocorrelation and autoresponse exponents are identical and the aging exponent for the response is equal to the aging exponent for the correlation. We investigate the non-equilibrium fluctuation-dissipation theorem for non-equilibrium states based on this quantity. In the non-linear response regime a certain dissipation-fluctuation ratio approximates unity for small waiting times but approaches the ratio of perturbed and unperturbed diffusion constants for larger waiting times.

This material is based upon work supported by the National Science Foundation under Grant No. DMR-0904999. Any opinions, findings, and conclusions or recommendations expressed in this material are those of the author and do not necessarily reflect the views of the National Science Foundation.

Contents

1 Introduction **1**

2 Correlation, Response and Relaxation **4**

2.1 Correlation function 4

2.2 Response function and susceptibility 5

2.3 Linear response theory 6

2.4 Aging 7

2.5 Fluctuation-dissipation theory of non-equilibrium states 8

3 Surface Growth Models **10**

3.1 Random deposition 11

3.2 The Family model 11

3.3 The Wolf-Villain Model 13

3.4 The Das Sarma-Tamborenea Model 14

3.5 Ballistic Deposition 14

3.6 The Restricted Solid on Solid Model 15

3.7 Competitive Growth Models 16

3.8 The Arrhenius Diffusion Model 17

3.9 The Siegert-Plischke Model 18

3.10 The Modified RDSR process 19

4 Langevin Equations for Surface Growth Processes **23**

4.1 Linear Langevin equations - The Edwards-Wilkinson and Mullins-Herring equations . . . 23
4.1.1 Asymptotic behavior . . . 25
4.1.2 Crossover points . . . 27
4.1.3 The Modified RDSR and the Edwards-Wilkinson equation . . . 29
4.2 Non-linear Langevin Equation - The Kardar-Parisi-Zhang equation . . . 29

5 Dynamic Scaling **34**
5.1 Family-Vicsek relation . . . 34
5.2 Generalized Family-Vicsek scaling relation . . . 35

6 Global Two-time Quantities I **41**
6.1 Correlation function for linear growth . . . 42
6.2 Response function for linear growth 1 : Changing the diffusion constant . . . 47
6.2.1 Dynamic phase diagram . . . 50
6.2.2 Small perturbation . . . 54
6.3 Response function for linear growth 2 : Changing the noise strength . . . 56
6.4 Fluctuation-dissipation ratios for linear growth . . . 59
6.5 Two-time Quantities for Non-linear Growth . . . 60
6.6 Summary . . . 63

7 Global Two-time Quantities II **65**
7.1 The quantity G_m . . . 65
7.2 The correlation function, the response function, and the fluctuation-dissipation ratio for the quantity G_m . . . 68
7.3 Non-equilibrium fluctuation-dissipation theory . . . 73

8 Conclusion **80**

Bibliography **83**

List of Figures

3.1 The random deposition (a), the Family model (b), and the Wolf-Villain model (c) for a $(1+1)$-dimensional system. The boxes surrounded by dashed boundaries indicate incoming particles. The arrows beside the particles show possible moves. 12

3.2 Log-log plot of the surface width vs. time for the RDSR process in systems with different sizes L. The data is averaged over 10000 realizations for each system size. The solid (dashed) line with slops 1/4 (1/2) is ploted for comparison. 13

3.3 The ballistic deposition for a $(1+1)$-dimensional system where the NN model (a) and the NNN model (b) are shown. The boxes surrounded by dashed boundaries indicate incoming particles. 15

3.4 The restricted solid on solid model for a $(1+1)$-dimensional system. The boxes surrounded by dashed boundaries indicate incoming particles. The crosses indicate where the depositions are not allowed. Here we show two cases with different values of S: (a) $S = 1$ and (b) $S = 2$. 16

3.5 Log-log plot of the surface width vs. time for the RSOS process in systems with different sizes L and different restricted heights S. The data is averaged over 1000 realizations for each system size and restricted height. The solid (dashed) line with slops 1/4 (1/3) is plotted for comparison. 17

3.6 Log-log plot of the surface width vs. time for the RD/RDSR process in systems with different sizes L and different probabilities p. The data is averaged over 1000 realizations for the cases where $p \leq 1/2$. The data for $p = 1$ are the same data as shown in Figure 3.2. The solid (dashed) line with slops 1/4 (1/2) is plotted for comparison. 18

3.7 Probabilities that for the shown configuration the particle, initially deposited on top of the middle column, comes to rest on top of one of the three columns. *J. Stat. Mech.* P08007. Used with permission of IOP Publishing Ltd and SISSA, 2010. 20

3.8 (a) Log-log plot of the surface width vs time for a system of size $L = 1000$ and different temperatures. The dashed lines have the slopes $1/2$ and $1/4$ expected in the random deposition and EW regimes, respectively. The location of both crossover points depend on temperature. The full lines are obtained from fitting the exact solution of the EW stochastic equation. Here and in the following error bars are smaller than the symbol sizes. (b) Time evolution of the effective exponent (3.14) for the data shown in (a). (c) Log-log plot of the surface width vs time for systems of different sizes evolving at the same temperature $T = 1$. (d) Time evolution of the effective exponent (3.14) for the data shown in (c). The full lines are derived from the fits to the exact solution of the EW stochastic equation (see Section 4.1.3 below). *J. Stat. Mech.* (2010) P08007. Used with permission of IOP Publishing Ltd and SISSA, 2010. . . . 22

4.1 The illustration of the integral Eq. (4.22). The functions $f(k)$ and $g(k)$ are shown as the gray solid curve and the black dashed line, respectively. The constant $\mathcal{C}$ is indicated by the area marked with orange color. The value of the parameter s is chosen to be $-3/2$ for this plot. 27

5.1 (a) Family-Vicsek scaling for the RD/RDSR process (see Figure 3.6 for the original plot) in systems with different sizes L and different probabilities p. A data collapse is only achieved for two of the three regimes. (b) A complete data collapse of all data sets is achieved when using our new scaling relation (5.6). The curves shown in the left panel completely fall one on top of the other and are no longer distinguishable. 36

5.2 The same as Fig. 5.1, but now for the RSOS model (see Figure 3.5 for the original plot) with different values S of the maximal nearest-neighbor height difference. Again a perfect data collapse is achieved when using the scaling relation (5.6). 36

5.3 (a) Log-log plot of the surface width vs time for the temperature dependent deposition model. Systems of different sizes at different temperatures are shown. (b) A complete data collapse of all data sets is also achieved for this model. *Phys. Rev. E* 79(5): 051605. Used with permission of American Physical Society, 2009. 39

5.4 Log-log plot of the rescaled surface width vs time for the one-dimensional linear Langevin equations with (a) $m = 2$ and (b) $m = 4$. The insets show the original data. 40

6.1 Six possible regimes for two-time functions. The regimes 2 and $2'$ (3 and $3'$) have the same leading behavior and, hence, belong to the same category. . . 44

6.2 Global correlation function when both times t and s are in the correlated regime. The symbols are obtained by numerically evaluating the exact expression (6.6) whereas the lines indicate the asymptotic power-laws (6.12). Panel (a) shows data for the EW case and dimensions $d = 1, 2$ (from top to bottom), panels (b) show data for the MH case and dimensions $d = 1, 2, 3, 4$ (from top to bottom). The different symbols correspond to different waiting times where $s_0 = 1000$ below the critical dimension and $s_0 = 200$ at the critical dimension (which is $d = 2$ for EW and $d = 4$ for MH). The linear extension of the system is $L = 2^{14}$ for $d = 1$, $L = 2^9$ for $d = 2$, $L = 2^7$ for $d = 3$, and $L = 2^6$ for $d = 4$. 46

6.3 (a-c) Time evolution of the width square in case the temperature is changed after 10^5 time steps. The full lines show the data obtained from numerical simulations of the temperature dependent deposition model (MRDSR). These data have been obtained for systems with L = 400 sites after averaging over 10,000 different growth events. The dashed lines show W_ν^2 for an unperturbed surface growing at the constant temperature T_f. In (a) the quench is to the RD regime, whereas in (b) and (c) the quenches are to the EW and saturation regimes, respectively. (d-e) The same cases as shown in (a-c), but now the difference $\Delta W^2 = \epsilon\chi$ is plotted. Qualitative different behavior is observed, depending on the regime that the unperturbed system has at the quench time. The circles are obtained from the exact solution of the EW equation. Note that the panel (f) is linear in t. 49

6.4 Contour plot of γ as a function of νs and μ/ν for $t/s = 64$. Four different regimes, separated by crossover regions, are identified. The two dashed lines separate the three qualitatively different types of behavior encountered when plotting the effective exponent as a function of t, see Fig. 6.6. *Phys. Rev. E* 80(6): 061602. Used with permission of American Physical Society, 2009. . . 52

6.5 (a) Contour plots of γ as a function of νs and μ/ν for $t/s = 64$ (full blue line), 256 (dashed green line), and 1024 (dotted red line). Only contours bounding the $\gamma = 0$, $-1/2$ and $-3/2$ regimes are shown. (b) The same contour plots as shown in (a) but as a function of νt and $\mu s/\nu t$. A collapse of the contours is observed. 52

6.6 The three different quench types illustrated by the time dependence of the effective exponent γ. In all cases the quench takes place at $s = 10^5$. Type (a) includes quenches with initial conditions νs and μ/ν located above the upper dashed line in Fig 6.4. For type (b) the starting point is located between the two dashed lines in Fig 6.4, whereas for type (c) the initial conditions put the starting point below the lower dashed line. 53

6.7 Global response to a change of the surface tension when both times t and s are in the correlated regime. The symbols are obtained by numerically evaluating the exact expression (6.19) whereas the lines indicate the asymptotic power-laws (6.30). Panel (a) shows data for the EW case and dimensions $d = 1, 2$ (from top to bottom), panels (b) show data for the MH case and dimensions $d = 1, 2, 3, 4$ (from top to bottom). The different symbols correspond to different waiting times where $s_0 = 1000$ below the critical dimension and $s_0 = 200$ at the critical dimension (which is $d = 2$ for EW and $d = 4$ for MH). The linear extension of the system is $L = 2^{14}$ for $d = 1$, $L = 2^9$ for $d = 2$, $L = 2^7$ for $d = 3$, and $L = 2^6$ for $d = 4$. 55

6.8 Global response to a change of the noise strength when both times t and s are in the correlated regime. The symbols are obtained by numerically evaluating the exact expression (6.34) whereas the lines indicate the asymptotic power-laws (6.38). Panel (a) shows data for the EW case and dimensions $d = 1, 2$ (from top to bottom), panels (b) show data for the MH case and dimensions $d = 1, 2, 3, 4$ (from top to bottom). The different symbols correspond to different waiting times where $s_0 = 1000$ below the critical dimension and $s_0 = 200$ at the critical dimension (which is $d = 2$ for EW and $d = 4$ for MH). The linear extension of the system is $L = 2^{14}$ for $d = 1$, $L = 2^9$ for $d = 2$, $L = 2^7$ for $d = 3$, and $L = 2^6$ for $d = 4$. 58

6.9 The global fluctuation-dissipation ratio for the one-dimensional EW case, with $m = 1$. The ratio (6.44) displays a different behavior in the different regimes. The data have been obtained by numerically evaluating the exact expressions derived in the previous subsections. The parameters are $L = 500$, $D = 1$, and $\nu = 0.001$. *J. Stat. Mech.* P08007. Used with permission of IOP Publishing Ltd and SISSA, 2010. 61

6.10 Log-log plots of global quantities as a function of t/s obtained from the one-dimensional KPZ equation in the correlated regime: (a) global correlation (b), global response to a change of the surface tension ν, and (c) global response to a change of the noise strength D. The data in (a) and (c) have been obtained with the Newman algorithm [76, 77], whereas the data in (b) result from the algorithm of Lam and Shin. We checked that both algorithms produce the same exponents and scaling functions for a given quantity. The system size is $L = 10000$, with $\lambda = 1$, $\nu = 1$, and $D = 1$. For the response shown in (b), ν has the value of 1.1 until time s at which point it is changed to the value 1, whereas for (c) D was changed from the value 1.1 to 1 at time s. The data shown have been obtained after averaging over 5×10^6 realizations for the correlation and 5×10^5 realizations for the response. The lines indicate the asymptotic power-law behavior. *J. Stat. Mech.* P08007. Used with permission of IOP Publishing Ltd and SISSA, 2010. 62

7.1 Two surfaces with same surface width but different values of G_m. 66

7.2 $\langle G_2 \rangle$ for various system sizes in one dimension as indicated in the figure. The inset shows the power-law decay for $G_{s,2} - \langle G_2 \rangle$ in the correlated regime. The symbols are obtained by numerically evaluating the exact expression Eq. (7.7). The dashed and solid lines are given by the asymptotic functions Eqs. (7.9) and (7.12). The parameters for the evaluations are $\nu = 0.001$ and $D = 1$ 69

7.3 The scaled data of $\langle G_2 \rangle$ shown in Figure 7.2. The inset shows the magnified portion around the saturation regime. Deviations are due to the finite-size effects. The dashed and solid lines are given by the asymptotic functions Eqs. (7.9) and (7.12). 69

7.4 Same as Figure 7.2 but here the plots show systems with various m and d. The system size is $L = 3600$ for $m = 2$ and $d = 1$; $L^2 = 6400$ for $m = 2$ and $d = 2$; $L = 14400$ for $m = 4$ and $d = 1$; and $L^2 = 25600$ for $m = 4$ and $d = 2$ 70

7.5 The correlation (a) and response (b) functions of G_2 in the (1+1)-dimensional system. The solid (open) symbols show the original (rescaled) data evaluated from Eqs. (7.15) and (7.17). The solid lines on both panels (a) and (b) are obtained from Eq. (7.24). The inset shows in log-log scale χ_G vs C_G together with a solid line given by Eq. (7.26). The parameters for the evaluations are $L = 2^{14}$, $\nu = 0.001$ and $D = 1$. 73

7.6 Contour plot of FDR $X(t, s)$ for the one-dimensional EW equation. The parameters for the evaluations are $L = 2^6$, $\nu = 0.001$ and $\mu = 0.99\nu$. The symbols $\tau_1 \equiv \log(t_1)$, $\tau_2 \equiv \log(t_2)$, and $\tau_x \equiv \log(1/2\nu)$ are used for simplicity. 74

7.7 The fluctuation-dissipation ratio as a function of waiting time s. The data are by numerically evaluating the correlation function Eq. (7.15) and response function Eq. (7.17). The solid (dashed) line indicates the value of $\frac{1}{2\nu}\left(\frac{L}{2\pi}\right)^m$ for $m = 2$ ($m = 4$). The linear extension for all the systems shown in the figure is $L = 2^6$. The parameters for the evaluations are $\nu = 0.001$ and $\mu = 0.99\nu$ and $t = s + 10^7$. 75

7.8 The numerical evaluation of the dissipation-fluctuation ratio Eq. (7.35) for the one dimensional EW equation. Panel (a) shows the systems with small perturbation and panel (b) shows the systems with large perturbation. The system size is $L = 2^6$, the diffusion constant for the unperturbed system is $\nu = 0.001$, and the observation time t is given by $\nu(t - s) = 100$ to ensure $2\nu(t - s) \gg 1$. Note the $Y \approx 1$ for small s and $Y \approx \mu/\nu$ for large s. 77

7.9 Contour plot of $Y(t, s)$. The non-equilibrium fluctuation-dissipation theorem Eq. (7.28) is valid for large observation times t and small waiting times s. . . 78

7.10 The numerical evaluation of the dissipation-fluctuation ratios Y (see Eq. (7.35)), Y_S and Y_T (see Eq. (7.43)) for the one-dimensional EW equation. The system size is $L = 2^6$, the diffusion constant for the unperturbed system is $\nu = 0.001$, the ratio of the diffusion constants is $\mu/\nu = 0.99$, and the observation time is given by $\nu(t - s) = 100$. 79

List of Tables

4.1 Values for the surface tension ν at different values of T/g that result from a fit of the numerical data of MRDSR to the exact solution of the Edwards-Wilkinson equation. 29

5.1 List of universality classes. The values of scaling exponents are valid for all dimensions for the RD universality class, for $d < d_c$ for both the EW and MH universality classes, and for $d = 1$ for the KPZ universality class. 35

6.1 Summary of the asymptotical dependence of the global correlation function for the different cases. RD corresponds to the random deposition regime, CR to the correlated regime, and SR to the saturation regime. The values of a and b, which depend on the case considered, can be read off from the equations in the main text. 44

6.2 The same as Table 6.1, but now for the response (6.19) to a small perturbation during which the surface tension is changed. The values of a, b and c, which depend on the case considered, can be read off from the equations in the main text. 54

6.3 The same as Table 6.2, but now for the response (6.33) to a change in the strength of the noise correlation. The values of a, b and c, which depend on the case considered, can be read off from the equations in the main text. . . 57

7.1 The numerically evaluated values of $I(m,d) \equiv \int_0^\pi \mathcal{P}(\mathbf{q})^{m/2}/q^m d\mathbf{q}$ 68

Chapter 1

Introduction

Temporal evolutions of surfaces and interfaces are widespread in nature and range from the macroscopic to the microscopic. Thus, orogenic events, weathering, and erosion make the surface of the earth evolve in time, without ever reaching an equilibrium state. Winds blowing over the surfaces of oceans, lakes and rivers generate rapid changing wind waves. A burning front propagating along a sheet of paper forms a one-dimensional moving edge. A drop of ink spread on a piece of paper yields an interface between wet and dry regions. Tumors that develop in living beings form interfaces between themselves and the host. A bacteria colony growing on an agar substrate is another example of an evolving interface in a biological system. Deposition processes, ranging from sedimentation in geology to processes such as electrochemical deposition, all yield surfaces and interfaces that evolve in time. Certainly, the complex behavior of an evolving surface results from numerous factors. In order to gain valuable insights into the universal properties of these ubiquitous phenomena, physicists try to identify the main ingredients responsible for the temporal evolution of surfaces. In general, there are two competing factors that are primarily responsible for time-dependent surfaces. On the one hand, fluctuations and noise make the surfaces become rougher as time progresses. On the other hand, dissipation and relaxation phenomena tend to smooth the surfaces. Obviously, both of these major mechanisms are influenced by control parameters such as temperature, pressure, chemical potential, or the thickness of the agar, for example. At fixed control parameters, it is usually assumed that the nature of the noise does not change in time. Relaxation forces, however, depend on the evolving surface itself: the rougher the surface is, the stronger the relaxation is. Starting from an initially flat surface, relaxation does not take place at the initial stages and the surface roughens. It follows that roughening is common for evolving surfaces. At a later stage dissipation and relaxation become effective, and the competition between the different mechanisms often yields in the long-time limit a saturated surface with a constant roughness. This saturation roughness is a power-law function of the surface size with some roughness exponent α. Interestingly, similar values of α are found for processes as different as paper combustion, paper wetting, fluid flow, and bacteria growth, pointing to universal, system independent properties of evolving surfaces.

Therefore, the study of the exponents governing surface growth processes helps us not only to understand their dynamic properties but also to classify the universality classes that reveal the commonalities of very different growth processes.

The major goal in modern statistical physics is to establish a general structure for systems out of equilibrium. Although this task is still a challenge, some theorems have been successfully extended to systems out of equilibrium. One of them is the linear response theorem that relates fluctuation and dissipation [6, 82]. Measuring the response of a system subjected to an external force or field has been a important method in experimental research for a long time. The magnetic susceptibility χ which measures the magnetization M of a material in response to an applied field is an example of such a quantity. Interestingly, the response can be expressed in terms of how the order parameter in a system correlates. Take the magnetic material as an example, where the magnetic susceptibility can be determined by calculating the correlation of the magnetization.[1] The regression hypothesis made by Onsager in 1935 also suggests a relation between the correlation and the response. It states that the linear response to a small non-equilibrium disturbance of a system can be treated as spontaneous thermal fluctuations of the system at equilibrium. This is a consequence of the fluctuation-dissipation theorem. Although the theorem for systems in equilibrium has been established for a long time, several researchers have recently worked on an extension to non-equilibrium systems.

Another approach in the search for general structures in non-equilibrium systems is to find common properties among distinctly different non-equilibrium phenomena. One example is categorizing the omnipresent slow relaxation processes into so-called aging phenomena. Coincidentally, it is the study of responses and correlations that help to establish this classification.

In this work we extend the study of surface roughening and growth processes to cases where the external conditions are changed during the growth. Combining analytical and numerical techniques, we aim at a classification of the possible responses of evolving surfaces to changing control parameters. Elucidating in our theoretical study the generic changes of surface morphology under a change of growth conditions, we propose specific protocols that allow the experimentalists to change the experimental conditions in order to tailor the roughness and morphology of their surfaces and interfaces. Putting our research in an even broader context, we notice that kinetic roughening and growth processes are paradigmatic examples of non-equilibrium processes. Our study therefore yields new insights into and enhances our understanding of systems that are far from equilibrium.

This thesis is organized in the following way. In Chapter 2 we discuss the general definition of correlation function, response function and linear response theory which links these two quantities. The tools introduced in this chapter will be extensively used in Chapters 6 and 7 to investigate surface growth. In Chapters 3 and 4 we introduce lattice models and equations of motion invented to mimic surface growth. Motivated by previous studies we

[1] Where one has $\chi = (\langle M^2 \rangle - \langle M \rangle^2)/k_B T$ with k_B the Boltzmann constant.

propose a lattice model with temperature-dependent growth properties that fits the famous Edwards-Wilkinson equation excellently. In Chapter 5 we discuss an important concept in the studies of surface growth, the Family-Vicsek scaling relation, which allows to classify growth universality classes. We propose a generalized version of this scaling relation which applies to larger classes of systems. Chapter 6 is devoted to the exact computation of the global two-time quantities related to the surface width in cases that are described by linear stochastic Langevin equations. The exact results allow us to comprehensively investigate all possible dynamical regimes. We also present our results for the one-dimensional Kardar-Parisi-Zhang equation where we highlight some commonalities with and differences to the linear systems. In Chapter 7 we discuss the global two-time quantities related to the quantity which is conjugated to the surface diffusion constant. Similar approaches as in Chapter 6 will be used. This quantity has interesting properties that allow us to discuss the generalized fluctuation-dissipation relation for non-equilibrium growth processes. Finally, Chapter 8 gives out conclusions.

Chapter 2

Correlation, Response and Relaxation

2.1 Correlation function

The two point correlation function of quantities ϕ and ψ

$$C_{\phi,\psi}(t,s) \equiv \langle \phi(t)\psi(s)\rangle, \tag{2.1}$$

is a measure of how these two quantities are correlated to each other. For systems in equilibrium the symbol $\langle\cdots\rangle$ denotes the thermal average, whereas for non-equilibrium processes it indicates the average over all possible trajectories that start from a specified distribution of initial configurations. The quantities of interest ϕ and ψ can be either local or global, and can be measured at the same time or at different times. The correlation of two quantities measured at the same time, $C_{\phi,\psi}(t) = \langle \phi(t)\psi(t)\rangle$, is called the equal-time correlation function. The equal-time correlation function for microscopic (local) variables at different positions is usually used to measure the order of a system. If the correlation between the same quantity is measured, one has $C_{\psi,\psi}(t,s) = \langle \psi(t)\psi(s)\rangle$, which is called autocorrelation function.[1] Normally, this quantity decays with time since thermal fluctuation progressively changes the value of ψ. The evaluation of $C_{\psi,\psi}(t,s)$, which is dependent on the separation between two times, records how the system loses its memory. For systems in the steady state, the autocorrelation function depends only on the difference between the two times, $C_{\psi,\psi}(t,s) = C_{\psi,\psi}(t-s)$. In other words, the correlation function has the property of time-translational invariance. The reason is that the equilibrium system has a steady state probability distribution which fulfills detailed balance. If the correlation between two variations $\delta\phi = \phi - \langle\phi\rangle$ and $\delta\psi = \psi - \langle\psi\rangle$ are calculated, we have

$$C_{\delta\phi,\delta\psi} = \Big\langle \Big(\phi - \langle\phi\rangle\Big)\Big(\psi - \langle\psi\rangle\Big)\Big\rangle = \langle\phi\psi\rangle - \langle\phi\rangle\langle\psi\rangle. \tag{2.2}$$

[1] For microscopic variable, the autocorrelation function is defined as the correlation at the same position, i.e. $\langle\psi(\mathbf{x},t)\psi(\mathbf{x},s)\rangle$.

This is called the connected correlation function of ϕ and ψ and is usually denoted as $\langle\phi\psi\rangle_c$. The connected autocorrelation function $C_{\delta\psi,\delta\psi} = \langle(\psi - \langle\psi\rangle)^2\rangle = \langle\psi^2\rangle - \langle\psi\rangle^2$, which is positive definite, measures the fluctuations in the quantity ψ.

2.2 Response function and susceptibility

To study how a system responds to an external perturbation, one introduces the response function. Assume that at time s a small impulse of a field h, which is conjugated to the observable ψ, is applied to the system. Therefore, the Hamiltonian of the system becomes

$$H(t) = H_0(t) - h\psi(t)\delta(t-s), \tag{2.3}$$

where H_0 is the Hamiltonian of the unperturbed system and $\delta(t-s)$ is the Dirac delta function. The measure of the difference of the observable ϕ between the perturbed and unperturbed system at time t is given by

$$R_{\phi,\psi}(t,s) \equiv \lim_{h\to 0} \frac{\langle\phi(t)\rangle_h - \langle\phi(t)\rangle}{h}, \tag{2.4}$$

where $\langle\cdots\rangle_h$ indicates the path average when the field h has been applied. This two-time function is called the response function. The response function is a measure of how the quantity ϕ reacts at time t when the quantity ψ has been perturbed at time s. Like the autocorrelation function the response function also decays for large time separation since the influence of the perturbation is gradually erased by the noise. For a system in the steady state, the response function also satisfies time-translational invariance due to the time-independent probability distribution and the detailed balanced dynamics.

The response function (2.4) is hard to measure experimentally due to the sharp impulse of the perturbation. Therefore, to increase the signal one often studies the cumulative response (it is also called the integrated response or susceptibility). The same measurement as before is made

$$\chi_{\phi,\psi}(t,s) \equiv \lim_{h\to 0} \frac{\langle\phi(t)\rangle_h - \langle\phi(t)\rangle}{h}. \tag{2.5}$$

However, the perturbation now is applied to the system during a certain time interval. Particularly, if a constant external filed h is turned on from the waiting time s to the observation time t, one has the zero-field cooled (ZFC) susceptibility

$$\chi^{\mathrm{ZFC}}_{\phi,\psi}(t,s) = \int_s^t ds' R_{\phi,\psi}(t,s'). \tag{2.6}$$

On the other hand, if the constant field is turned on at $t = 0$ until the waiting time s, one obtains the thermoremanent susceptibility (TRM)

$$\chi^{\mathrm{TRM}}_{\phi,\psi}(t,s) = \int_0^s ds' R_{\phi,\psi}(t,s'). \tag{2.7}$$

By the definition of the ZFC and TRM susceptibilities, one has

$$\chi^{\rm ZFC}_{\phi,\psi}(t,0) = \chi^{\rm TRM}_{\phi,\psi}(t,s) + \chi^{\rm ZFC}_{\phi,\psi}(t,s), \tag{2.8}$$

where $\chi^{\rm ZFC}_{\phi,\psi}(t,0) = \chi^{\rm FC}_{\phi,\psi}(t)$ is also called the field-cooled susceptibility.

2.3 Linear response theory

Onsager's regression hypothesis states that the response of a system at equilibrium to a small external perturbation is equivalent to the spontaneous thermal fluctuations of the system. This hypothesis can be explained as follows. In thermal equilibrium, a system in a configuration X described by a Hamiltonian $H_0(X)$ has the probability distribution function

$$P(X) = \frac{1}{Z} e^{-H_0(X)/k_BT}, \tag{2.9}$$

where T is the temperature, k_B is the Boltzmann constant and $Z = \int dX e^{-H_0(X)/k_BT}$ is the partition function. The expectation value of observable ϕ in the system is given by

$$\langle \phi \rangle = \int dX P(X)\phi(X). \tag{2.10}$$

Consider that the system is now perturbed by the external field h such that the perturbed Hamiltonian becomes $H(X) = H_0(X) - h\psi(X)$. In this case, one has the perturbed probability distribution

$$P_h(X) = \frac{1}{Z_h} e^{-H(X)/k_BT}, \tag{2.11}$$

where the perturbed partition function becomes $Z_h = \int dX e^{-H(X)/k_BT}$. To calculate the expectation value of the observable ϕ in the perturbed system, one can expand the perturbed partition function about the unperturbed one to first order

$$Z_h = \int dX [1 + h\psi(X)/k_BT + \mathcal{O}(h^2)] e^{-H_0(X)/k_BT} \tag{2.12}$$

which further yields

$$P_h(X) = P(X)\left\{1 + h\left[\psi(X) - \langle\psi\rangle\right]/k_BT + \mathcal{O}(h^2)\right\}. \tag{2.13}$$

Therefore, the expectation value of ϕ for the perturbed system is given by

$$\begin{aligned} \langle\phi\rangle_h &= \int dX P_h(X)\phi(X) \\ &= \langle\phi\rangle + h\Big\{\langle\phi\psi\rangle - \langle\phi\rangle\langle\psi\rangle\Big\}/k_BT + \mathcal{O}(h^2). \end{aligned} \tag{2.14}$$

For a small perturbation, the higher order can be neglected and one obtains the linear response theory for an equilibrium state

$$\chi_{\phi,\psi} = \lim_{h\to 0} \frac{\langle\phi\rangle_h - \langle\phi\rangle}{h} = \frac{1}{k_B T}\Big\{\langle\phi\psi\rangle - \langle\phi\rangle\langle\psi\rangle\Big\}. \tag{2.15}$$

In a more compact form, on has

$$R_{\phi,\psi}(t,s) = \pm\frac{d}{ds}\chi_{\phi,\psi}(t,s) = \frac{1}{k_B T}\frac{d}{ds}\Big\langle\phi(t)\psi(s)\Big\rangle_c, \tag{2.16}$$

where one has $+(-)$ if $\chi_{\phi,\psi} = \chi^{\rm TRM}_{\phi,\psi}$ ($\chi^{\rm ZFC}_{\phi,\psi}$). This equation links microscopic fluctuations and macroscopic relaxation. It is also called the fluctuation-dissipation theorem.

2.4 Aging

Slow relaxation processes are non-equilibrium processes that are encountered in many circumstances, ranging from domain growth, phase separation, weakly driven systems, granular materials, and spin glasses to structural glasses. Some of those systems evolve extremely slow and may never reach their equilibrium state in the experimental time window. This is for example the case in glassy systems. In addition to the slowly, non-exponential dynamics, several other common properties have been observed in those systems. First, time-translational invariance and fluctuation-dissipation theorem are broken. These make the slow relaxation processes distinct from the non-equilibrium steady states. Second, the change of the physical properties of the system proceeds slower as the system becomes older. This defines the *age* of the system. To quantify this property two-time quantities such as the autocorrelation function and autoresponse function are studied. It is found that there often exist dynamic scaling relations for the correlation function and response function. In addition, there exists a time-dependent length scale $L(t)$ describing the correlated domain size. Dynamic processes with the above properties are summarized by the term *aging* [27, 28, 47].

For a simple case where the time-dependent length scale displays a power-law growth, one has $L(t) \sim t^{1/z}$, where z is the so-called dynamic exponent. The autocorrelation function and the autoresponse function are usually observed to have the scaling forms

$$C(t,s) = s^{-b} f_C(t/s) \tag{2.17}$$

$$R(t,s) = s^{-1-a} f_R(t/s) \tag{2.18}$$

where a and b are aging exponents and $f_{C,R}(y)$ are scaling functions. Generally, the scaling functions display a power-law decay in the long time limit $y \gg 1$

$$f_C(y) \sim y^{-\lambda_C/z} \tag{2.19}$$

$$f_R(y) \sim y^{-\lambda_R/z} \tag{2.20}$$

where λ_C and λ_R are called the autocorrelation and autoresponse exponents respectively. When a system enters the aging regime, the fluctuation-dissipation theorem Eq. (2.16) no longer holds. It has been suggested to study instead the fluctuation-dissipation ratio

$$X_{\phi,\psi} = k_B T \frac{\chi_{\phi,\psi}}{C_{\phi,\psi}}. \tag{2.21}$$

It follows that by defining an effective temperature T_{eff} such that $k_B T_{\text{eff}}\ \chi_{\phi,\psi}/C_{\phi,\psi} = 1$, one has $T_{\text{eff}} = T/X_{\phi,\psi}$. In many cases, the effective temperature T_{eff} is larger then the heat bath temperature T since $X_{\phi,\psi} < 1$ is usually observed. It is worth noting that $X_{\phi,\psi}$ is not guaranteed to be observable independent for systems out of equilibrium. Hence, the effective temperature is denoted as $T_{\text{eff}}^{(\phi,\psi)}$ if the observable dependence is highlighted.

2.5 Fluctuation-dissipation theory of non-equilibrium states

Effective temperatures are often studied when the fluctuation-dissipation theory is violated. However, if that temperature is found to depend on the observable, it is hard to give a physical meaning to the effective temperature. Recently, theoretical studies focused on other approaches in the search for a non-equilibrium fluctuation-dissipation theorem. One successful approach introduced by Baiesi et. al. provides a novel way to interpret the fluctuation-dissipation relation [6]. They compare the path probability density between the perturbed and unperturbed systems, denoted by $P_h[\omega(t)]$ and $P[\omega(t)]$ respectively, where $\omega(t)$ describes the trajectory in configuration space. Hence, the expectation value of the observable ϕ in the unperturbed system at time t is given by $\langle\phi(t)\rangle = \int_0^t [D\omega(t')]P[\omega(t')]\phi[\omega(t')]$, where we integrate over all possible trajectories. To study time-reversibility one defines a time-reversal operator θ which reverses the trajectory ω. Writing that

$$P_h[\omega] = e^{-A[\omega]} P[\omega], \tag{2.22}$$

the action $A[\omega]$ can be decomposed into two part

$$-A[\omega] = \frac{1}{2} S[\omega] - \frac{1}{2} T[\omega], \tag{2.23}$$

where $S[\omega] \equiv A[\theta\omega] - A[\omega]$ is time antisymmetric, and $T[\omega] \equiv A[\theta\omega] + A[\omega]$ is time symmetric. The time-antisymmetric part can be viewed as a difference in entropy flux from the system to the environment between the perturbed and unperturbed dynamics,

$$\begin{aligned} S[\omega] &= \frac{1}{k_B T} \int_0^t ds h_s \frac{d}{ds} \psi[\omega(s)] \\ &= \frac{1}{k_B T} \left\{ h_t \psi(t) - h_0 \psi(0) - \int_0^t ds \frac{dh_s}{ds} \psi[\omega(s)] \right\}. \end{aligned} \tag{2.24}$$

The first two terms on the right-hand side of this equation give the change of energy due to the perturbation, while the third term is the work done on the system by the external field h_s. The time-symmetric term is given by the change of the escape rate from a trajectory due to the perturbation. This term is called the excess *dynamical activity* or *traffic*. Denoting $W(x,y)$ as the transition rate from state x to state y, the escape rate from state x is given by $\sum_y W(x,y)$. For a Markov process, the transition rate $W(x,y)$ is perturbed by the external field h_s, $W(x,y) \to W(x,y)e^{h_s[\psi(y)-\psi(x)]/k_BT}$. Therefore, the excess activity over a trajectory is given by

$$\begin{aligned} T[\omega] &= \int_0^t ds \sum_y W(x,y)(e^{h_s[\psi(y)-\psi(x)]/k_BT} - 1) \\ &= \frac{1}{k_BT}\int_0^t ds \left\{ h_s \sum_y W(x,y)[\psi(y)-\psi(x)] + \mathcal{O}(h_s^2) \right\} \\ &= \frac{1}{k_BT}\int_0^t ds \left\{ h_s \frac{d\psi}{ds} + \mathcal{O}(h_s^2) \right\}. \end{aligned} \tag{2.25}$$

In the linear response regime, ons has $\langle \phi(t) \rangle_h = \langle \phi(t) \rangle + \int_0^t ds h_s R_{\phi\psi}(t,s)$. Expanding $\langle \phi(t) \rangle_h$ about the unperturbed system to first order in h and then applying Eq. (2.23), one obtains

$$\begin{aligned} \int_0^t ds h_s R_{\phi\psi}(t,s) &= \Big\langle \phi(t) \Big\rangle_h - \Big\langle \phi(t) \Big\rangle \\ &\approx \Big\langle -\phi(t) A[\omega] \Big\rangle \\ &= \frac{1}{2}\Big\langle \phi(t) S[\omega] \Big\rangle - \frac{1}{2}\Big\langle \phi(t) T[\omega] \Big\rangle \end{aligned} \tag{2.26}$$

Plugging in Eqs. (2.24) and (2.25), one finally has

$$R_{\phi\psi}(t,s) = \frac{1}{2k_BT}\frac{d}{ds}\Big\langle \phi(t)\psi(s) \Big\rangle - \frac{1}{2k_BT}\Big\langle \phi(t)\frac{d}{ds}\psi(s) \Big\rangle. \tag{2.27}$$

We will test this equation by applying it to the non-equilibrium surface growth (through the exact results obtained from linear Langevin equations) in Chapter 7.

Chapter 3

Surface Growth Models

In this chapter, we discuss the most important discrete lattice models used for the study of surface growth. We start from the classical models which can be described by linear stochastic equations of motion (see Chapter 4). These growth processes can basically be classified according to the effective Hamiltonian of the equation of motion. The first type we will discuss is that with an effective Hamiltonian proportional to the total surface slope, while the other type has an effective Hamiltonian which is proportional to the total surface curvature. The surface growth generated by particle sedimentation under the influence of gravity belongs to the first type, originally studied by Edwards and Wilkinson [37] (see also Chapter 4). A related discrete lattice model, which is called random deposition with surface relaxation (RDSR), was proposed later by Family [40]. It is interesting that the scaling exponents obtained by the simulations agree with those derived from the analytical work. So far it has been found that the vicinal steps of an oxide surface [78], non-interacting flux lines in a superconductor as well as single-file diffusion [19] belong to the Edwards-Wilkinson universality class. The second type of effective Hamiltonian yields another universality class, which includes the Mullins-Herring equation [74] (see also Chapter 4), the Wolf-Villain model [92], the Das Sarma-Tamborenea model [33] and an experimental study of step fluctuations on Ag(111) films [35]. In addition, we will discuss models which are believed to be associated with the Kardar-Parisi-Zhang equation [55] (see also Chapter 4). These models include the ballistic deposition and the restricted solid on solid model. Thereafter, systems based on fundamental models with an adjustable parameter will be introduced. Some models, called competitive growth models, result from the combination of two fundamental models which are selected with different probabilities. The properties of the surface evolution are controlled by the selected probabilities. In other models the effect of temperature is modeled through rules that accept a new configuration with a probability proportional to the Boltzmann factor. These models include the Arrhenius diffusion model [26, 33, 52, 65, 80, 89], the Siegert-Plischke model [86] and the modified RDSR model [24, 23].

3.1 Random deposition

The random deposition process is one of the simplest mechanisms causing the evolution of a surface. Random deposition can be described by a surface growth model where particles drop randomly upon the surface and then stick directly on the top of the surface [40, 8]. For simplicity, people usually deal with a discrete lattice model and make the following assumptions. First, the particle is a $(d+1)$-dimensional hypercube with uniform linear size a which is usually assumed to be unity. Second, under the first assumption, the d-dimensional substrate is divided into A columns, where A denotes the area of the substrate. Third, the flux of incoming particles is constant. It is a convention to assume that there are A particles dropped per unit time. The roughness of a growing surface is characterized by the time dependent mean interface width, the square of which is defined as the variance of surface height

$$W^2(t) = \frac{1}{A}\sum_i \left[h_i(t) - \bar{h}(t)\right]^2, \tag{3.1}$$

where h_i is the surface height of the ith column, and $\bar{h}$ is the mean height. After $N = tA$ particles have been deposited on a flat substrate, the probability of finding a column with height h is a binominal distribution,

$$f(N,h) = \frac{N!}{h!(N-h)!}p^h q^{N-h}, \tag{3.2}$$

where $p = 1/A$ and $q = 1 - p$. Hence, the mean and variance are given respectively by

$$\begin{aligned} \bar{h} &= Np = t, \\ W^2 &= Npq \approx t. \end{aligned} \tag{3.3}$$

The second equation, where a large enough substrate area has been assumed in order to ensure the approximation, can be rewritten as $W \approx t^\beta$ with $\beta = 1/2$. The exponent β, which describes how the surface width evolves with time, is called the growth exponent. An illustration of the $(1+1)$-dimensional model is shown in Figure 3.1(a).

3.2 The Family model

The Family model [40] is a discrete lattice model which imitates particle sedimentation under the influence of gravity. In addition to the roughening process caused by the random deposition, a smoothing effect is introduced. This step, the so-called surface relaxation, is described as follows. After the particle reaches the top of the surface site, the particle can go to one of its neighbor columns with lowest height as shown in Figure 3.1 (b). This procedure generates a surface current which is driven by gravity. Sometimes people use the name random deposition with surface relaxation (RDSR) for the Family model to emphasize

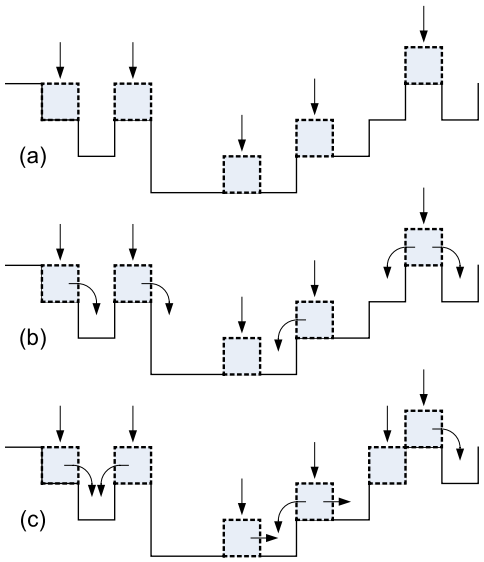

Figure 3.1: The random deposition (a), the Family model (b), and the Wolf-Villain model (c) for a $(1+1)$-dimensional system. The boxes surrounded by dashed boundaries indicate incoming particles. The arrows beside the particles show possible moves.

the mechanism of the process and to contrast it with random deposition. In RDSR there are three regimes characterized by different growth behaviors of the surface width [40] (see also Figure 3.2 for our simulation data). Starting form a flat substrate, a random growth, where $W^2 \approx t$, is expected in the very early time regime since the nearly flat surface produces almost no diffusion steps. After enough particles have been deposited, the relaxation processes are turned on and hence correlations between columns are built up. In this correlated regime, an evolution of the surface width,

$$W(t) \sim t^{\beta} \tag{3.4}$$

where the growth exponent $\beta \approx 1/4$ for $d = 1$, is observed. In this regime, the roughening process prevails over the relaxation and therefore the surface width is increasing. However, roughening does not dominate all the way. As the surface becomes rougher, the frequency of diffusion is higher. Eventually, these two competing mechanisms balance each other, the surface width stops increasing and the system enters the saturation regime. The surface width of saturation regime is called the saturation width W_s. One finds that the saturation width and the crossover time t_x between correlated and saturation regimes are algebraic functions of the system size,

$$\begin{aligned} W_s &\sim L^{\alpha}, \\ t_x &\sim L^{z}. \end{aligned} \tag{3.5}$$

The exponents α and z describing the size dependent properties of the saturation width

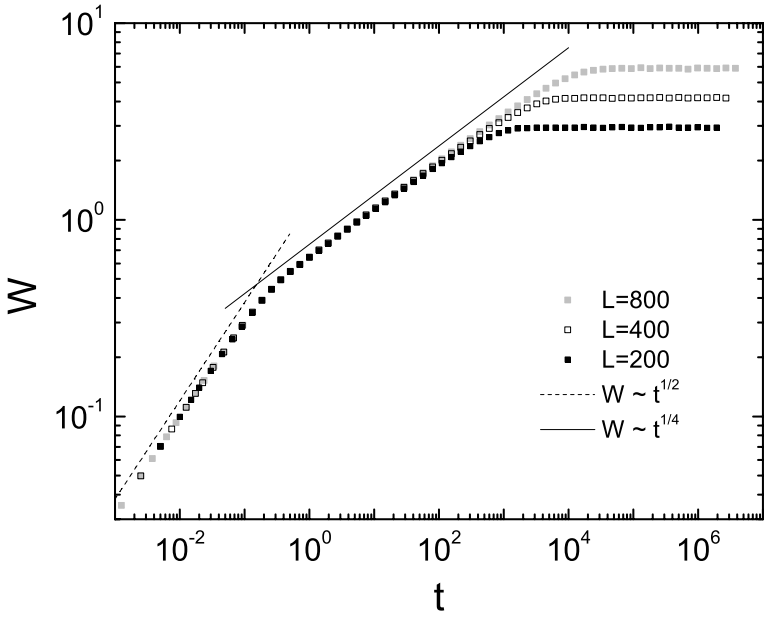

Figure 3.2: Log-log plot of the surface width vs. time for the RDSR process in systems with different sizes L. The data is averaged over 10000 realizations for each system size. The solid (dashed) line with slops 1/4 (1/2) is ploted for comparison.

and time are called roughness and dynamic exponents. It is observed that $\alpha \approx \frac{2-d}{2}$ and $z \approx 2$ by inspecting the data obtained from simulations [40]. Not all the scaling exponents are independent to each other. There exists a scaling relation

$$\alpha/\beta = z \tag{3.6}$$

which will be derived in Chapter 5. Note that a related model, where the particles can diffuse up to the lth neighbor, has also been studied [40, 33]. Results show that the scaling exponents are independent of l.

3.3 The Wolf-Villain Model

Wolf and Villain studied a discrete lattice model where the surface current is driven by the chemical potential [92]. In this model newly arrived particles hop to a site with the largest contact area. This site offers the largest binding energy and ensures that the particle is at a location where the chemical potential has a local minimum. The possible moves of the model are shown on Figure 3.1 (c). This model yields results very similar to the Family model. The system starts from random deposition described by Eq. (4.1) and then crosses over to the correlated regime before entering the saturation regime. However, the scaling exponents

are different. For $d = 1$, $\alpha \approx 3/2$, $\beta \approx 3/8$ and $z \approx 4$ are measured [92]. For $d = 2$ one has $\alpha \approx 2/3$ and $\beta \approx 1/5$ [59, 87].

3.4 The Das Sarma-Tamborenea Model

The Das Sarma-Tamborenea (DST) model (or the kink diffusion model) was introduced to simulated molecular beam epitaxy (MBE) growth, a technology for the formation of single particles by deposition [33]. In this model, each new arriving particle is assigned a probability p to hop to the nearest kink site within a diffusion distance l after having been randomly deposited. The simplest case, where $p = 1$ and $l = 1$, is very similar to the Wolf-Villain model. In this case the particle hops randomly to one of its nearest neighboring sites provided the number of contacts is increased, whereas in the WV model the particle seeks a site with largest contacts nearby. The simulation result shows $\beta \approx 3/8$ for $d = 1$ which indicates that the DST model might share the scaling exponents with the WV model [33]. However, later studies [31, 59, 87] revealed that the two models do not belong to the same universality class for $d = 2$, as here $\alpha \approx 1$ and $\beta \approx 1/4$ have been observed for the DST model [31].

3.5 Ballistic Deposition

The ballistic aggregation model was initially developed to study colloidal aggregration [90, 88]. In this model a particle is ejected from a randomly selected position and moves along a linear (ballistic) trajectory in a random direction until it collides with the growing cluster to which it sticks. The model can be modified to simulate surface deposition, and is then called ballistic deposition (BD) [69]. In ballistic deposition, instead of moving in a random direction, all particles are assumed to move parallel with each other. Although a particle moves toward the substrate, the angle of incidence is not required to be equal to zero. The early studies on incident angles and the related directions of growing columns can be found in [69, 68]. Here we stress two versions of BD where the particles fall vertically upon the substrate, namely the nearest-neighbor (NN) model and next-nearest-neighbor (NNN) model. In the NN (NNN) BD model a particle, which falls from a randomly chosen site, stays at the first site along the trajectory where its (next) nearest neighbor is occupied, as shown in figure 3.3. Therefore, the growth rules of NN and NNN BD models can be described as follows

$$h_{i,n+1} = \max\left(h_{i+1,n}, h_{i,n} + 1, h_{i-1,n}\right), \tag{3.7}$$

for NN and

$$h_{i,n+1} = \max\left(h_{i+1,n}, h_{i,n}, h_{i-1,n}\right) + 1, \tag{3.8}$$

for NNN, where $h_{i,n}$ indicates the surface height of the ith column at the nth time step. The scaling exponents found for the two models are the same, namely $\alpha \approx 1/2$ and $\beta \approx 1/3$ [69]

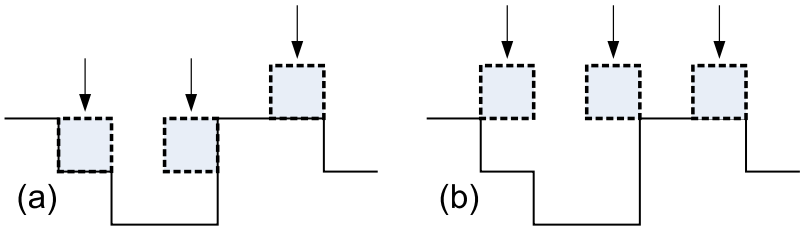

Figure 3.3: The ballistic deposition for a $(1+1)$-dimensional system where the NN model (a) and the NNN model (b) are shown. The boxes surrounded by dashed boundaries indicate incoming particles.

although the two models are different in detail. This difference of growth rules only reflects on non-universal parameters such as the growth rate [8] and the coefficient of the nonlinear term λ in the corresponding KPZ equation [61] (see Chapter 4) which is believed to belong to the same universality class as the BD model. It is found that the structure generated by this model is very similar to the one which is observed in the experiment of vapor deposition of thin films. One similarity between this model and vapor deposition is that the particles are not allowed to relax [7].

3.6 The Restricted Solid on Solid Model

The solid on solid (SOS) model is the collective name for growth models where the deposited particles can only fall on top of already existing particles. Therefore, overhangs and vacancies are not allowed. The restricted solid on solid (RSOS) model proposed by Kim et. al. further confines the maximum local slope. In their model, a particle is added to a randomly chosen site provided that the differences of surface heights between any two adjacent columns are restricted such that $|\Delta h| \leq S$ at every stage [56]. The integer S sets the absolute value of maximum local slope for this model. This model has very good scaling properties over a large range of substrate dimensions d. It has been verified numerically that $\beta = 1/(d+2)$ and $\alpha = 1/(d+3)$ up to $d = 4$ which leads to a dimensional independent relation $\alpha + z = 2$. The integer S does not affect the scaling exponents, but shifts the first crossover time to larger values for larger values of S [22] (see also our simulation results in Figure 3.5 (a)). The relation between the first crossover point and the value S is

$$W_1^2 = t_1 \propto S^2. \tag{3.9}$$

The model can be generalized such that the maximum height difference becomes a non-integer number by the following procedure. For any non-integer value S, we split the number into an integer I and a decimal D,

$$S = I + D, \tag{3.10}$$

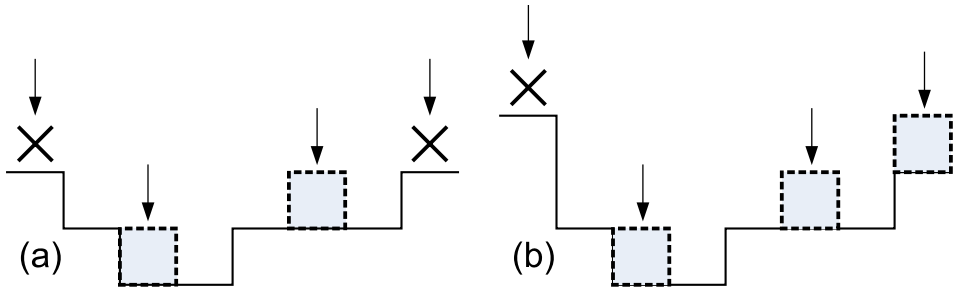

Figure 3.4: The restricted solid on solid model for a $(1+1)$-dimensional system. The boxes surrounded by dashed boundaries indicate incoming particles. The crosses indicate where the depositions are not allowed. Here we show two cases with different values of S: (a) $S = 1$ and (b) $S = 2$.

where $I = \text{Floor}(S)$ is the largest integral value that is not greater than S. By using the equality

$$S = I(1 - D) + (I + 1)D, \tag{3.11}$$

we define a mixture of two RSOS processes where the one with restricted height difference I takes place with probability $(1 - D)$ and the other with $I + 1$ occurs with probability D. The average value of the restricted height difference for this generalized model is therefore a positive non-integer number S.

3.7 Competitive Growth Models

In recent years the study of non-equilibrium growth systems has shifted to more complex cases as for example competitive growth models, see e.g. [33, 51, 48, 21, 49, 57, 75, 13, 53, 50, 1, 79, 58]. In a competitive growth model one considers a mixture of two different deposition processes where one of them takes place with probability p whereas the other takes place with probability $1 - p$. One example is the RD/RDSR model [51] where the deposition happens according to the RDSR rules with probability p and to the RD rules with probability $1 - p$. Whereas for $p = 1$ and $p = 0$ only one of the processes is realized, for general values of p the mixture of the two processes leads to a crossover between the two regimes where the crossover time and width depend on the value of p. Our simulation results for the RD/RDSR model for two different system sizes with various values of p are shown in Figure 3.6.

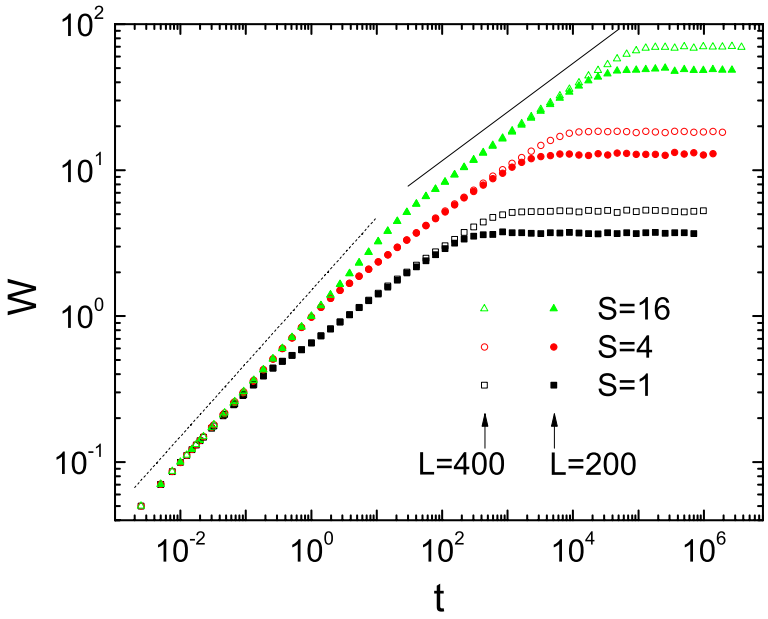

Figure 3.5: Log-log plot of the surface width vs. time for the RSOS process in systems with different sizes L and different restricted heights S. The data is averaged over 1000 realizations for each system size and restricted height. The solid (dashed) line with slops 1/4 (1/3) is plotted for comparison.

3.8 The Arrhenius Diffusion Model

In molecular-beam-epitaxy growth the incoming atoms are dropped with a deposition rate R_D. The atoms on the surface diffuse continuously following the Arrhenius law [26, 33, 65, 52, 89, 80]. Each surface atom has a probability $R = (2k_BT/h)e^{-E_A/(k_BT)}$ to surmount the energy barrier, where E_A is the activation energy, whereas k_B and h are the Boltzmann and the Planck constants respectively. The activation energy is usually given by $E_A = E_0 + nE_B$, where E_0 is the diffusion barrier for a free atom, E_B is the binding energy per bond, and n is the number of nearest neighbors.[1] After activation, atoms are free to hop to one of its nearest-neighbor sites, provided that the newly selected site is not higher than the original one. The Arrhenius law allows deposited atoms to hop, with the exception of those that are fully surrounded by others atoms. The diffusion rate vanishes at zero temperature and monotonically increases when the temperature increases. Therefore, one can expect to have the growth exponent $\beta = 1/2$ when $T \to 0$, since random deposition is the only active process. On the contrary, at high temperature the diffusion process is highly active, the surface atoms can travel distances long enough to find a local minimum where the hopping stops. Therefore, the surface becomes smoother at higher temperatures. This kind of temperature effect has been studied systematically for $1+1$ dimensional systems [89]. The

[1]The parameters are chosen to be $E_0 = 0.3$ eV and $E_B = 1$ eV for Si and GaAs systems [33].

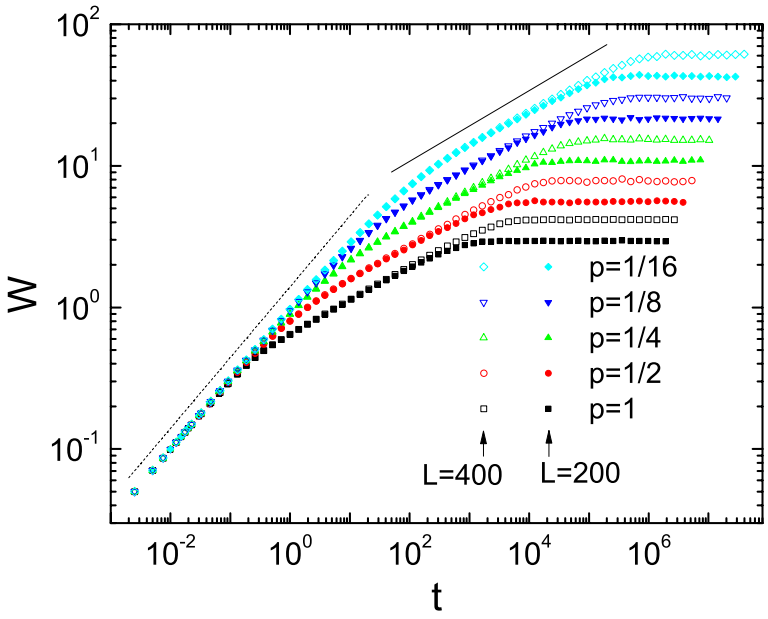

Figure 3.6: Log-log plot of the surface width vs. time for the RD/RDSR process in systems with different sizes L and different probabilities p. The data is averaged over 1000 realizations for the cases where $p \leq 1/2$. The data for $p = 1$ are the same data as shown in Figure 3.2. The solid (dashed) line with slops 1/4 (1/2) is plotted for comparison.

RD regime in the low temperature limit and the smoothing regime at high temperatures are indeed revealed in simulations. More interestingly, a regime with $\beta \approx 3/8$ is observed at intermediate temperatures. One can also directly look at how the ratio R/R_D changes the properties of the surface. In this aspect, the regime with $\beta \approx 3/8$ is found around $R/R_D \approx 1$ where we have one diffusion per deposition [33, 89]. This provides evidence that at intermediate temperatures the one-dimensional Arrhenius diffusion model belongs to the same universality class as the WV and DST models.

3.9 The Siegert-Plischke Model

In the Siegert-Plischke model [86], a Hamiltonian

$$H = \sum_{\langle i,j \rangle} \left[g_2 (h_i - h_j)^2 + g_4 (h_i - h_j)^4 + g_6 (h_i - h_j)^6 \right] \tag{3.12}$$

is assigned to a surface configuration $\{h_i\}$, where $\langle i, j \rangle$ denotes a summation over the nearest-neighbor pairs. In the surface evolution process, a site is chosen randomly for either depositing a new particle or hopping of a surface particle to one of its neighboring sites. The rate for deposition and diffusion are τ and $1 - \tau$, respectively. Therefore, the surface evolution

recovers the random deposition for $\tau = 1$, and a diffusion process with conserved number of particles for $\tau = 0$. If the diffusion is selected, the direction of move is chosen randomly and the acceptance probability for the hopping of the particle is given by $P_{i\to j} = 1/(1+e^{\Delta H/k_B T})$, where ΔH is the change of the surface energy.

3.10 The Modified RDSR process

In the following we briefly discuss the behavior of a simple deposition model that turns out to be an excellent representative of the Edwards-Wilkinson (EW) universality class (see Chapter 4 for exact result for the Edwards-Wilkinson equation). (This section is based on material published in [23]). This model is then used to motivate the different protocols discussed in Chapter 6 for measuring the global response. Our deposition model is based on Family's original random deposition with surface relaxation (RDSR) process [40] and differs from this model by the diffusion step. In the RDSR process a particle deposited on the surface is allowed to jump to one of the neighboring sites if this site has a lower height than the site of deposition. In our model we assign an energy $E_i(t) = g\, h_i(t)$ to the column at site i where $h_i(t)$ is the height of that column at time t. The constant g can be thought of as the gravitation constant, for example. Starting from an initially flat substrate, particles of mass one are deposited on randomly chosen sites and then allowed to diffuse locally after deposition. For a diffusion step taking place at time t, we select one of the neighboring sites j at random and accept the jump with the temperature and time dependent (Metropolis like) probability

$$P_{i\to j}(T,t) = \begin{cases} 1 \quad \text{if} \;\; E_j(t) \le E_i(t) \\ e^{-[E_j(t)-E_i(t)]/k_B T} = e^{-g[h_j(t)-h_i(t)]/k_B T} \\ \qquad\qquad\qquad\qquad \text{if} \;\; E_j(t) > E_i(t) \end{cases} . \tag{3.13}$$

In the following we choose units thus that the Boltzmann constant $k_B = 1$. In contrast to the original model there is a non-vanishing probability that a deposited particle jumps to a neighboring site with a higher height than the deposition site. We assume this jump to be thermally activated and to depend on T (the temperature of the substrate). As we discuss in the following, the ratio T/g is a parameter that governs the morphology of the growing interface and allows us to study the response of the surface to a change in external conditions.

It is instructive to look at the behavior of the model in the limits of $T \to 0$ and $T \to \infty$. At zero temperature no jumps to sites with higher height are allowed, and the particle is incorporated into the aggregate at the selected neighboring site if the column at that site is shorter than at the initial site. Thus, for $T \to 0$ we recover the RDSR process [40]. In the opposite limit, $T \to \infty$, however, a particle will always jump to the selected neighboring column, irrespective of the height difference. As a result, the different columns will grow independently, yielding an uncorrelated surface as for the RD process. For intermediate

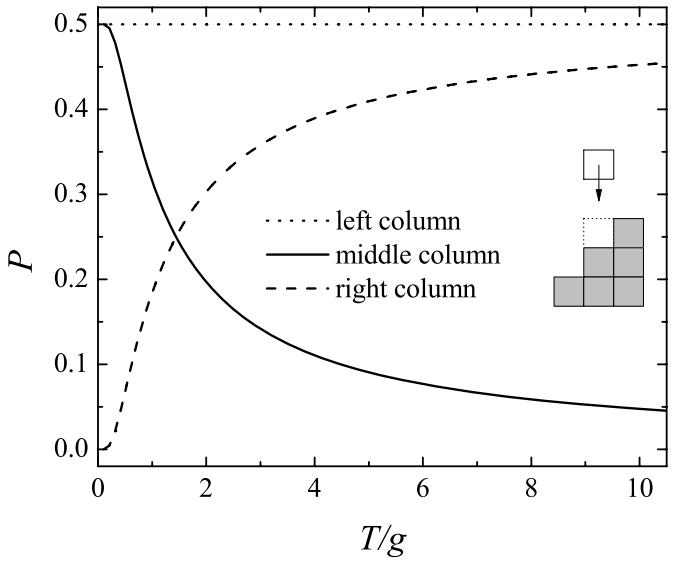

Figure 3.7: Probabilities that for the shown configuration the particle, initially deposited on top of the middle column, comes to rest on top of one of the three columns. *J. Stat. Mech.* P08007. Used with permission of IOP Publishing Ltd and SISSA, 2010.

temperatures, a crossover between the RD and the RDSR processes is observed, with the crossover point depending on the temperature.

The temperature dependence of the model is illustrated in Figure 3.7. Suppose a particle is deposited on top of the middle column in the configuration shown, the plot provides the T/g dependence of the probabilities for having this particle end up at one of the three sites. In the original Family model the particle would always come to rest on top of the left column.

Of course, temperature has been introduced in theoretical studies of growth processes prior to our work (see [32, 70, 10, 63, 38] for some examples). For a typical microscopic model studied in this context one often assumes that the atom's hopping follows an Arrhenius-like rate that is proportional to e^{-E_n/k_BT}, where the activation energy E_n is itself proportional to the number of bonds formed by the atom before the hopping attempt. Whereas this is surely a rather realistic modeling of diffusion processes on a crystal surface, we have opted here for a simpler approach where the probability for a particle to hop depends on the height difference between the actual site and the proposed new site. (Note that jumps to sites with higher heights have also been allowed in other microscopic growth models [32, 44]). As we will show in the following, all aspects of our simple model agree perfectly with the solution of the stochastic Edwards-Wilkinson equation with a *single* fit parameter.

In the following we are interested in the dependence of the surface width W on time t, on the ratio T/g, and on system size L (in this section we only discuss the one-dimensional case). In our simulations, we have a wide range of T/g values and several L's up to 1000. For simplicity, we always start from a flat surface, i.e. $W = 0$ for $t = 0$. For the data discussed

below, the unit of t is one Monte Carlo Step (i.e., L particles deposited) and we averaged over 1000 independent runs with different random numbers.

In Figure 3.8a,c we show the time dependence of the surface width for, respectively, the case with fixed $L = 1000$ at different T/g's and the case with a fixed $T/g = 1$ and various L's. As for the RDSR process one distinguishes three regimes separated by two crossover points: a random deposition (RD) regime, followed by a EW regime, with a final crossover to the saturation regime. In contrast to Family's original model, the initial RD process is not confined to very early times $t \leq 1$ but extends to larger times. In fact, the crossover time t_1 between the RD and the EW regimes is shifted to higher values for increasing temperatures and diverges in the limit of infinite temperatures. As the crossover is smeared out, we identify the crossover point with the intersection point of the straight lines fitted to the two linear regimes in the log-log plots. Due to the nature of the uncorrelated deposition of particles (Poisson process), we have the identity $W^2 = t$ in the RD regime, yielding the width $W_1 = \sqrt{t_1}$ at the crossover point. In the EW regime the relation between width and deposition time changes to $W \propto t^{1/4}$. This regime extends up to a second crossover point (t_2, W_2), whose precise location also depends on the value of T and beyond which the final saturation regime prevails. The crossover between the different regimes is further illustrated in Fig. 3.8b,d where we show the time evolution of the effective exponent

$$\beta_{eff} = \frac{d \ln W}{d \ln t} \tag{3.14}$$

for the two cases. The evolution of the width shown in Fig. 3.8 is very reminiscent of the behavior encountered in competitive growth models. In both cases two different scaling regimes are found whose ranges depend on a system parameter. In the MRDSR model, the ratio T/g plays the role of the quantity p, the main difference being that we do not artificially choose between the different processes, as in our system the competition is intrinsic and governed by the value of the temperature.

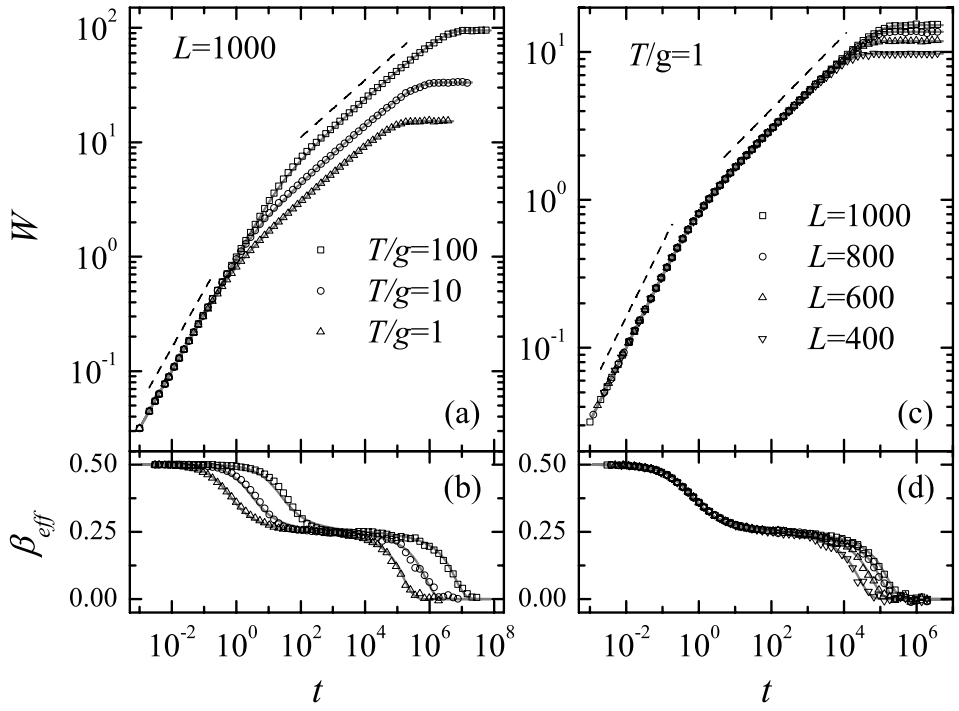

Figure 3.8: (a) Log-log plot of the surface width vs time for a system of size $L = 1000$ and different temperatures. The dashed lines have the slopes 1/2 and 1/4 expected in the random deposition and EW regimes, respectively. The location of both crossover points depend on temperature. The full lines are obtained from fitting the exact solution of the EW stochastic equation. Here and in the following error bars are smaller than the symbol sizes. (b) Time evolution of the effective exponent (3.14) for the data shown in (a). (c) Log-log plot of the surface width vs time for systems of different sizes evolving at the same temperature $T = 1$. (d) Time evolution of the effective exponent (3.14) for the data shown in (c). The full lines are derived from the fits to the exact solution of the EW stochastic equation (see Section 4.1.3 below). *J. Stat. Mech.* (2010) P08007. Used with permission of IOP Publishing Ltd and SISSA, 2010.

Chapter 4

Langevin Equations for Surface Growth Processes

In addition to the investigation of microscopic models, the study of coarse-grained continuum equations of motion provides another way to investigate the evolution of surfaces. In this chapter we will discuss two linear Langevin equations, namely the Edwards-Wilkinson [37] and Mullins-Herring [74] equations, and a nonlinear Langevin equation, namely the Kardar-Parisi-Zhang equation [55]. These are the fundamental equations in the field of surface growth. The linear Langevin equations can be solved analytically. We will then use these exact results to study the surface width. The evolution of the surface width has three regimes which are controlled by a length scale l. Following that, we will compare the result of the Edwards-Wilkinson equation with the MRDSR process. For the nonlinear equation there is no simple analytical method that can be used to derive the exact solution. Therefore, we will introduce various numerical integration methods.

4.1 Linear Langevin equations - The Edwards-Wilkinson and Mullins-Herring equations

The surface motion under the influence of random fluctuations can be described by the stochastic equation

$$\frac{\partial h(\mathbf{x},t)}{\partial t} = \eta(\mathbf{x},t). \tag{4.1}$$

where $h(\mathbf{x},t)$ is the surface height measured in the reference frame moving with the mean height and $\eta(\mathbf{x},t)$ is uncorrelated noise with zero average,

$$\begin{aligned} \langle \eta(\mathbf{x},t) \rangle &= 0, \\ \langle \eta(\mathbf{x},t)\eta(\mathbf{x}',t') \rangle &= D\delta^d(\mathbf{x}-\mathbf{x}')\delta(t-t'). \end{aligned} \tag{4.2}$$

By integrating equation (4.1) and then calculating the average of h and h^2 using equation (4.2), it is easy to show that

$$W^2(t) = \langle h(\mathbf{x},t)^2\rangle - \langle h(\mathbf{x},t)\rangle^2 = Dt. \tag{4.3}$$

Comparing with Eq. (3.3) derived from the lattice model described in Chapter 3, we have $D = 1$. The equation for surface growth with relaxation can be derived from the continuity equation

$$\frac{\partial h(\mathbf{x},t)}{\partial t} = -\nabla\cdot\mathbf{j}(\mathbf{x},t) + \eta(\mathbf{x},t), \tag{4.4}$$

where $\mathbf{j}(\mathbf{x},\mathbf{t})$ is the surface current. If the surface current is driven by the gravitational potential, the current is proportional to the surface height gradient:

$$\mathbf{j} = -\nu\nabla h. \tag{4.5}$$

The negative sign indicates a downhill current and the proportional constant ν is usually called the surface tension or diffusion constant. If, instead, the surface current is driven by the chemical potential difference, one has

$$\mathbf{j} = -K\nabla\mu \tag{4.6}$$

Since the chemical potential (or binding energy) is proportional to the contact area, it is also proportional to the negative of the surface curvature, $\mu \propto -\nabla^2 h(\mathbf{x},t)$. Plugging the surface current Eq. (4.5) into the continuity equation Eq. (4.4) yields the Edwards-Wilkinson (EW) equation [37],

$$\frac{\partial h(\mathbf{x},t)}{\partial t} = \nu\nabla^2 h(\mathbf{x},t) + \eta(\mathbf{x},t). \tag{4.7}$$

On the other hand, the surface current Eq. (4.6) generates the noisy Mullins-Herring (MH) equation [74],

$$\frac{\partial h(\mathbf{x},t)}{\partial t} = -K\nabla^4 h(\mathbf{x},t) + \eta(\mathbf{x},t). \tag{4.8}$$

The two equations Eqs. (4.7) and (4.8) can be summarized by the equation

$$\frac{\partial h(\mathbf{x},t)}{\partial t} = -\nu(i\nabla)^m h(\mathbf{x},t) + \eta(\mathbf{x},t), \tag{4.9}$$

where m is an even number. For $m = 2$ we recover the EW equation and for $m = 4$ we obtain the MH equation. We will show that the dynamical exponent z is equal to m later. Writing both the height $h(\mathbf{x},t)$ and the noise $\eta(\mathbf{x},t)$ as Fourier transformations

$$\begin{aligned} h(\mathbf{x},t) &= \sum_{\mathbf{q}} h_{\mathbf{q}}(t)\exp(i\mathbf{q}\cdot\mathbf{x}), \\ \eta(\mathbf{x},t) &= \sum_{\mathbf{q}} \eta_{\mathbf{q}}(t)\exp(i\mathbf{q}\cdot\mathbf{x}), \end{aligned} \tag{4.10}$$

where $\mathbf{q}$ runs over all the reciprocal lattice vectors, equations (4.9) and (4.2) become

$$\frac{\partial h_{\mathbf{q}}}{\partial t} = -\nu \mathbf{q}^m h_{\mathbf{q}} + \eta_{\mathbf{q}} \tag{4.11}$$

and

$$\langle \eta_{\mathbf{q}}(t)\eta_{\mathbf{q}'}(t')\rangle = DL^{-d}\delta^d_{\mathbf{q}+\mathbf{q}'}\delta(t-t'). \tag{4.12}$$

The general solution of (4.11) is readily obtained to be

$$h_{\mathbf{q}}(t) = \exp(-\nu\mathbf{q}^m t)h_{\mathbf{q}}(0) + \int_0^t d\tau \exp\left(-\nu\mathbf{q}^m(t-\tau)\right)\eta_{\mathbf{q}}(\tau). \tag{4.13}$$

Assuming an initially flat surface, $h_{\mathbf{q}}(0) = 0$ for every $\mathbf{q}$, one obtains the following two-point correlation function of the surface height in $\mathbf{q}$-space:

$$\langle h_{\mathbf{q}_1}(t_1)h_{\mathbf{q}_2}(t_2)\rangle = \frac{D}{L^d\nu}e^{-\nu(q_1^m t_1 + q_2^m t_2)}\frac{1}{q_1^m + q_2^m}\left(e^{\nu(q_1^m+q_2^m)t_<} - 1\right)\delta^d_{\mathbf{q}_1+\mathbf{q}_2}, \tag{4.14}$$

where $q_i = |\mathbf{q}_i|$ and $t_<$ is the smaller of the times t_1 and t_2. This well-known result will be useful in the following. The square of the surface width, which is evaluated by averaging over the area of substrate for a given system, can also be evaluated by averaging over many repetition of the process for a fixed position. By taking both averages, the square of the surface width (3.1) can be written in terms of the Fourier components of the height as

$$\left\langle W^2(t)\right\rangle = \left\langle \frac{1}{L^d}\sum_{\mathbf{x}}\left(\sum_{\mathbf{q}\neq 0} h_{\mathbf{q}}(t)\exp\left(i\mathbf{q}\cdot\mathbf{x}\right)\right)^2\right\rangle, \tag{4.15}$$

where we took into account that the average height of the surface is equal to the zero mode of the surface height. Plugging Eq.(4.14) into Eq.(4.15) one has

$$\left\langle W^2(t)\right\rangle = \frac{D}{2\nu L^d}\sum_{\mathbf{q}\neq 0}\frac{1}{\mathbf{q}^m}\left(1 - e^{-2\nu t\mathbf{q}^m}\right). \tag{4.16}$$

4.1.1 Asymptotic behavior

The behavior of the surface width is controlled by the length scale $l \equiv (2\nu t)^{1/m}$. If $l < 1/q_{max}$, we have $(l\mathbf{q})^m < 1$ for all $\mathbf{q}$. One then can simply expand the function inside the parentheses into power series and sum over the leading terms to approximate the summation,

$$\left\langle W^2(t)\right\rangle \approx \frac{Dl^m}{2\nu L^d}\sum_{\mathbf{q}\neq 0}\left\{1 - \frac{1}{2}(l\mathbf{q})^m + \mathcal{O}\left[(l\mathbf{q})^{2m}\right]\right\} \approx Dt, \tag{4.17}$$

where $\sum_{\mathbf{q}\neq 0} 1 = L^d$ has been applied in the second step. This result shows that the random deposition in the early time regime of the surface evolution is a common property of the

linear Langevin equations (4.9) for the possible combinations of d and m. If, on the contrary, $l \gg 1/q_{min}$, we have $\exp\left[-(l\mathbf{q})^m\right] \ll 0$ for all $\mathbf{q}$, and one can drop all the exponential terms in Eq. (4.16). The summation yields a t-independent value which is the so called saturation width,

$$\left\langle W_s^2 \right\rangle \approx \frac{D}{2\nu L^d} \sum_{\mathbf{q}\neq 0} \frac{1}{\mathbf{q}^m}. \tag{4.18}$$

The summation in Eq. (4.18) is L-dependent since $\mathbf{q}$ and the number of terms which is summed over are both functions of L. To examine the L-dependence of saturation width, we replace $\mathbf{q}$ by $\frac{2\pi}{L}\mathbf{n}$, where $\mathbf{n} = \sum_{i=1}^{d} n_i \hat{e}_i$, to obtain

$$\left\langle W_s^2 \right\rangle \approx \frac{DL^{m-d}}{2^{m+1}\pi^m \nu} \sum_{\mathbf{n}\neq 0} \frac{1}{\mathbf{n}^m}. \tag{4.19}$$

For a one-dimensional system, the summation can be replaced by the Riemann zeta function $\zeta(m)$, provided that the system is large enough. In general, the summation is proportional to the integral $\Omega_d \int_1^{L/2} n^{d-m-1} dn$, where $\Omega_d = 2\pi^{d/2}/\Gamma(d/2)$ is the solid angle of a d-dimensional sphere.[1] In the large L limit, this integral is approximately given by $\Omega_d \frac{1}{m-d}$ for $d < m$ and $\Omega_d \ln(L/2)$ for $d = m$. Therefore, one has

$$\left\langle W_s^2 \right\rangle \sim \frac{D\Omega_d}{2^{m+1}\pi^m \nu} \begin{cases} \frac{1}{m-d} L^{m-d} & \text{if } d < m \\ \ln(L/2) & \text{if } d = m \end{cases}. \tag{4.20}$$

The roughness exponent, $\alpha = \frac{m-d}{2}$, for $d < m$, then follows immediately.[2] For $1/q_{max} < l < 1/q_{min}$, every single term in the summation can have a significant contribution for a certain range of l. One can replace the sum by an integral to capture the t-dependent behavior of the summation. By assuming that $k \equiv (lq)^m$, one has

$$\left\langle W^2(t) \right\rangle \sim \frac{D\Omega_d l^{m-d}}{2\nu(2\pi)^d m} \int_{(2\pi l/L)^m}^{(\pi l)^m} k^{d/m-2} \left(1 - e^{-k}\right) dk. \tag{4.21}$$

Since the integrand has two limiting behaviors on the two sides of $k = 1$, we can split it into two parts plus a correction term as

$$\int_a^b k^s (1 - e^{-k}) dk = \int_a^1 k^{s+1} dk + \int_1^b k^s dk - \mathcal{C}, \tag{4.22}$$

provided that $a \ll 1$ and $b \gg 1$. The correction $\mathcal{C}$, which is the area between the original curve, $f(k) = k^s(1 - e^{-k})$, and the combinational curve, $g(k) = k^{s+1}$ for $k \leq 1$ and $g(k) = k^s$ for $k > 1$, should not sensitively depend on a and b since it is subjected to $a \ll 1$ and $b \gg 1$. The illustration of the integral is shown in Figure 4.1. After some simplification, we have

[1] The summation approximates the integral in the continuum limit.

[2] The roughness exponent defined in Eq. (3.5) gives the L dependence of saturation width W_s which stands for $\langle W_s \rangle$ generally. Here we derive the exponent from $\left\langle W^2 \right\rangle$. This is valid as long as the variance of the surface width $\sigma \equiv \left\langle W^2 \right\rangle - \langle W \rangle^2$ is much smaller than $\left\langle W^2 \right\rangle$. In this case we have $\langle W \rangle \approx \sqrt{\langle W^2 \rangle}$ and all the definitions related to $\langle W \rangle$ apply to $\sqrt{\langle W^2 \rangle}$. We will sometimes write W^2 for $\left\langle W^2 \right\rangle$.

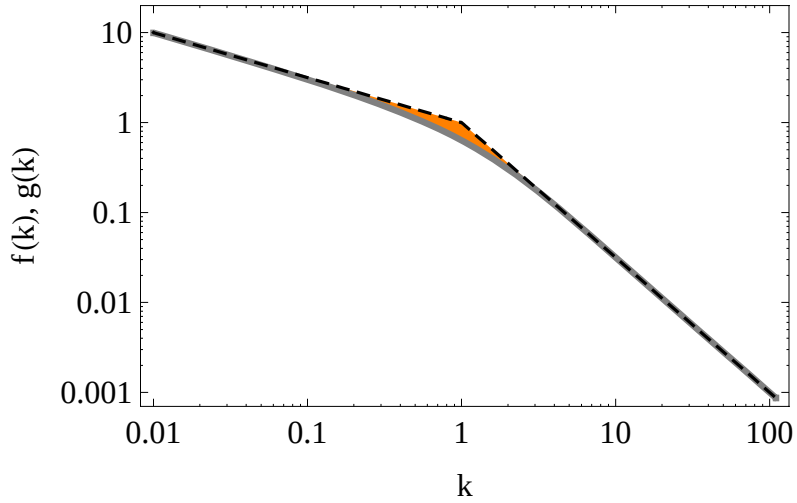

Figure 4.1: The illustration of the integral Eq. (4.22). The functions $f(k)$ and $g(k)$ are shown as the gray solid curve and the black dashed line, respectively. The constant $\mathcal{C}$ is indicated by the area marked with orange color. The value of the parameter s is chosen to be $-3/2$ for this plot.

$$\left\langle W^2(t) \right\rangle \sim \frac{D\Omega_d}{2\nu(2\pi)^d} \begin{cases} \frac{m}{(m-d)d}(2\nu t)^{1-d/m} & \text{if } d < m \\ \frac{1}{m}\ln(2\nu t) & \text{if } d = m \end{cases} . \tag{4.23}$$

The result for $d < m$ gives the growth exponent $\beta = \frac{m-d}{2m}$. Applying the relation among scaling exponents, $z = \alpha/\beta$, one has that the dynamic exponent $z = m$.

4.1.2 Crossover points

We can also roughly estimate the crossover points by making use of the fact that the three regimes are separated by two crossover points around $l_1 \sim 1/q_{max}$ and $l_2 \sim 1/q_{min}$, where $l_i \equiv (2\nu t_i)^{1/m}$ with $i = 1$ and 2. The q_{max} and q_{min} are the largest and shortest radii of hyperspheres inside the first Brillouin zone of the reciprocal lattice, and have the values $q_{max} = \pi\sqrt{d}$ and $q_{min} = 2\pi/L$. Therefore, one immediately has the two crossover times as

$$\begin{aligned} t_1 &\sim \frac{1}{2\nu}\left(\frac{1}{\pi\sqrt{d}}\right)^m , \\ t_2 &\sim \frac{1}{2\nu}\left(\frac{L}{2\pi}\right)^m . \end{aligned} \tag{4.24}$$

and the ratio

$$\frac{t_2}{t_1} \sim \left(\frac{\sqrt{d}}{2}L\right)^m . \tag{4.25}$$

We apply the definition of the growth exponent Eq. (3.4), which indicates the slope of correlated growth in the $\log(t)$-$\log(W)$ plane, to arrive at

$$\log\left(\frac{W_2}{W_1}\right) = \beta \log\left(\frac{t_2}{t_1}\right). \tag{4.26}$$

This gives us

$$\frac{W_2}{W_1} \sim \left(\frac{\sqrt{d}}{2}L\right)^{\frac{m-d}{2}}. \tag{4.27}$$

We further use the approximation Eq. (4.17) to estimate the two crossover widths

$$\begin{aligned} W_1 &\sim \frac{1}{\sqrt{2\nu}}\left(\frac{1}{\pi\sqrt{d}}\right)^{m/2}, \\ W_2 &\sim \frac{1}{\sqrt{2\nu}}\left(\frac{1}{\pi\sqrt{d}}\right)^{m/2}\left(\sqrt{\frac{d}{2}}L\right)^{\frac{m-d}{2}}. \end{aligned} \tag{4.28}$$

As expected, the saturation width is a power function of the system size L. Basically, the transition between the two regimes is not sharp. Therefore, it is more appropriate to use crossover regions instead of crossover points. For this reason, people sometimes use the intersection between two straight lines (in the log-log plot) to determine the crossover points. We can also use this concept to estimate the crossovers (the calculation shown here is published in [25]). We first compute the first crossover time t_1 in the limit of infinite L for the 1D EW equation (see also [3]). Since this point is defined as the intersection of the RD regime ($W^2 = t$) and the EW regime ($W^2 \cong At^{1/2}$), we have

$$t_1 = A^2 \tag{4.29}$$

so that the problem reduces to finding the amplitude A associated with EW growth. For $L \to \infty$, the sum in expression (4.16) can be replaced by an integral, which can be computed to extract A. Further simplification occurs if we consider $\partial_t W^2 = \int_{-\pi}^{\pi} e^{-2\nu t\theta^2} d\theta/2\pi$. Imposing the ansatz $W^2 \cong At^{1/2}$, we arrive at

$$At^{-1/2} \cong \frac{1}{\pi}\int_{-\pi}^{\pi} e^{-2\nu t\theta^2} d\theta. \tag{4.30}$$

Transforming to $\xi \equiv \sqrt{2\nu t}\theta$, we have

$$A \cong \frac{1}{\sqrt{2\nu}\pi}\int_{-\pi\sqrt{2\nu t}}^{\pi\sqrt{2\nu t}} e^{-\xi^2} d\xi \frac{1}{\sqrt{2\pi\nu}}. \tag{4.31}$$

So, as $t \to \infty$ (or, to be precise, $L \gg t \gg \nu^{-1}$), we arrive at $W^2(t) = At^{1/2}$ as well as

$$t_1 = A^2 = \frac{1}{2\pi\nu}. \tag{4.32}$$

T/g	0.1	1	10	100
ν	0.2300	0.1768	0.0379	0.0046

Table 4.1: Values for the surface tension ν at different values of T/g that result from a fit of the numerical data of MRDSR to the exact solution of the Edwards-Wilkinson equation.

Of course, this approach can also be used to extract t_2. Equating this W^2 (i.e., $At^{1/2}$) to the saturation W^2 (i.e., $(L/8\pi^2\nu)\sum_n n^{-2} = L/24\nu$), we arrive at

$$t_2 = \left(\frac{L}{24\nu A}\right)^2 = \frac{\pi}{288\nu}L^2 \ .$$

This provides

$$\frac{t_2}{t_1} = \left(\frac{\pi L}{12}\right)^2 , \tag{4.33}$$

which is very close to the result derived in Eq. (4.25).

4.1.3 The Modified RDSR and the Edwards-Wilkinson equation

Next, we turn our attention to the comparison of the MRDSR model and the EW equation (4.7) (for the one-dimensional case). In the expression (4.16), we must fix $D = 1$ in order to agree with $W^2 = t$ in the RD regime. This leaves us with just one free parameter, namely, $\nu\,(T/g)$, which can be obtained by fitting the numerical data to the theoretical expression, see Table 4.1. The result of this procedure can be summarized by

$$\nu = \frac{1}{a + b\,T/g} \tag{4.34}$$

with $a = 4.23$ and $b = 2.13$. As the solid lines in Figure 3.8 show, excellent fits are achieved with these values of ν. Clearly, the theoretical curves are in very good agreement with the data over the entire range of L's and T/g's explored. Note in addition that it is possible to collapse *all* data onto a single curve [24] (see also Chapter 5). It is worth mentioning that a $1/T$ dependence of the surface tension ν is typically encountered in experiments on step fluctuations [9, 34, 35, 12] or on surface smoothing [78] which are described theoretically by linear Langevin equations. This section is published in [23].

4.2 Non-linear Langevin Equation - The Kardar-Parisi-Zhang equation

The first attempt to introduce a nonlinear Langevin equation for surface growth was made by Kardar, Parisi and Zhang [55] in 1986. They added the simplest nonlinear term $(\nabla h)^2$ to

the Edwards-Wilkinson equation and arrived at an equation, which is now called the KPZ equation,

$$\frac{\partial h(\mathbf{x},t)}{\partial t} = \nu\nabla^2 h(\mathbf{x},t) + \lambda\left(\nabla h(\mathbf{x},t)\right)^2 + \eta(\mathbf{x},t). \tag{4.35}$$

As they explained, the nonlinear term results from the leading order behavior of the local growth which is in the direction perpendicular to the surface. On the one hand, the KPZ equation can be mapped to the Burgers equation, which describes the velocity field $\mathbf{v}$ of a vorticity-free fluid with a randomly stirring force $\nabla\eta$,

$$\frac{\partial \mathbf{v}}{\partial t} + \lambda\mathbf{v}\cdot\nabla\mathbf{v} = \nu\nabla^2\mathbf{v} - \nabla\eta \tag{4.36}$$

by the transformation $\mathbf{v} = -\nabla h$. Replacing $\mathbf{v}$ by $-\nabla h$, we have $\lambda\mathbf{v}\cdot\nabla\mathbf{v} = \nabla(\nabla h)^2$ which yields the nonlinear term in the KPZ equation. On the other hand, by applying the Hopf-Cole transformation $h = (\nu/\lambda)\ln(\phi)$, the KPZ equation can be mapped to the equation of the restricted partition function ϕ for a directed polymer in a medium with quenched impurities η,

$$\frac{\partial \phi(\mathbf{x},t)}{\partial t} = \nu\nabla^2\phi(\mathbf{x},t) + \frac{\lambda}{\nu}\phi(\mathbf{x},t)\eta(\mathbf{x},t). \tag{4.37}$$

The advantage of this equation is that the nonlinear term disappears. However, the multiplication of the noise and the field still prohibits a simple analysis. By rescaling the surface height and time as $h' = (\lambda/D)^{1/3}h$ and $t' = (D\lambda^2)^{1/3}t$, one can rewrite the KPZ equation as

$$\frac{\partial h'(\mathbf{x},t')}{\partial t'} = \frac{\nu}{(D\lambda^2)^{1/3}}\nabla^2 h'(\mathbf{x},t') + \left(\nabla h'(\mathbf{x},t')\right)^2 + \zeta(\mathbf{x},t'), \tag{4.38}$$

where we have $\langle\zeta(\mathbf{x}_1,t_1')\zeta(\mathbf{x}_2,t_2')\rangle = \delta^d(\mathbf{x}_1-\mathbf{x}_2)\delta(t_1'-t_2')$.[3] This equation shows that the KPZ equation has one effective parameter $\nu' \equiv \nu/(D\lambda^2)^{1/3}$. Systems which have the same value of ν' can be therefore rescaled and described by the same equation. In $1+1$ dimensional systems, the scaling exponents derived by Kardar, Parisi, and Zhang are exactly $\alpha = 1/2$ and $z = 3/2$. One can associate with the KPZ equation a Fokker-Planck equation [45]

$$\frac{\partial P[h(x),t]}{\partial t} = -\int d\mathbf{x}\frac{\delta}{\delta h}\left\{\left[\nu\nabla^2 h + \lambda(\nabla h)^2\right]P\right\} + \frac{D}{2}\int d\mathbf{x}\frac{\delta^2 P}{\delta h^2}\ , \tag{4.39}$$

where $P[h(x),t]$ is a time dependent probability functional of the surface height. It is well known that there exists a steady state solution

$$P_s[h(x),t] = \exp\left[-\frac{\nu}{D}\int dx\left(\nabla h\right)^2\right] \tag{4.40}$$

for $1+1$ dimensional systems.[4] The fact that the solution is also the steady-state solution for the EW equation indicates that the nonlinear term does not affect the evolution after the

[3] One can also rewrite the KPZ equation as $\partial h'/\partial t' = \nabla^2 h' + (\nabla h')^2 + \epsilon\zeta$ if one rescales the variables $h' = (\lambda/\nu)h$, $t' = \nu t$ and $\epsilon' = (D/\nu^3)^{1/2}\lambda$, or as $\partial h'/\partial t' = \nabla^2 h' + \lambda'(\nabla h')^2 + \zeta$ if $h' = (\nu/D)^{1/2}h$, $t' = \nu t$ and $\lambda' = (D/\nu^3)^{1/2}\lambda$ is used, see [20, 2].

[4] For Burgers fluid, this probability is nothing but just the Boltzmann factor with kinetic energy.

surface has reached the steady state. Because of the nonlinearity, the KPZ equation cannot be solved exactly.[5] Therefore, numerical integrations have been extensively studied in the last two decades [20, 2, 72, 4, 11, 73, 76, 77, 14, 15, 91]. We next summarize the various discretization schemes for the $1+1$ dimensional KPZ equation (the corresponding discrete equations for higher dimensional systems can be derived immediately). To discretize the KPZ equation, one writes

$$\frac{h_{i,n+1}-h_{i,n}}{\Delta t}=\nu L(h_{i,n})+\lambda N(h_{i,n})+\eta_{i,n}, \tag{4.41}$$

where we use the suffixes i and n to denote that the indicated variables are evaluated at the ith lattice site and the nth time step. $L(h_{i,n})$ and $N(h_{i,n})$ represent the special discretizations of linear and nonlinear terms respectively and will be discussed later. The $\eta_{i,,n}$ is the discretized noise with zero mean and correlation $\langle \eta_{i,n}\eta_{j,m}\rangle = \frac{D}{a\Delta t}\delta_{i,j}\delta_{n,m}$, where a is the lattice constant and is conventionally set to be equal to 1. One can decrease the time step Δt to increase the accuracy of the numerical intergration. Therefore, by confirming that a further decrease of the time step does not change the result, one can check for convergence of the result. Next, we focus on the spatial discretization schemes. For simplicity, we will not write down the temporal discretization explicitly but denote it as $\partial h_i/\partial t$ thereafter. We drop the suffix of time step n whenever there is no need to indicate it explicitly. The linear term is obtained straightforwardly as

$$L(h_i)=\frac{1}{a^2}\left[(h_{i+1}-h_i)-(h_i-h_{i-1})\right]. \tag{4.42}$$

A simple and widely studied discretization scheme for the nonlinear term is the Euler scheme [20, 2, 72, 4, 73].

$$N(h_i)=\frac{1}{4a^2}\left[(h_{i+1}-h_{i-1})^2\right]. \tag{4.43}$$

This approach is also called the standard or post-point discretization. It has to be pointed out that the Euler scheme has some intrinsic problems such as an unsuitable symmetric lattice feature,[6] and an instability even in the absence of noise [39, 76]. In addition, it cannot well approximate the continuum KPZ equation since the diffusion coefficient is found to be inconsistent with the one derived from the continuum equation [62]. To avoid these undesirable features one can implement the spatial discretization of Eq. (4.37),

$$\frac{\partial \phi_i}{\partial t}=\nu L(\phi_i)+\frac{\lambda}{\nu}\phi_i\eta_i\ , \tag{4.44}$$

where $\partial\phi_i/\partial t=(\phi_{i,n+1}-\phi_{i,n})/\Delta t$. As shown by Newman and Swift [77], by defining that $\tilde{\phi}_i=\phi_i+(\lambda/\nu)\Delta t\phi_i\eta_i$, which yields $\tilde{h}_i\approx h_i+\Delta t\eta_i$ under the Hopf-Cole transformation, with

[5] Except a recent study which gives an exact result for a special initial condition in $1+1$ dimensional systems [85], there are no general exact solutions for the KPZ equation.

[6] The nonlinear term vanishes when $h_{i+1}=h_{i-1}$ which is not the case in the continuum limit.

$\tilde{h}_i = (\nu/\lambda)\ln(\tilde{\phi}_i)$ for $(\lambda/\nu)\Delta t < 1$, the Eq. (4.44) can be approximated by

$$h_{i,n+1} = \tilde{h}_{i,n} + \frac{\nu}{\lambda}\ln\left\{1 + \frac{\nu\Delta t}{a^2}\left[\exp\left(\frac{\lambda}{\nu}(\tilde{h}_{i+1,n} - \tilde{h}_{i,n})\right) + \exp\left(\frac{\lambda}{\nu}(\tilde{h}_{i-1,n} - \tilde{h}_{i,n})\right) - 2\right]\right\} \tag{4.45}$$

In the strong-coupling limit $\lambda \gg \nu$, this equation can be further simplified as

$$h_{i,n+1} = \max\left(\tilde{h}_{i+1,n}, \tilde{h}_{i,n}, \tilde{h}_{i-1,n}\right) \ . \tag{4.46}$$

This simple dynamics is very similar to the algorithm of ballistic deposition where the overhang property is exhibited, see Eqs. (3.7) and (3.8). Therefore, a connection between strong-coupling KPZ equation and the BD model may be suggested. In fact the numerical integration for one dimensional system shows that $\beta \approx 0.308$ which is close to the results for BD. In the regime where $\lambda \ll \nu$, the temporal discretization can be achieved by using $\partial\phi_i/\partial t = (\lambda/\nu)\phi_i \partial h_i/\partial t$. This leads to another discretization scheme after performing the inverse Hopf-Cole transformation,

$$\frac{\partial h_i}{\partial t} = \frac{\nu^2}{\lambda a^2}\left[\exp\left(\frac{\lambda}{\nu}(h_{i+1} - h_i)\right) + \exp\left(\frac{\lambda}{\nu}(h_{i-1} - h_i)\right) - 2\right] + \eta_i \ . \tag{4.47}$$

The series expansion up to second order in h_i yields the so called antistandard or prepoint discretization [76, 14, 91],

$$N(h_i) = \frac{1}{2a^2}\left[(h_{i+1} - h_i)^2 + (h_i - h_{i-1})^2\right] \ . \tag{4.48}$$

Therefore, the antistandard discretization scheme is accurate only when $(h_{i+1} - h_i) < \nu/\lambda$. The numerical integrations we have discussed so far provide ways to investigate the KPZ equation. It has been shown that the discretization more or less gives the correct exponents for the KPZ universality class in various schemes. However, it is still an open question whether a finite difference approach really yields the same solution as the continuum equation. The major issue includes the accuracy and stability in the long time regime where the fluctuations become large. Moreover, the conventional discretizations can not yield a steady state probability distribution for the corresponding discrete surfaces, even though this distribution exists for the one dimensional continuum KPZ equation. In other words, for a specified surface configuration $\mathbf{h} \equiv \{h_i\}$, assuming that there exists a discretized steady state probability distribution

$$P_s[\mathbf{h}] = \exp\left[-\frac{\nu}{a^2 D}\sum_{i=1}^{L}(h_{i+1} - h_i)^2\right], \tag{4.49}$$

this probability distribution does not satisfy the discrete Fokker-Planck equation

$$\frac{\partial P[\mathbf{h}]}{\partial t} = -\sum_{i=1}^{L}\frac{\partial}{\partial h_i}\left\{[\nu L(h_i) + \lambda N(h_i)]\, P\right\} + \frac{D}{2}\sum_{i=1}^{L}\frac{\partial^2 P}{\partial h_i^2} \tag{4.50}$$

in the steady state where $\partial P_s/\partial t = 0$. This has first been remarked by Lam and Shin who introduced a discretization scheme which is able to solve this problem [62]. In their discretization, the nonlinear term is given by

$$N(h_i) = \frac{1}{3a^2}\left[(h_{i+1}-h_i)^2 + (h_{i+1}-h_i)(h_i-h_{i-1}) + (h_i-h_{i-1})^2\right]. \tag{4.51}$$

It can be shown that this nonlinear term satisfies $\sum \partial(N(h_i)P_s)/\partial h_i = 0$ under perodic boundary conditions. Since $\partial P_s/\partial h_i = \nu L(h_i)P$ leads to the cancellation for the first and third terms on the right-hand side in Eq. (4.50), the probability $P_s[\mathbf{h}]$ is the steady state solution for nonzero λ for Lam and Shin's approach. Later, it was pointed out by Becuta [14] that the Euler, antistandard, and Lam-Shin schemes can be summarized by the generalized discretization

$$N^{(\gamma)}(h_i) = \frac{1}{2\gamma+1}\left[(h_{i+1}-h_i)^2 + 2\gamma(h_{i+1}-h_i)(h_i-h_{i-1}) + (h_i-h^i_{i-1})\right], \tag{4.52}$$

with the corresponding parameter $\gamma = 1$, 0, and 1/2 respectively. Instead of seeking a proper discretization of the KPZ equation with a steady state distribution given by Eq. (4.49), Becuta shows that there exists a modified steady state probability

$$P_s[\mathbf{h}] = \exp\left\{-\frac{\nu}{D}\sum_{i=1}^{L}\left[\frac{1}{a^2}(h_{i+1}-h_i)^2 + \frac{\sigma}{a^4}(h_{i+1}-2h_i+h_{i-1})^3\right]\right\}, \tag{4.53}$$

where

$$\sigma = \frac{\lambda}{72\nu}\left(\frac{1-2\gamma}{1+\gamma}\right) \tag{4.54}$$

for the generalized discretization Eq. (4.52). There are two cases for which the probability distribution recovers the simple form Eq. (4.49), namely $\gamma = 1/2$ and $\lambda = 0$. The first one is when the generalized discretization becomes the Lam-Shin scheme. The second one is due to the vanishing of the nonlinear term in the discrete KPZ equation. Therefore, one should recover the steady state probability for the discrete EW equation. It is worth to note that the Lam-Shin approach and Becuta's generalization give different discrete representations of $(\nabla h)^2$ in the KPZ equation and in the steady state probability distribution. This implies that we still lack a perfect discretized KPZ equation.[7]

[7]Actually, there is no finite renormalization-group fixed point for $d > 1$. Therefore, it is not even clear that there is universality at all.

Chapter 5

Dynamic Scaling

In this chapter, we discuss the celebrated Family-Vicsek scaling relation. This important concept has led to the successful development of universality classes in surface growth. We then discuss a parameter free scaling relation that yields a complete data collapse for large classes of non-equilibrium growth processes. We illustrate the power of this new scaling relation through various growth models, as for example the competitive growth model RD/RDSR, the RSOS and the MRDSR. The new scaling relation is compared to the Family-Vicsek relation. The major results described in this chapter are published in [24].

5.1 Family-Vicsek relation

As we have discussed in previous chapters, many surface growth processes share a general property: there are three regimes separated by two crossover points, t_1 and t_2. Starting from an initially flat surface, a surface grows in the same way as the RD process at very early times with $t < t_1 \sim 1$, since no (or only very few) diffusion steps occur in that regime. For $t > t_1$ the width increases as a power law of time with a growth exponent β, before entering a saturation regime after a crossover time t_2 (see Figures 3.2, 3.5, 3.6 and 3.8). Both the saturation width W_2 and the crossover time t_2 are powers of the substrate size L, see Eq. (3.5). If one disregards the RD regime, one can achieve a data collapse for the different system sizes by shifting the second crossover point in a log-log plot to the origin. This procedure is summarized in the celebrated Family-Vicsek scaling relation [41]

$$W = W_2 f(t/t_2), \tag{5.1}$$

where $f(x)$ is a scaling function which has the property

$$f(x) = \begin{cases} 1 & \text{for} \quad x \gg 1 \\ x^{\beta} & \text{for} \quad x \ll 1 \end{cases} . \tag{5.2}$$

Discrete Models	Continuum Equations	α	β	z
RD	RD Eq. (4.1)		1/2	
RDSR, MRDSR	EW Eq. (4.7)	$(2-d)/2$	$(2-d)/4$	2
WV	MH Eq. (4.8)	$(4-d)/2$	$(4-d)/8$	4
BD, RSOS	KPZ Eq. (4.35)	1/2	1/3	3/2

Table 5.1: List of universality classes. The values of scaling exponents are valid for all dimensions for the RD universality class, for $d < d_c$ for both the EW and MH universality classes, and for $d = 1$ for the KPZ universality class.

One can alternatively rewrite the scaling law as

$$W = L^{\alpha} f(t/L^{z}). \tag{5.3}$$

In this case the second crossover points for different system sizes are shifted to a common point $(t_2/L^z,\ W_2/L^\alpha)$, and the scaling function has to be modified as

$$f(x) = \begin{cases} W_2/L^{\alpha} & \text{for} \quad x \gg t_2/L^{z} \\ Ax^{\beta} & \text{for} \quad x \ll t_2/L^{z} \end{cases}, \tag{5.4}$$

where A is a constant. One can furthermore obtain from the scaling law that $W \propto L^{\alpha}(t/L^{z})^{\beta}$ when $t \ll t_2$. For Eq. (3.4) to be valid, one needs to have the relation Eq. (3.6), introduced in Chapter 3. It is worth noting that the Family-Vicsek relation neglects the RD regime at early times and exclusively focuses on the two regimes connected by the crossover point at $t = t_2$. We take the RD-RDSR (Figure 3.6) and RSOS (Figure 3.5) models as examples. After applying the Family-Vicsek relation, we see partial data collapse as indicated in Figure 5.1 (a) for RD/RDSR and Figure 5.2 (a) for RSOS. The scaling relations (3.5) and the scaling law (5.3) are generic for growing interfaces and have been verified analytically, numerically, and experimentally in a large variety of systems. Various universality classes have been identified which differ by the values of the scaling exponents. Thus the RDSR process belongs to the Edwards-Wilkinson universality class with the exponents $\beta = 1/4$ and $z = 2$ for a one-dimensional substrate. The WV process belongs to the Mullins-Herring universality class with the exponents $\beta = 3/8$ and $z = 4$ for a one-dimensional substrate. The RD process is in an universality class of its own which is characterized by the values $\beta = 1/2$. Another well known universality class, directly related to technologically relevant growth processes, is the KPZ universality class. A summary of the most important universality classes is given in Table 5.1.

5.2 Generalized Family-Vicsek scaling relation

In simple growth processes the random deposition regime is restricted to very early times. This is fundamentally different in more complex systems where the initial regime can extend

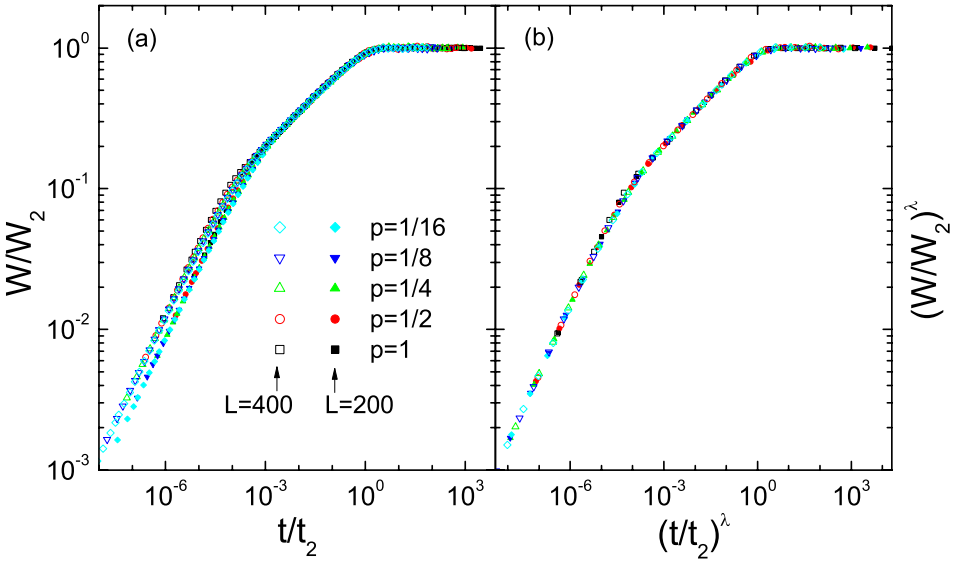

Figure 5.1: (a) Family-Vicsek scaling for the RD/RDSR process (see Figure 3.6 for the original plot) in systems with different sizes L and different probabilities p. A data collapse is only achieved for two of the three regimes. (b) A complete data collapse of all data sets is achieved when using our new scaling relation (5.6). The curves shown in the left panel completely fall one on top of the other and are no longer distinguishable.

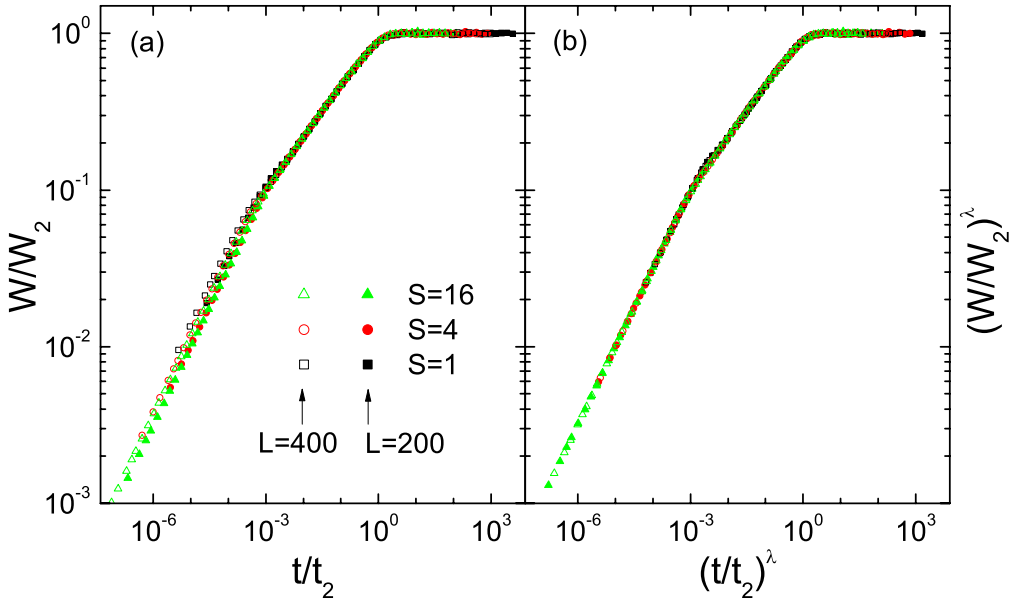

Figure 5.2: The same as Fig. 5.1, but now for the RSOS model (see Figure 3.5 for the original plot) with different values S of the maximal nearest-neighbor height difference. Again a perfect data collapse is achieved when using the scaling relation (5.6).

over very large times [51, 48, 21, 49, 57, 75, 13, 53, 50, 1, 79, 58, 22]. As already mentioned, the Family-Vicsek scaling relations (5.1) and (5.3) assign a new set of coordinates to the second crossover point. This does however not yield a complete data collapse for growth processes with two crossover points if one considers systems of different sizes (see Figures 5.1 (a) and 5.2 (a)). For the competitive growth models some phenomenological scaling relations have been proposed in the past, but these modified scaling relations also only allow a partial collapse of the different curves [51, 57, 13, 58]. However, a scaling relation leading to a complete data collapse of *all* curves obtained for different system sizes and different values of the system parameters can indeed be obtained for any growth system that exhibits two different crossover points. This data collapse is achieved in a two-step process. First we translate all curves in a log-log plot such that the second crossover point is now located at the origin. This is achieved by plotting $\log\left(\frac{W}{W_2}\right)$ as a function of $\log\left(\frac{t}{t_2}\right)$. We show this step in 5.1 (a) for the RD/RDSR and 5.2 (a) for the RSOS processes. In the second step we rescale both axes by the common scale factor $\lambda = 1/\log\left(\frac{W_2}{W_1}\right)$ such that in the log-log plot the first crossover point is fixed at the rescaled width $\log W_2' = -1$.[1] This isotropic rescaling, which conserves the slope of the region between the two crossover points, renders the length of the line connecting the two crossover points the same for all curves, and a complete data collapse, encompassing all three regimes, follows. This second step is shown in 5.1 (b) and 5.2 (b) for the RD/RDSR and RSOS respectively. Our proposed scaling relation can be cast in the following equation:

$$\frac{\log\left(\frac{W}{W_2}\right)}{\log\left(\frac{W_2}{W_1}\right)} = F\left[\frac{\log\left(\frac{t}{t_2}\right)}{\log\left(\frac{W_2}{W_1}\right)}\right] \tag{5.5}$$

where $F(x)$ is a scaling function. Introducing $\lambda = 1/\log\left(\frac{W_2}{W_1}\right)$, we can rewrite this as

$$W^\lambda = W_2^\lambda\, G\left[\left(\frac{t}{t_2}\right)^\lambda\right] \tag{5.6}$$

with a new scaling function $G(y)$,

$$G(y) = \begin{cases} 1 & \text{for} \quad y \gg 1 \\ y^\beta & \text{for} \quad 1 \gg y \gg 10^{-1/\beta} \\ y^{1/2} & \text{for} \quad y \ll 10^{-1/\beta} \end{cases} . \tag{5.7}$$

In fact, the first step of relation (5.6) is just the Family-Vicsek relation (5.1). Therefore, we see that we recover the Family-Vicsek relation by setting $\lambda = 1$. This nicely shows that it is the isotropic rescaling in the log-log plot by the factor $\frac{1}{\log(W_2/W_1)}$ that ultimately is responsible for the success of the new scaling relation. As shown in Figures 5.1 (b) and 5.2 (b) for the RD/RDSR and RSOS processes, the proposed scaling relation (5.6) yields a complete data collapse for different system sizes L and different values of the system parameters. This

[1] Alternatively, one can use $\lambda = 1/\log\left(\frac{t_2}{t_1}\right)$ to fix the second crossover point at rescaled time $\log t_2' = -1$.

perfect scaling behavior should be compared with the incomplete scaling proposed in the literature [51, 57, 13, 58]. Obviously, the scaling relation (5.6) is of universal use in growth systems with two crossover points and replaces the Family-Vicsek relation in these systems. This class of systems encompasses competitive growth models, but also the simple growth systems, for which the Family-Vicsek relation has been proposed originally, belong to this class. It is also worth noting that the properties of the different models only enter in our relation (5.6) implicitly through the dependence of the positions of the crossover points on the different system parameters.

A complete collapse can also be achieved when first moving the first crossover point to the origin in a log-log plot, yielding the relation

$$\frac{\log\left(\frac{W}{W_1}\right)}{\log\left(\frac{W_2}{W_1}\right)} = \tilde{F}\left[\frac{\log\left(\frac{t}{t_1}\right)}{\log\left(\frac{W_2}{W_1}\right)}\right] \tag{5.8}$$

or

$$W^\lambda = W_1^\lambda \tilde{G}\left[\left(\frac{t}{t_1}\right)^\lambda\right] \tag{5.9}$$

where $\tilde{F}$ and $\tilde{G}$ are again scaling functions. This scaling relation is completely equivalent to the first one, only the scales are shifted. By locating the two crossover points, we are able to use the expression (5.9) to collapse the data we obtain from the one-dimensional MRDSR model (see Figure 5.3). Since the first crossover point (t_1, W_1) of this model is proportional to $(1/\nu, 1/\sqrt{\nu})$ (see Chapter 4), applying the fitted relation between ν and T we can rewrite the scaling relation (5.9) in the form

$$W^\lambda = (a' + b'T/g)^{\lambda/2}\, G\left[\frac{t^\lambda}{(a' + b'T/g)^\lambda}\right] \tag{5.10}$$

where $a' = 0.28$ and $b' = 0.57$,[2] with $\lambda(L) = 1/\log(c\,L^\alpha)$ and $c = 0.535$, whereas $\alpha = 1/2$ is the roughness exponents of the EW universality class.[3] Eq. (5.10) directly reveals for our model the dependence of the generalized scaling relation on the system size and on the temperature.

The two-parameter linear Langevin equation (4.9) can be rescaled into a one-parameter equation

$$\frac{\partial h'(\mathbf{x}, t')}{\partial t'} = -(i\nabla)^m h'(\mathbf{x}, t') + \eta(\mathbf{x}, t') \tag{5.11}$$

[2]The values of a' and b' are fitted using Eq. (5.10) such that we can obtain good data collapse. We do not recover that $a' = a/2\pi$ and $b' = b/2\pi$, which is suggested by $2\pi\nu t_1 = 1$, since this is a rough estimation. To apply the scaling relations (5.6) and/or (5.9), we require to shift one of the crossovers exactly to the origin in the log-log scale.

[3]One can also simply assume that $\lambda = 1/\log(L)$ to achieve good data collapse as long as c is much smaller than L. The expression of $\lambda = 1/\log(cL^\alpha)$ is used for ensuring that the second crossover width is fixed at the rescaled width $\log W_2' = 1$.

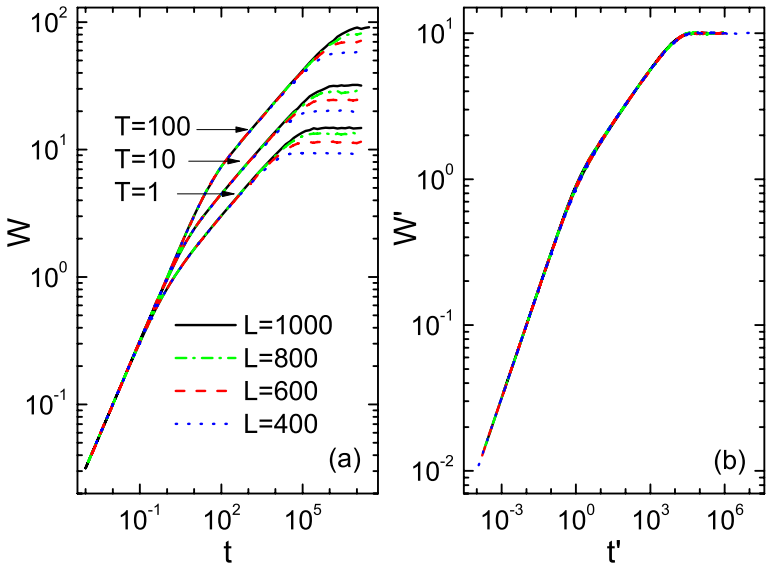

Figure 5.3: (a) Log-log plot of the surface width vs time for the temperature dependent deposition model. Systems of different sizes at different temperatures are shown. (b) A complete data collapse of all data sets is also achieved for this model. *Phys. Rev. E* 79(5): 051605. Used with permission of American Physical Society, 2009.

by setting $t = t'/\nu$ and $h = h'/\sqrt{\nu}$ but keeping $\langle \eta(\mathbf{x}_1, t'_1)\eta(\mathbf{x}_2, t'_2)\rangle = D\delta(\mathbf{x}_1, t'_1)\delta(\mathbf{x}_2, t'_2)$. This rescaling together with the definition of width in Eq. (3.1) yields that $\sqrt{\nu}W = f(\nu t)$, where f is a scaling function. This is, basically, the Family-Vicsek scaling relation with shifting the first crossover points, which are proportional to $(1/\nu, 1/\sqrt{\nu})$, onto a single point. However, using this form only allows us to collapse curves with different diffusion constants ν but it does not allow to collapse curves from systems with different sizes L. The L dependence feature of surface width is revealed by the summation in Eq. (4.16). Due to the simplicity of this equation, we can obtain the information on the location of the two crossover points (see Chapter 4). In this way we find that, as usual, only the crossover to the saturation regime depends on the system size. In addition, the coordinates of both crossover points display a linear dependence on the inverse of the diffusion constant. Taking these observations into account, the scaling relation (5.9) can be rewritten in the from

$$W^{\lambda} = (r\nu)^{\lambda/2} G\left[(r\nu t)^{\lambda}\right], \tag{5.12}$$

where r is a fitting parameter which ensures that the first crossover point is shifted to the origin in a log-log plot. The results of applying the scaling relation to the one-dimensional EW and MH equations are shown in Figure 5.4 (a), (b) respectively. We find that $r = 2/\pi^2$ yields a good data collapse for the 1D EW equation, and $r = (2\pi)^4$ for the 1D MH equation. The value $\lambda = 1/\log L$ is used for the fittings.

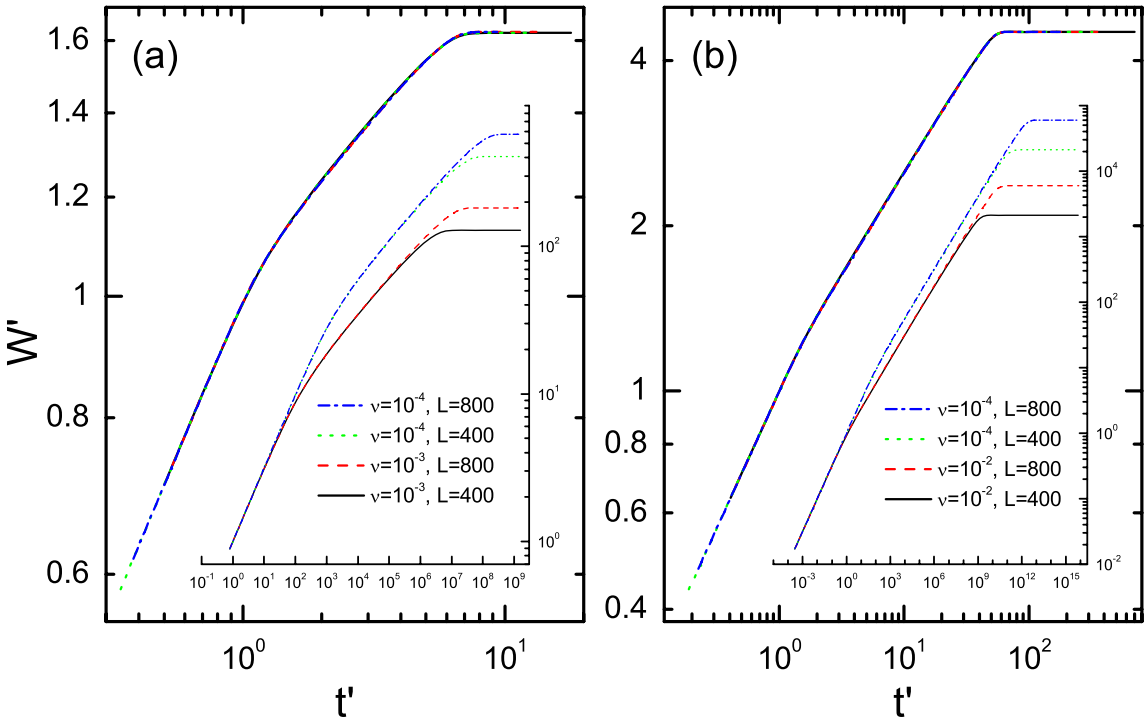

Figure 5.4: Log-log plot of the rescaled surface width vs time for the one-dimensional linear Langevin equations with (a) $m = 2$ and (b) $m = 4$. The insets show the original data.

Chapter 6

Global Two-time Quantities I

Two-time quantities are nowadays routinely studied in the context of non-equilibrium relaxation and ageing phenomena [47] where in most cases the focus is on local quantities. For example when studying a magnetic system one usually investigates the spin-spin correlation function or the response of a spin to a local magnetic field. Incidentally, the study of aging in magnetic systems has revealed that additional insights can be gained by looking at global quantities, as for example the magnetization-magnetization correlation or the response of the magnetization to a spatially constant magnetic field [66, 81, 5, 18, 36].

In the studies of growth processes mainly local two-time quantities have been investigated in the past [54, 83, 84, 16, 15, 25, 78, 46]. Examples include the two-time height-height correlation function [54, 83, 84, 16, 15, 46] or the response of the height to a local perturbation [83, 84, 16, 15, 46]. Some attention has also been paid to slightly more complex quantities as for example the two-time roughness or the two-time incoherent scattering function [16, 15].

Both the local height-height autocorrelation function $C_\ell(t,s)$ and the local autoresponse function $R_\ell(t,s)$ display simple aging scaling forms [54, 83, 84, 46], irrespective of whether the system is linear or non-linear:

$$C_\ell(t,s) = s^{-b_\ell}\, f_{C_\ell}(t/s) \quad , \quad R_\ell(t,s) = s^{-1-a_\ell}\, f_{R_\ell}(t/s) \tag{6.1}$$

where the scaling functions f_{C_ℓ} and f_{R_ℓ} are power-laws in the long time limit, i.e. $f_{C_\ell}(y) \sim y^{-\lambda_{C,\ell}/z}$ and $f_{R_\ell}(y) \sim y^{-\lambda_{R,\ell}/z}$ for $y \gg 1$ [47]. The values of the dynamical exponent z as well as of the scaling exponents b_ℓ, a_ℓ, $\lambda_{C,\ell}$, and $\lambda_{R,\ell}$ depend on the dynamical universality class. For growth processes the dynamical exponent z is related to the roughness exponent α and the growth exponent β by the relation $z = \alpha/\beta$. As shown in the studies [54, 83, 84, 46] the local autocorrelation and autoresponse exponents are identical and given by $\lambda_{C,\ell} = \lambda_{R,\ell} = d$ where d is the dimensionality of the substrate. In addition, the scaling exponent of the correlation function, b_ℓ, is given by $b_\ell = -2\alpha/z$, whereas for the scaling exponent of the response function the relation $a_\ell = d/z - 1$ can be conjectured. As for the linear stochastic equations we have that $\alpha = (z-d)/2$, it follows that in linear systems both scaling exponents

have the same value, $a_\ell = b_\ell = d/z - 1$. This is different for the non-linear Kardar-Parisi-Zhang equation [55] where for a one-dimensional substrate we have $\alpha = 1/2$ and $z = 3/2$, yielding $b_\ell = -2/3$ and $a_\ell = -1/3$ [46, 30].

In this chapter we study the aging behavior of certain global two-time quantities, namely the correlation function of the squared width and the response of the squared width to a global perturbation. We show that the scaling behavior of the global response depends in linear systems on how the system is perturbed, yielding different results for different protocols. This observation is of interest as the global response should be readily accessible in smoothening experiments [78], for example. Exploiting the fact that exact solutions can be obtained for growth processes described by linear Langevin equations, we comprehensively study the scaling behavior of these global two-time quantities for the Edwards-Wilkinson [37] and the noisy Mullins-Herring equations [74], thereby distinguishing between various limiting cases. In order to gain some understanding of the behavior of these quantities in non-linear systems, we also discuss some data that have been obtained by numerically integrating the non-linear Kardar-Parisi-Zhang equation [55]. Our results indicate that in the non-trivial correlated regime the two-time global quantities generically exhibit a behavior of full aging. We also discuss the global fluctuation-dissipation ratio and show how this quantity can be used for the characterization of growth processes. The content of this chapter has been published in [25, 23].

6.1 Correlation function for linear growth

The first global quantity that we are going to discuss is the connected correlation function

$$C(t,s) = \langle W^2(t)\, W^2(s)\rangle - \langle W^2(t)\rangle\langle W^2(s)\rangle \tag{6.2}$$

where W^2 is the square of the surface width at time t on top of a d-dimensional substrate of linear extension L. We assume in the following that $t > s$ and call s the waiting time and t the observation time. Starting from Eq. (4.15) we have

$$\begin{aligned}\langle W^2(t)W^2(s)\rangle &= \frac{1}{L^{2d}}\sum_{\mathbf{x},\mathbf{x}'}\sum_{\mathbf{q},\mathbf{q}',\mathbf{p},\mathbf{p}'\neq 0}\langle h_{\mathbf{q}}(t)h_{\mathbf{q}'}(t)h_{\mathbf{p}}(s)h_{\mathbf{p}'}(s)\rangle \\ &\quad \exp\left[i(\mathbf{q}+\mathbf{q}')\cdot\mathbf{x}\right]\exp\left[i(\mathbf{p}+\mathbf{p}')\cdot\mathbf{x}'\right].\end{aligned} \tag{6.3}$$

The calculation of (6.2) is therefore reduced to the determination of the four-point correlation function of surface height in $\mathbf{q}$-space. Using Wick's theorem, this four-point function can be expressed through two-point functions of the form (4.14), yielding

$$\begin{aligned}\langle h_{\mathbf{q}_1}(t_1)h_{\mathbf{q}_2}(t_2)h_{\mathbf{q}_3}(t_3)h_{\mathbf{q}_4}(t_4)\rangle &= \langle h_{\mathbf{q}_1}(t_1)h_{\mathbf{q}_2}(t_2)\rangle\langle h_{\mathbf{q}_3}(t_3)h_{\mathbf{q}_4}(t_4)\rangle \\ &\quad +\langle h_{\mathbf{q}_1}(t_1)h_{\mathbf{q}_3}(t_3)\rangle\langle h_{\mathbf{q}_2}(t_2)h_{\mathbf{q}_4}(t_4)\rangle \\ &\quad +\langle h_{\mathbf{q}_1}(t_1)h_{\mathbf{q}_4}(t_4)\rangle\langle h_{\mathbf{q}_2}(t_2)h_{\mathbf{q}_3}(t_3)\rangle.\end{aligned} \tag{6.4}$$

Inserting this into (6.3) and using the identity

$$\sum_{n=0}^{N-1} \exp\left(\frac{2\pi inm}{N}\right) = N\delta_{m,0} \tag{6.5}$$

yields the expression

$$\begin{aligned}\langle W^2(t)W^2(s)\rangle &= \frac{D^2}{L^{2d}\nu^2}\left\{\sum_{\mathbf{q},\mathbf{p}\neq 0}\frac{1}{4q^m p^m}\left(1-e^{-2q^m\nu t}\right)\left(1-e^{-2p^m\nu s}\right)\right. \\ &\left. + \sum_{\mathbf{q}\neq 0}\frac{1}{2q^{2m}}e^{-2q^m\nu t}\left(e^{2q^m\nu s}+e^{-2\nu q^m s}-2\right)\right\}.\end{aligned}$$

The first term on the right-hand side being just $\langle W^2(t)\rangle\langle W^2(s)\rangle$, we finally obtain

$$C(t,s) = \frac{D^2}{2L^{2d}\nu^2}\sum_{\mathbf{q}\neq 0}\frac{1}{q^{2m}}e^{-2q^m\nu t}\left(e^{2q^m\nu s}+e^{-2q^m\nu s}-2\right). \tag{6.6}$$

The behavior of $C(t,s)$ is controlled by two length scales: $l_t \equiv (2\nu t)^{1/m}$ and $l_s \equiv (2\nu s)^{1/m}$, with $l_t > l_s$. Depending on the values of l_t and l_s and their relations to the maximum and minimum values of q, $q_{max} = \pi\sqrt{d}$ and $q_{min} = 2\pi/L$, different regimes are encountered. For example, if at time t the length $l_t < 1/q_{max}$[1], one still is in the short time regime where the random deposition process prevails. On the other hand, if at time t one has that $l_t > 1/q_{min}$, one is in the saturation regime. Finally, the system is in the correlated regime when $1/q_{max} < l_t < 1/q_{min}$. To carry out the summation Eq. (6.6), one can replace the sum by an integral

$$\sum_{\mathbf{q}} f(q) \to (L/2\pi)^d \Omega_d \int_0^\pi q^{d-1} f(q) dq \tag{6.7}$$

for the general cases. However, if $l_t > 1/q_{min}$ such that the exponential terms with smallest q dominate, we simply have

$$\sum_{\mathbf{q}} f(q) \to 2df(q_{min}). \tag{6.8}$$

We discuss in the following the functional form of the correlation function for the different regimes shown in the diagram Figure 6.1 according to the approximations Eqs. (6.7), and (6.8). A summary of the asymptotic behavior in the corresponding regimes is shown in Table 6.1.

1. If $l_t < 1/q_{max}$ we are in the short time regime. In that case all exponentials in (6.6) can be expanded and only the leading terms need to be retained, i.e. $e^{-2q^m\nu t} \approx 1 - 2q^m\nu t$

[1]By $l_t < 1/q_{max}$ we mean that the order of l_t has to be much smaller than the order of $1/q_{max}$. There are complicated crossover effects showing up when l_t and $1/q_{max}$ are of comparable magnitude that we are not going to discuss. Of course, the same remark applies when comparing one of the length scales to $1/q_{min}$.

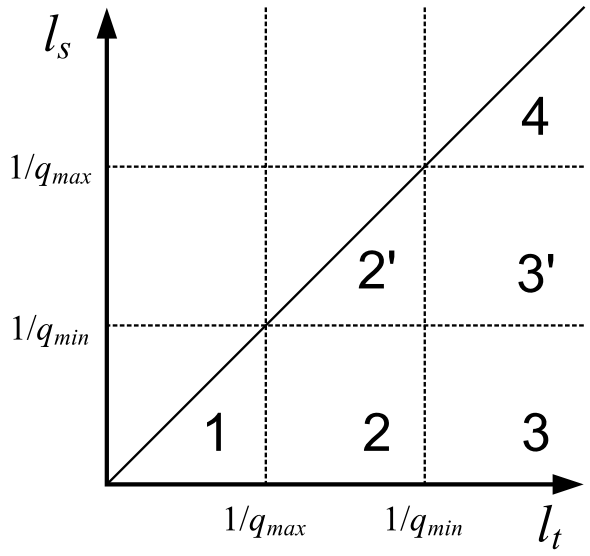

Figure 6.1: Six possible regimes for two-time functions. The regimes 2 and 2′ (3 and 3′) have the same leading behavior and, hence, belong to the same category.

$s \setminus t$	RD	CR	SR
SR	–	–	$ae^{-b(t-s)}$
CR	–	$as^{2-d/m}\,(t/s)^{-d/m}$	$a\,s^2\,e^{-bt}$
RD	$a\,s^2\,(1-b\,t)$	$as^{2-d/m}\,(t/s)^{-d/m}$	$a\,s^2\,e^{-bt}$

Table 6.1: Summary of the asymptotical dependence of the global correlation function for the different cases. RD corresponds to the random deposition regime, CR to the correlated regime, and SR to the saturation regime. The values of a and b, which depend on the case considered, can be read off from the equations in the main text.

and $e^{2q^m\nu s}+e^{-2q^m\nu s}-2 \approx (2q^m\nu s)^2$ for all q. Replacing the sum by an integral, we obtain

$$\begin{aligned} C(t,s) &\approx \frac{2D^2s^2}{L^{2d}}\left(\frac{L}{2\pi}\right)^d \Omega_d \int_0^\pi q^{d-1}\left(1-2q^m\nu t\right) dq \\ &\approx \frac{2^{2-d}D^2\pi^{d/2}}{L^d\Gamma(d/2)d}s^2\left(1-\frac{2d}{d+m}\pi^m\nu t\right), \end{aligned} \tag{6.9}$$

where $\Omega_d = 2\pi^{d/2}/\Gamma(d/2)$ is the solid angle of the d-dimensional sphere. Therefore, in the short time regime the correlation function decreases linearly with time.

2. If the final time is in the correlated regime, i.e. if $1/q_{max} < l_t < 1/q_{min}$, one has to distinguish between two different cases, depending on whether $l_s < 1/q_{max}$ (the system was in the RD regime at time s) or $1/q_{max} < l_s < l_t$ (the system was in the correlated regime at time s). In the first case we can again replace $e^{2q^m\nu s}+e^{-2q^m\nu s}-2$ by $(2q^m\nu s)^2$ and obtain the expression

$$\begin{aligned} C(t,s) &\approx \frac{2D^2s^2}{L^{2d}}\left(\frac{L}{2\pi}\right)^d \Omega_d \int_0^\infty q^{d-1}e^{-2q^m\nu t}dq \\ &= A_{m,d}s^2t^{-d/m}, \end{aligned} \tag{6.10}$$

where

$$A_{m,d} = \frac{2^{2-d-d/m}D^2\Gamma(d/m)}{L^d\pi^{d/2}m\nu^{d/m}\Gamma(d/2)}\ , \tag{6.11}$$

yielding a power-law decay with an exponent d/m. In the second case ($2'$ in Figure 6.2), which is the most interesting one as both times are in the correlated regime, we expand all exponentials in (6.6) and integrate term by term. This yields

$$\begin{aligned} C(t,s) &= A_{m,d}s^2\left\{t^{-d/m}+\frac{s^2}{12}\frac{\partial^2}{\partial t^2}t^{-d/m}+\frac{s^4}{360}\frac{\partial^4}{\partial t^4}t^{-d/m}+\cdots\right\} \\ &= A_{m,d}s^2t^{-d/m}\left\{1+\frac{1}{12}\frac{d}{m}\left(\frac{d}{m}+1\right)\left(\frac{s}{t}\right)^2+\right. \\ &\quad \left.\frac{1}{360}\frac{d}{m}\left(\frac{d}{m}+1\right)\left(\frac{d}{m}+2\right)\left(\frac{d}{m}+3\right)\left(\frac{s}{t}\right)^4+\cdots\right\} \\ &\approx A_{m,d}s^2t^{-d/m} \end{aligned} \tag{6.12}$$

where the last line gives the asymptotic form for $t \gg s$. Interestingly, we recover asymptotically the same leading behavior as for the case $l_s < 1/q_{max}$, i.e. in the long time limit any memory of the regime that prevailed at time s is lost. Looking closer at the expressions (6.10) and (6.12), we see that in both cases the global correlation function can be cast in the standard form [47] $C(t,s) = s^{-b}f_C(t/s)$ where $b = d/m-2$ and $f_C(t/s)$ is a scaling function that only depends on the ratio t/s. In addition, the

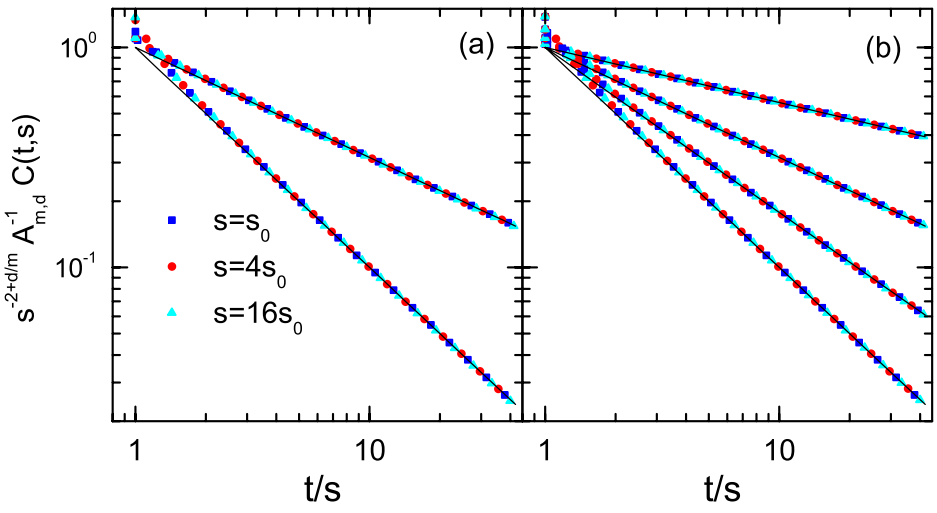

Figure 6.2: Global correlation function when both times t and s are in the correlated regime. The symbols are obtained by numerically evaluating the exact expression (6.6) whereas the lines indicate the asymptotic power-laws (6.12). Panel (a) shows data for the EW case and dimensions $d = 1, 2$ (from top to bottom), panels (b) show data for the MH case and dimensions $d = 1, 2, 3, 4$ (from top to bottom). The different symbols correspond to different waiting times where $s_0 = 1000$ below the critical dimension and $s_0 = 200$ at the critical dimension (which is $d = 2$ for EW and $d = 4$ for MH). The linear extension of the system is $L = 2^{14}$ for $d = 1$, $L = 2^9$ for $d = 2$, $L = 2^7$ for $d = 3$, and $L = 2^6$ for $d = 4$.

scaling function is asymptotically given by a power-law, $f_C(t/s) \sim (t/s)^{-\lambda_C/z}$, with the autocorrelation exponent $\lambda_C = d$ and the dynamical exponent $z = m$. In Figure 6.2a,b we compare the correlation function (6.6), where the sum has been evaluated numerically, with the asymptotic power-law (6.12), see Figure 6.2a for the EW case and Figure 6.2b for the MH case. In all cases the asymptotic regime is accessed very rapidly. We can now also compare for this regime the global correlation function with the local height-height correlation, see [54, 83, 84]. For the local correlation function one obtains the scaling exponents $b_\ell = d/m - 1$ and $\lambda_{C,\ell} = d$. Thus, for both the local and global quantities the long-time behavior is governed by the same power-law exponent, $\lambda_C = \lambda_{C,\ell}$, but the value of the scaling exponent b is different from the value of b_ℓ. This yields interesting differences at the upper critical dimension which is $d = 2$ for EW and $d = 4$ for MH. Indeed, whereas the local exponent b_ℓ then vanishes and the scaling function of the local correlation shows a logarithmic dependence on time (which makes the extraction of the correct scaling behavior from experimental or simulation data rather tedious) [83], the global exponent remains different from zero and no logarithms are occulting the scaling behavior of the global correlation, making this a much better quantity for studying dynamical scaling close to the upper critical dimension.

3. In case the observation time is in the saturation regime with $l_t > 1/q_{min}$, the leading contribution is given by the term in $e^{-2q^m_{min}\nu t}$. If the waiting time is such that $l_s < 1/q_{min}$, then we can approximate for $q = q_{min}$ the term involving s by $(2q^m_{min}\nu s)^2$ which yields

$$C(t,s) \approx \frac{4dD^2s^2}{L^{2d}} e^{-2q^m_{min}\nu t} \ . \tag{6.13}$$

4. If both the observation time and the waiting time are in the saturation regime, we have $l_s > 1/q_{min}$ and therefore

$$C(t,s) \approx \frac{dD^2L^{2(m-d)}}{(2\pi)^{2m}\nu^2} e^{-2q^m_{min}\nu(t-s)}, \tag{6.14}$$

i.e. the global correlation is time-translation invariant. This is of course expected, as the saturation regime corresponds to the steady state regime. It is worth noting that in both cases the decay time in the exponential, $\tau = 1/(2q^m_{min}\nu)$, depends on the diffusion mechanism through the values of ν and m but does not depend on the dimensionality of the substrate.

6.2 Response function for linear growth 1 : Changing the diffusion constant

Experimentally, a quantity that can be changed easily and that gives way to a global perturbation is the temperature. If an experimental system is described by a stochastic Langevin equation, temperature can enter either through the surface tension ν (also called diffusion constant or mobility, depending on the physical context) or through the noise. We will study the responses to two different global perturbations: either we keep the noise unchanged and suddenly change ν (as it is the case in surface smoothening experiments or in step fluctuation studies) or we keep the surface tension constant and change the noise (as it is the case in some deposition experiments where the noise in the particle flux can be changed experimentally). Both protocols have been used for studying the change in morphology of a growing surface when changing experimental conditions [64, 25]. We will discuss the first protocol in this section and the second protocol in the next section. In order to measure the global response we are going to perturb the growing system through a change in the surface tension ν. Having thus perturbed our system, we then study its relaxation to the state that is realized when the system evolves all the time at fixed values of ν. We start from an initially flat surface and let the system evolve with a surface tension μ until the waiting time s after which we set the surface tension to the final value ν. In order to monitor the relaxation of the system for $t > s$, we compute the function

$$\chi(t,s) = \frac{\langle W^2\rangle_{\mu\to\nu}(t,s) - \langle W^2\rangle_{\nu}(t)}{\epsilon} \tag{6.15}$$

where the index "$\mu \to \nu$" indicates the perturbed system, whereas the index "ν" stands for the system that is evolving at a fixed value ν of the surface tension. The quantity $\epsilon \equiv \nu - \mu$ measures the strength of the perturbation. Usually one is interested in small perturbations for which $|\epsilon| \ll 1$. However, as we discuss later, the response (6.15) displays simple aging and dynamical scaling even for very strong perturbations. It has to be noted that the response $\chi(t,s)$ is a time integrated response that gives the reaction of the system to a perturbation lasting until time s. This time integrated response is related to the response R due to an instantaneous perturbation by $\chi(t,s) = \int_0^s du\, R(t,u)$. Assuming a standard scaling behavior for R, i.e. $R(t,s) = s^{-1-a} f_R(t/s)$, it follows that the time integrated response should scale as $\chi(t,s) = s^{-a} f_\chi(t/s)$ [47]. The expression for $\chi(t,s)$ is readily obtained by remarking that the solution of the Langevin equation becomes for $t \geq s$

$$h_{\mathbf{q}}(t) = e^{-\nu \mathbf{q}^m (t-s)} h_{\mathbf{q},\mu}(s) + \int_s^t d\tau e^{-\nu \mathbf{q}^m (t-\tau)} \eta_{\mathbf{q}}(\tau), \tag{6.16}$$

where

$$h_{\mathbf{q},\mu}(s) = \int_0^s d\tau e^{-\mu \mathbf{q}^m (s-\tau)} \eta_{\mathbf{q}}(\tau) \tag{6.17}$$

is the solution of a surface that, starting from a flat initial state, evolves until time s at the constant surface tension μ. Inserting this expression into Eq. (4.15) yields

$$\langle W^2 \rangle_{\mu\to\nu}(t,s) = \frac{D}{2L^d} \sum_{\mathbf{q}\neq 0} \frac{1}{q^m} \left\{ \frac{1}{\mu} e^{-2q^m \nu (t-s)} - \frac{1}{\mu} e^{-2q^m [\nu(t-s)+\mu s]} \frac{1}{\nu} \left(1 - e^{-2q^m \nu (t-s)} \right) \right\} \tag{6.18}$$

for $t \geq s$, which finally gives the expression

$$\chi(t,s) = \frac{D}{2L^d \epsilon} \sum_{\mathbf{q}\neq 0} \frac{1}{q^m} e^{-2q^m \nu (t-s)} \left\{ \frac{1}{\mu} \left(1 - e^{-2q^m \mu s} \right) - \frac{1}{\nu} \left(1 - e^{-2q^m \nu s} \right) \right\} \tag{6.19}$$

for our response function. To give a rough idea of how the response function behaves in the different time regimes we will next focus on the result for the one-dimensional Edwards-Wilkinson equation Eq. (4.7), where $d = 1$ and $m = 2$, before general discussions in the following subsections. As we discussed in Chapters 3 and 4, the 1D EW equation can be simulated by the MRDSR model by relating the surface tension ν to the temperature. Therefore, the perturbation with respect to the surface tension ν can be realized by changing the temperature. We will start with the discussion of the results obtained both from the exact solution of the EW equation and simulations of the MRDSR model. To set the stage for discussions, we begin with the data for some typical cases, all with $s = 10^5$, shown in Figure 6.3. In order to be able to discuss the different cases for a fixed s, we must work with a relatively small system: $L = 400$. The data are obtained by averaging over 10,000 different growth events. The dashed lines in (a-c) represent $W_\nu^2(t)$ in an unperturbed system. With $T_f = 10^9, 10^3$, and 1 (the corresponding fitted values of the surface tension ν are shown in Table 4.1), the surface is, at the time of the quench, in the (a) RD, (b) EW, and (c) saturation regimes, respectively. The corresponding differences, $\Delta W^2(t,s) = \epsilon\chi$, are shown in Figure

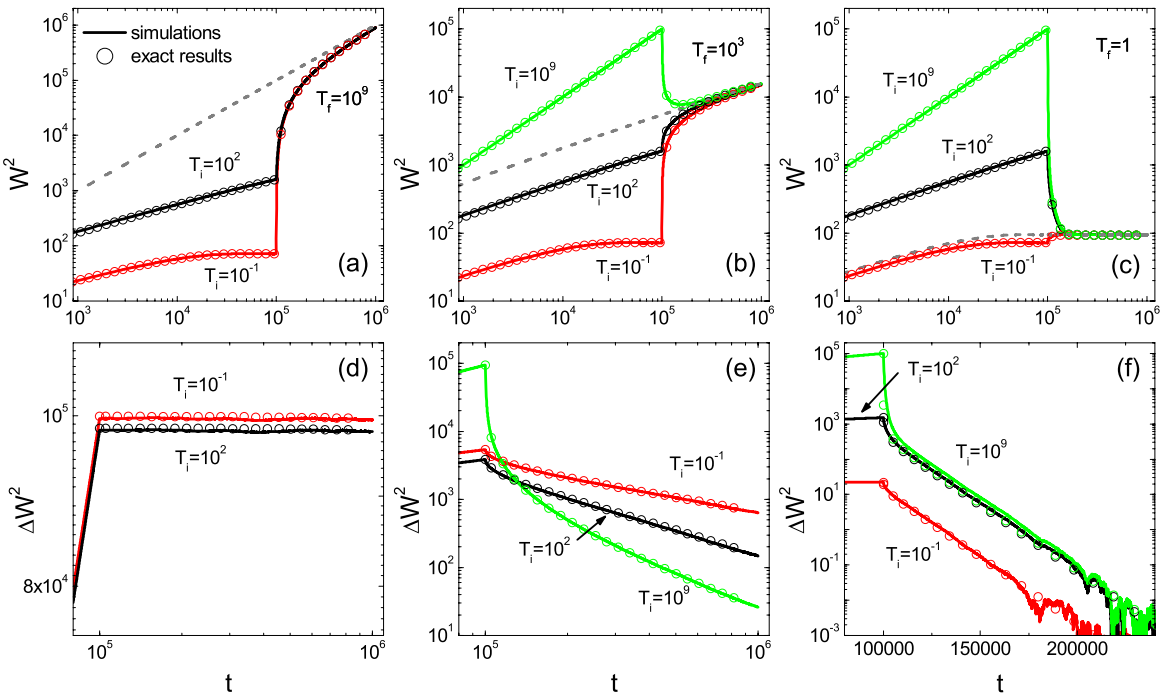

Figure 6.3: (a-c) Time evolution of the width square in case the temperature is changed after 10^5 time steps. The full lines show the data obtained from numerical simulations of the temperature dependent deposition model (MRDSR). These data have been obtained for systems with L = 400 sites after averaging over 10,000 different growth events. The dashed lines show W_ν^2 for an unperturbed surface growing at the constant temperature T_f. In (a) the quench is to the RD regime, whereas in (b) and (c) the quenches are to the EW and saturation regimes, respectively. (d-e) The same cases as shown in (a-c), but now the difference $\Delta W^2 = \epsilon\chi$ is plotted. Qualitative different behavior is observed, depending on the regime that the unperturbed system has at the quench time. The circles are obtained from the exact solution of the EW equation. Note that the panel (f) is linear in t.

6.3 (d-f). The effects of two up-quenches into the RD regime, from the EW ($T_i = 10^2$) and the saturation ($T_i = 10^{-1}$) regimes, are displayed in Figure 6.3 (a). As Figure 6.3 (d) shows, for quenches into RD, the width $W^2_{\mu\to\nu}(t,s)$ cannot reach that of the reference system, $W^2_\nu(t)$. The "best" $\Delta W^2(t,s)$ can achieve is a constant. The physical origin of this behavior lies in the linear growth of W^2 in the RD regime. Thus, for two unperturbed systems started at different times (say, $t = t_0$ and t_1), the difference $W_0^2 - W_1^2$ is just a constant: $t_1 - t_0$. In our case, the correlated growth up to time s endowed our surface with a smaller $W^2_{\mu\to\nu}(t,s)$ than the reference $W^2_\nu(s)$. Immediately after the quench, correlated growth is simply replaced by independent growth of different columns and the width $W^2_{\mu\to\nu}(s)$ is "frozen" in as a kind of "initial condition" (at $t = s$). As a result, the difference $\Delta W^2 = W^2_\nu(t) - W^2_{\mu\to\nu}(t,s)$ remains at the value $W^2_\nu(s) - W^2_{\mu\to\nu}(s,s)$. Of course, if we follow these two systems further in time, ΔW^2 will eventually vanish. Turning next to quenches to the EW regime, we found the most interesting behavior (see Figure 6.3 (b, e)). The difference ΔW^2 initially decreases rapidly before crossing over to a slower, power-law decay at larger times ($t \gg s$):

$$\Delta W^2 \sim t^\gamma \tag{6.20}$$

Here, we observed the exponent γ to be typically $-1/2$ or $-3/2$. We will discuss in more detail the conditions under which these values can be expected in the next subsection. Finally, for a quench to the saturation regime, ΔW^2 decays exponentially:

$$\Delta W^2 \sim \exp(-\kappa t) \tag{6.21}$$

with a decay constant κ that depends on the value of the final temperature T_f. Up to now, we have shown only the simplest situation where the system is well within a given initial regime at the moment of the quench and, in addition, that it has time to relax into a well defined regime of the reference system. Clearly, as we let the final system evolve further, it may cross over to a different regime (e.g., in case of Fig. 6.3a,d a crossing over to the EW and saturation regimes will take place for larger t). Therefore, we should expect the general relaxation process to be quite complex.

6.2.1 Dynamic phase diagram

The closed form Eq. (6.19) is not particularly transparent, as it involves all possible crossover behaviors. To shed some light on the various scenarios, we consider some limiting cases where simple properties (exponentials and powers) can be extracted. We note that Eq. (6.19) is controlled by three length scales, l_t, $l_\nu \equiv l_s$ and $l_\mu \equiv (2\mu s)^{1/m}$. In this section we will focus on how the competition between l_ν and l_μ affects these simple properties for $t \gg s$. For the following discussion, we define $g(l_\nu, l_\mu) \equiv \frac{1}{\mu}\left(1 - e^{-l_\mu^m q^m}\right) - \frac{1}{\nu}\left(1 - e^{-l_\nu^m q^m}\right)$.

1. If both l_ν and l_μ are larger than $1/q_{min}$, one has $g(l_\nu, l_\mu) \approx \frac{1}{\mu} - \frac{1}{\nu}$, which implies

$$\chi \approx \frac{dD}{L^d\epsilon}\left(\frac{1}{\mu} - \frac{1}{\nu}\right)\frac{1}{q_{min}^m} e^{-2q_{min}^m \nu(t-s)}, \tag{6.22}$$

since the condition $t \gg s$ yields $l_t > 1/q_{min}$ as well.

2. If $l_\nu > 1/q_{min}$ but $l_\mu < 1/q_{max}$, one has $g(l_\nu, l_\mu) \approx 2q^m s$. By the same method as in case 1. we have
$$\chi \approx \frac{2dDs}{L^d \epsilon} e^{-2q_{min}^m \nu(t-s)} \tag{6.23}$$

3. In the opposite limit, where $l_\nu < 1/q_{max}$ but $l_\mu > 1/q_{min}$, we have $g(l_\nu, l_\mu) \approx -2q^m s$. Since we are not required to be in the large l_t limit, summing over $\mathbf{q}$ yields
$$\chi \sim s(t-s)^{-\frac{d}{m}} \tag{6.24}$$

4. Another case which yields a power-law decay is when both l_ν and l_μ are less than $1/q_{max}$. In this case we have $g(l_\nu, l_\mu) \approx 2(\nu - \mu)s^2 q^{2m}$. The summation over $\mathbf{q}$ yields
$$\chi \sim s^2(t-s)^{-1-\frac{d}{m}} \tag{6.25}$$

5. If we further impose that $l_t \ll 1/q_{max}$, we have
$$\chi \sim s^2 \tag{6.26}$$

To examine the behavior of the response function Eq. (6.19) comprehensively, we define $\chi \sim t^\gamma$ and evaluate γ numerically. We note that the function $\nu\epsilon\chi$ depends only on three scaling variables, μ/ν, νs, and t/s. In the presence of a power-law, the response function can be rewritten as $\nu\epsilon\chi = a(t/s)^\gamma$, where a is a constant. The exponent γ is now a function of μ/ν, νs, and t/s and can be defined effectively as $d\log(\nu\epsilon\chi)/d\log(t) = d\log(\chi)/d\log(t)$.[2] In the following, we consider the 1D EW equation as an example. In Fig. 6.4 we show the contour plot of γ as a function of μ/ν and νs for $t/s = 64$. This plot reveals four different regimes. First, the regime of exponential decay for large νs corresponds to the cases 1 and 2. Second, two power-law regimes correspond to the limits where νs is small. In the large μs limit (the case 3) we observe that $\gamma = -1/2$ which is exactly $-d/m$, and in the small μs limit (the case 4) we have $\gamma = -3/2$ which is $-1 - d/m$. Finally, the regime where χ or $\nu\epsilon\chi$ is constant (labeled by $\gamma = 0$) corresponds to case 5. The different regimes are separated by crossover regions where the effective exponent does not lock-in into one of the values 0, $-1/2$, or $-3/2$. Fig. 6.5a shows how the extensions of the four regimes depend on the value of t/s in cases where $t/s \gg 1$. Interestingly, an increase of the value of t/s mainly shifts the contours in the $\log(\nu s)$ *vs.* $\log(\mu/\nu)$ plot along the $(-1, 1)$ direction. This is shown in Fig. 6.5b where we plot $\log(\nu t)$ *vs.* $\log(\mu s/\nu t)$. This way of plotting indeed leads to an approximate data collapse, which gets better for larger values of t/s. That this data collapse is only approximate also follows from inspection of the exact solution (6.19). Still, Fig. 6.5b nicely allows us to visualize the extend of the different dynamic regimes for large ratios t/s. Finally, in Fig. 6.6, we discuss the change of the effective exponent γ as a function of t for

[2]Since γ is no longer a constant, to evaluate it we need to look at the slope of $\nu\epsilon\chi$ in a log-log plot, which is the derivative. After taking the derivative of $\log(\nu\epsilon\chi)$ or $\log(\chi)$ with respect to $\log(t)$, we obtain γ, which is, indeed, a function of μ/ν, νs, and t/s.

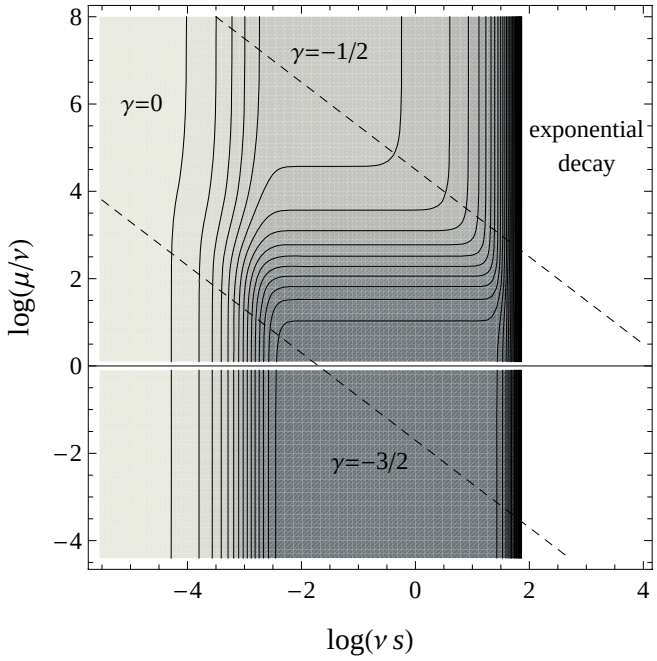

Figure 6.4: Contour plot of γ as a function of νs and μ/ν for $t/s = 64$. Four different regimes, separated by crossover regions, are identified. The two dashed lines separate the three qualitatively different types of behavior encountered when plotting the effective exponent as a function of t, see Fig. 6.6. *Phys. Rev. E* 80(6): 061602. Used with permission of American Physical Society, 2009.

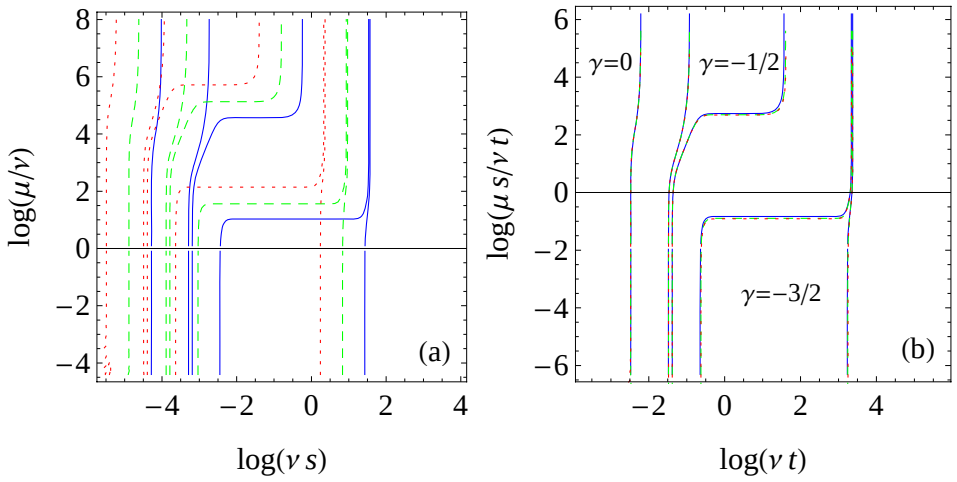

Figure 6.5: (a) Contour plots of γ as a function of νs and μ/ν for $t/s = 64$ (full blue line), 256 (dashed green line), and 1024 (dotted red line). Only contours bounding the $\gamma = 0$, $-1/2$ and $-3/2$ regimes are shown. (b) The same contour plots as shown in (a) but as a function of νt and $\mu s/\nu t$. A collapse of the contours is observed.

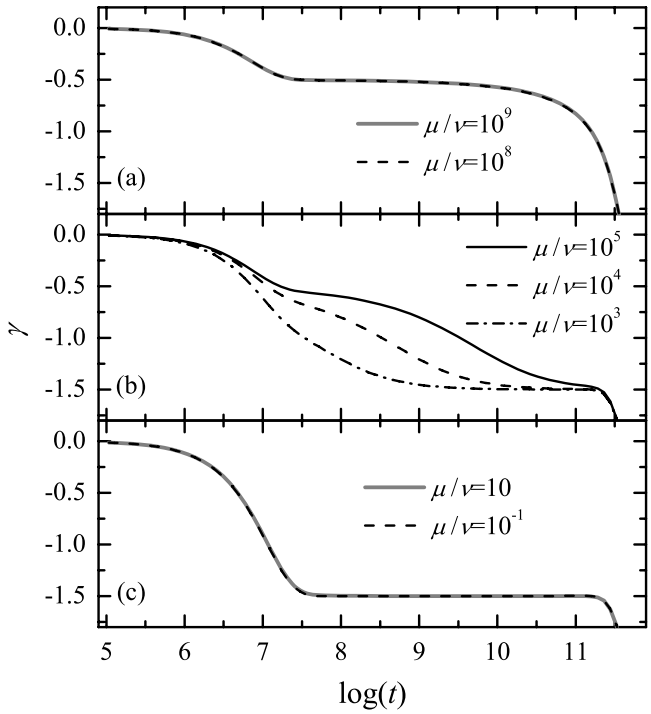

Figure 6.6: The three different quench types illustrated by the time dependence of the effective exponent γ. In all cases the quench takes place at $s = 10^5$. Type (a) includes quenches with initial conditions νs and μ/ν located above the upper dashed line in Fig 6.4. For type (b) the starting point is located between the two dashed lines in Fig 6.4, whereas for type (c) the initial conditions put the starting point below the lower dashed line.

various values of μ/ν (and $s = 10^5$). Note that an increasing time t corresponds in Fig. 6.4 approximately to a cut along the $(-1, 1)$ direction, so that we can distinguish three typical scenarios, separated by the dashed lines there. Along the upper dashed line, Fig. 6.6a shows the effective exponent decreasing to the $\gamma = -1/2$ plateau where it remains for a long time before crossing over to the regime where the difference $\Delta W^2 = \epsilon\chi$ vanishes exponentially fast ("$\gamma = -\infty$"). For the region above this line in Fig. 6.4, we can expect similar results. Along the lower dashed line, the same behavior is seen, except that the plateau value is now $\gamma = -3/2$ (Fig. 6.6c). This can also be expected for the region below this lower dashed line in Fig. 6.4. Between these two protocols, a more complex behavior is encountered, as the effective exponent shows some tendency to lock-in at both values $-1/2$ and $-3/2$ (see Fig. 6.6b). We should remind the reader that the $\gamma(t)$ curves shown here are applicable for all varieties of quenches (different quench times, as well as initial and final temperatures) as long as the rescaled time νs is fixed.

$s \setminus t$	RD	CR	SR
SR	–	–	$ae^{-b(t-s)}$
CR	–	$as^{1-d/m}\,(t/s)^{-d/m-1}$	$a\,s^2\,e^{-b(t-s)}$
RD	$a\,s^2\,(1-b\,t-c\,s)$	$as^{1-d/m}\,(t/s)^{-d/m-1}$	$a\,s^2\,e^{-b(t-s)}$

Table 6.2: The same as Table 6.1, but now for the response (6.19) to a small perturbation during which the surface tension is changed. The values of a, b and c, which depend on the case considered, can be read off from the equations in the main text.

6.2.2 Small perturbation

Having a general idea of the behavior of the response function, we next focus on the special case of small perturbations. For small perturbations, where $|\epsilon| \ll 1$, three length scales reduce to two: $l_\mu \approx l_\nu = l_s$. Therefore, we can proceed as for the correlation function in the previous section. As we have the same cases and therefore can use the same approximation schemes (see Figure 6.1), we shall only quote the final expressions (see Table 6.2 for a summary).

1. At early times, where t is still in the RD regime, we have a linear decay,

$$\chi(t,s) \approx \frac{D\pi^{d/2+m}}{2^{d-1}\Gamma(d/2)(d+m)} s^2 \left\{ 1 - 2\frac{d+m}{d+2m}\pi^m \left[\nu(t-s) + \frac{1}{3}(\nu+\mu)s \right] + \mathcal{O}(\nu t)^2 \right\} . \tag{6.27}$$

2. When t is in the correlated regime, we obtain for a perturbation that lasted only until some time s in the RD regime the following expression for the response:

$$\chi(t,s) \approx B_{m,d} s^2 (t-s)^{-d/m-1}, \tag{6.28}$$

with

$$B_{m,d} = \frac{Dd\,\Gamma(d/m)}{2^{d+d/m}\pi^{d/2} m^2\,\Gamma(d/2)\nu^{d/m+1}} . \tag{6.29}$$

If, however, the perturbation ended inside the correlated regime (the regime $2'$ in Figure 6.1), we have

$$\begin{aligned} \chi(t,s) &= B_{m,d} s^2 (t-s)^{-\frac{d}{m}-1} \left\{ 1 - \frac{\nu+\mu}{3\nu}\left(\frac{d}{m}+1\right)\left(\frac{t}{s}-1\right)^{-1} + \cdots \right\} \\ &\approx B_{m,d} s^2 (t-s)^{-\frac{d}{m}-1}, \end{aligned} \tag{6.30}$$

yielding the same leading behavior as for a perturbation that already stopped in the RD regime. In the correlated regime we can therefore cast the response in the standard form $\chi(t,s) = s^{-a} f_\chi(t/s)$ with $a = \frac{d}{m} - 1$ and $f_\chi(t/s) \sim (t/s)^{-\lambda_R/z}$ for t/s large, with

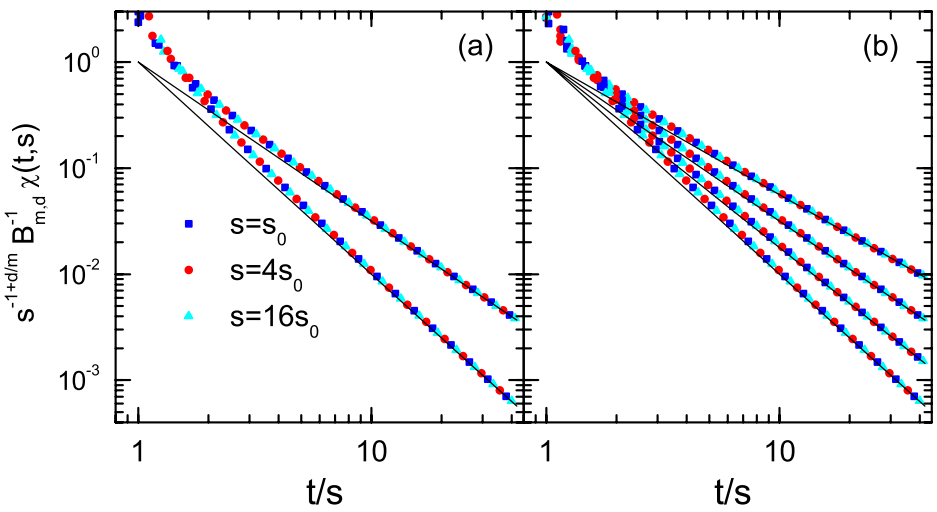

Figure 6.7: Global response to a change of the surface tension when both times t and s are in the correlated regime. The symbols are obtained by numerically evaluating the exact expression (6.19) whereas the lines indicate the asymptotic power-laws (6.30). Panel (a) shows data for the EW case and dimensions $d = 1, 2$ (from top to bottom), panels (b) show data for the MH case and dimensions $d = 1, 2, 3, 4$ (from top to bottom). The different symbols correspond to different waiting times where $s_0 = 1000$ below the critical dimension and $s_0 = 200$ at the critical dimension (which is $d = 2$ for EW and $d = 4$ for MH). The linear extension of the system is $L = 2^{14}$ for $d = 1$, $L = 2^9$ for $d = 2$, $L = 2^7$ for $d = 3$, and $L = 2^6$ for $d = 4$.

$\lambda_R = d + m$. We show this scaling behavior in Figure 6.7 a,b for the EW and for the MH case and compare the scaling function to the asymptotic power-law. One can now also compare the values of the exponents with those obtained for the global correlation function Eq. (6.2) as well as with those obtained for the response of the height to a local perturbation, see [83]. Comparing with the global correlation, one notes that we have the interesting situation that $a \neq b$ and $\lambda_R \neq \lambda_C$. It is rather uncommon that the response of some quantity and the correlation of the same quantity display a different asymptotic behavior in the aging regime [47]. Mathematically, this intriguing observation can be traced back to the fact that in the expression Eq. (6.6) for the correlation q^{2m} shows up in the denominator whereas q^m is encountered in the denominator of the corresponding expression (6.19) for the response function. In order to compare the global response with the local response, we need to look at the time integrated local response. Inserting the expressions given in [83] for the local response R_ℓ (where $R_\ell \sim (t-s)^{-d/m}$) into the integral $\chi_\ell(t,s) = \int_0^s du\, R_\ell(t,u)$ yields for the local time integrated response the form $\chi_\ell(t,s) = s^{-a_\ell} f_{\chi_\ell}(t,s)$ where the exponent a_ℓ has the value $a_\ell = \frac{d}{m} - 1$, whereas the exponent governing the scaling function in the long time regime is $\lambda_{R,\ell} = d$. We therefore have that the scaling exponent $a = a_\ell$ is the same for both responses but that the global and the local autoresponse exponents differ, $\lambda_R = \lambda_{R,\ell} + m$.

3. If the observation time is in the saturation regime, we obtain that

$$\chi(t,s) \approx \frac{2^{d+m} D \pi^m}{L^{m+d}} s^2 e^{-2q_{min}^m \nu (t-s)} \tag{6.31}$$

for a perturbation that comes to an end before entering the saturation regime.

4. Finally, if both the observation time and waiting time are in the saturation regime, we have

$$\chi(t,s) \approx \frac{D L^{m-d}}{2^{m-d+1} \pi^m \mu \nu} e^{-2q_{min}^m \nu (t-s)}. \tag{6.32}$$

6.3 Response function for linear growth 2 : Changing the noise strength

For the second protocol we proceed analogously. We again start from an initially flat surface and let the system evolve with the strength D' of the noise correlation until the waiting time s at which we set this strength to the final value D. We then compute the function

$$\chi_D(t,s) = \frac{\langle W^2 \rangle_{D' \to D}(t,s) - \langle W^2 \rangle_D(t)}{\epsilon} \tag{6.33}$$

$s \setminus t$	RD	CR	SR
SR	–	–	$ae^{-b(t-s)}$
CR	–	$as^{1-d/m}\,(t/s)^{-d/m}$	$a\,s\,e^{-bt}$
RD	$a\,s\,(1-b\,t)$	$as^{1-d/m}\,(t/s)^{-d/m}$	$a\,s\,e^{-bt}$

Table 6.3: The same as Table 6.2, but now for the response (6.33) to a change in the strength of the noise correlation. The values of a, b and c, which depend on the case considered, can be read off from the equations in the main text.

with $\epsilon = D' - D$. This is again a time integrated response. A straightforward calculation yields the expression

$$\chi_D(t,s) = \frac{1}{2L^d\nu}\sum_{\mathbf{q}\neq 0}\frac{1}{q^m}e^{-2q^m\nu t}\left(e^{2q^m\nu s}-1\right) \tag{6.34}$$

for this global response. Again, we briefly discuss the limiting cases in the following (see Table 6.3).

1. At early times with $l_t < 1/q_{max}$ we have again a linear decrease of the global response:

$$\chi_D(t,s) \approx \frac{s\pi^{d/2}}{2^{d-1}\Gamma(\frac{d}{2})d}\left(1-\frac{2d}{d+m}\pi^m\nu t\right)\ . \tag{6.35}$$

2. In the correlated regime we obtain for a perturbation ending before the end of the RD regime:

$$\chi_D(t,s) \approx C_{m,d}\,s\,t^{-d/m} \tag{6.36}$$

with

$$C_{m,d} = \frac{\Gamma(\frac{d}{m})}{2^{d+d/m-1}\nu^{d/m}\pi^{d/2}m\Gamma(\frac{d}{2})}\ . \tag{6.37}$$

If the perturbation only ends in the correlated regime, the result is

$$\chi_D(t,s) = C_{m,d}\,s\,t^{-d/m}\left(1+\frac{d}{2m}\frac{s}{t}+\cdots\right)\ , \tag{6.38}$$

yielding the same asymptotic behavior. This scaling behavior is shown in Fig. 6.8a,b for the EW and MH cases. Comparing the expressions (6.38) and (6.30) we see that the scaling properties of the response of the square of the surface width depends on how the growing interface has been perturbed. More precisely we find that (1) the scaling exponent a is independent of the protocol, but that (2) the autoresponse exponent λ_R is now equal to d, i.e. the response of the system decays in the long time limit slower when the perturbation is due to a change of the noise strength. Interestingly, the global response to a change in D has the same power-law as the global autocorrelation.

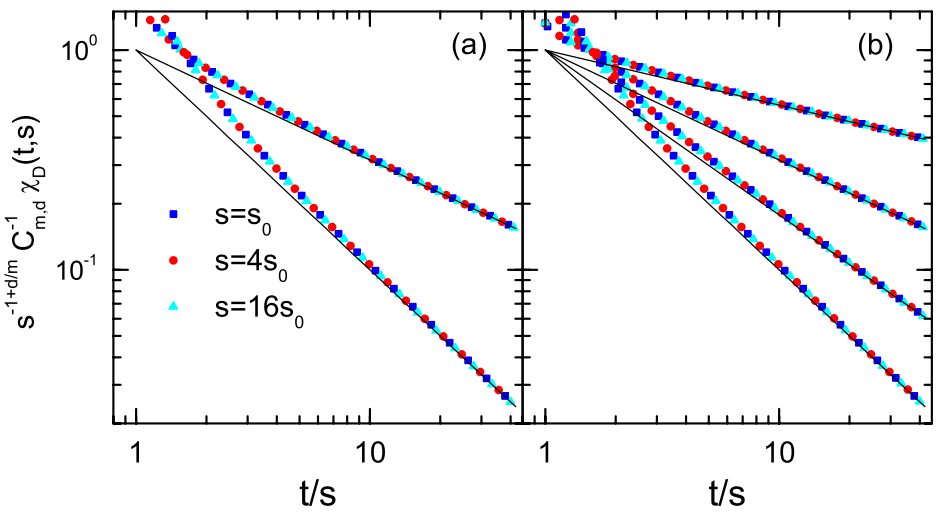

Figure 6.8: Global response to a change of the noise strength when both times t and s are in the correlated regime. The symbols are obtained by numerically evaluating the exact expression (6.34) whereas the lines indicate the asymptotic power-laws (6.38). Panel (a) shows data for the EW case and dimensions $d = 1, 2$ (from top to bottom), panels (b) show data for the MH case and dimensions $d = 1, 2, 3, 4$ (from top to bottom). The different symbols correspond to different waiting times where $s_0 = 1000$ below the critical dimension and $s_0 = 200$ at the critical dimension (which is $d = 2$ for EW and $d = 4$ for MH). The linear extension of the system is $L = 2^{14}$ for $d = 1$, $L = 2^9$ for $d = 2$, $L = 2^7$ for $d = 3$, and $L = 2^6$ for $d = 4$.

3. If we measure in the saturation regime the response to a perturbation that ended before reaching that final regime, we have that

$$\chi_D(t,s) \approx \frac{2ds}{L^d} e^{-2q_{min}^m \nu t} \ . \tag{6.39}$$

4. Finally, if the perturbation continues until the saturation regime is reached, then

$$\chi_D(t,s) \approx \frac{dL^{m-d}}{2^m \pi^m \nu} e^{-2q_{min}^m \nu (t-s)} \ . \tag{6.40}$$

6.4 Fluctuation-dissipation ratios for linear growth

The fluctuation-dissipation ratio [27] has been introduced as a generalization of the celebrated fluctuation-dissipation theorem to non-equilibrium systems (see Chapter 2). Whereas this ratio has some appealing features, as for example its simplicity and the possibility to assign an effective temperature to a non-equilibrium system [29], many studies in model systems have revealed major problems with that quantity, ranging from observable dependent effective temperatures [42, 17] to the appearance of negative temperatures [67, 43]. As a result, the usefulness of the fluctuation-dissipation ratio is in general very restricted, even though it might occasionally yield interesting insights in specific systems. The fluctuation-dissipation ratios of local quantities and the related effective temperatures have also been studied for the one-dimensional EW equation [16] (higher dimensional cases and the MH cases can be inferred from the equations given in [83]). This study shows that the ratio of the response $R_\ell(t,s)$ of the height to the height-height correlation $C_\ell(t,s)$ allows in the linear systems to characterize the different growth regimes through an effective temperature.

We will next study the fluctuation-dissipation ratios due to a global perturbation. To do so we need to find a suitable pair of global conjugate variables. Let us consider a configuration where the height of the column at site i is h_i. Setting the lattice constant in vertical direction to be 1 and setting the potential energy of the initial flat surface to be zero, the potential energy U_i stored in a column of height h_i is (with the mass of a deposed particle set to 1)

$$\frac{U_i}{T} = \frac{g}{T} + 2\frac{g}{T} + \cdots + (h_i - 1)\frac{g}{T} = h_i(h_i-1)\frac{g}{2T} \ . \tag{6.41}$$

Shifting the value zero of the potential energy to the average height $\overline{h} = \frac{1}{N}\sum_{i=1}^{N} h_i$, where $N = L^d$ is the number of sites on the substrate, we obtain for the total potential energy of our configuration the value

$$\frac{U}{T} = \sum_{i=1}^{N} \frac{U_i}{T} = \frac{g}{2T}\sum_{i=1}^{N}\Big(h_i(h_i-1) - \overline{h}(\overline{h}-1)\Big) = \frac{g}{2T}\sum_{i=1}^{N}\Big(h_i^2 - \overline{h}^2\Big) = \frac{gN}{2T}W^2 \tag{6.42}$$

where $W^2 = \frac{1}{N}\sum_{i=1}^{N}\left(h_i^2 - \overline{h}^2\right) = \frac{1}{N}\sum_{i=1}^{N}\left(h_i - \overline{h}\right)^2$ is the squared width. From this it follows that $\frac{N}{2}W^2$ is the quantity conjugated to g/T and, as $g/T \sim \nu$, to ν. Therefore, by rescaling the global correlation and response functions as

$$\begin{aligned} \widetilde{C}(t,s) &\equiv \frac{L^{2d}}{4}C(t,s) \\ \widetilde{\chi}(t,s) &\equiv \frac{L^{d}}{2}\chi(t,s) \end{aligned} \tag{6.43}$$

we can discuss the fluctuation-dissipation ratio

$$X(t,s) = \frac{\partial_s \chi(t,s)}{\partial_s C(t,s)} = \frac{\chi(t,s)}{C(t,s)} \tag{6.44}$$

and measure the limit value $X_\infty = \lim_{s\longrightarrow\infty}\lim_{t\longrightarrow\infty} X(t,s)$ [47]. Note that the last equality in Eq. 6.44 is valid when $\chi(t,s)$ and $C(t,s)$ have the same s-dependent part. This is indeed the case for our system (see Tables 6.1 and 6.2.) Strictly speaking, taking this limit does not yield non-trivial results for our global quantities. Assuming this system to be infinite (such that one remains in the correlated regime in the long-time limit), one immediately sees from the Tables 6.1 and 6.2 that the trivial value $X_\infty = 0$ is obtained for the global fluctuation-dissipation ratio, and it is not possible to introduce a meaningful effective temperature. Still, the quantity $X(t,s)$ does yield at finite times a behavior that is characteristic for the different regimes, as shown in Figure 6.9 for the ratio formed by the global response to a change in ν and the global correlation. In order to understand this figure, let us look at a case (the case $s = 1$ in the figure) where the waiting time is in the RD regime. If $t \approx s$, i.e. t is also in that regime, the ratio (6.44) is constant: $X = \frac{d\pi^m}{D(d+m)}$. If t is such that $1/q_{max} < l_t < 1/q_{min}$, i.e. t is in the correlated regime, X is inversely proportional to t: $X = \frac{d}{2D\nu m}t^{-1}$. The same behavior, albeit with a different pre-factor, is obtained if we consider the global response to a change in D instead. Finally, in the saturation regime, with $l_t > 1/q_{min}$, X is again constant, with $X = \frac{2^{d+m-1}\pi^m}{dDL^m}$. These three regimes are separated by crossover regimes when $l_t \approx 1/q_{max}$ or $l_t \approx 1/q_{min}$. If we choose a different waiting time, $s = 100$ or $s = 10000$ in Figure 6.9, the ratio $X(t,s)$, after some non-universal behavior for $t - s \ll 1$, rapidly evolves towards the same master curve as the $s = 1$ data.

6.5 Two-time Quantities for Non-linear Growth

In order to assess the importance of non-linearities, we also studied global quantities derived from the one-dimensional KPZ equation. We thereby complement the studies [15, 46] which focused on local quantities.

The KPZ equation has been shown to describe faithfully kinetic roughening and to be a paradigmatic model for the description of a large range of non-equilibrium systems [45].

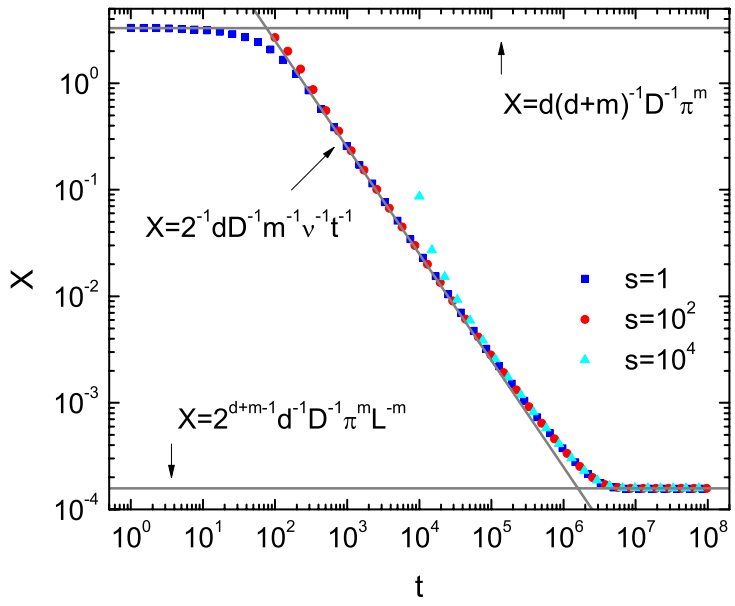

Figure 6.9: The global fluctuation-dissipation ratio for the one-dimensional EW case, with $m = 1$. The ratio (6.44) displays a different behavior in the different regimes. The data have been obtained by numerically evaluating the exact expressions derived in the previous subsections. The parameters are $L = 500$, $D = 1$, and $\nu = 0.001$. *J. Stat. Mech.* P08007. Used with permission of IOP Publishing Ltd and SISSA, 2010.

This well-known equation is given by the expression Eq. (4.35) and differs from the EW equation by the non-linear term proportional to the parameter λ. Here $\eta(\mathbf{x}, t)$ is the usual Gaussian white noise with zero mean and covariance $\langle \eta(\mathbf{x}, t)\eta(\mathbf{y}, s)\rangle = D\delta^d(\mathbf{x} - \mathbf{y})\delta(t - s)$. The numerical integration of (4.35) has been the subject of many studies and different discretization schemes have been proposed in order to handle the non-linearity (see, for example, [76, 62, 14, 71, 91] and Chapter 4).

We also studied for this system the global correlation and response functions introduced in the previous sections. In order to make sure that our results are independent of the integration schemes, we computed these quantities using different approaches, namely the scheme of Lam and Shin [62] as well as the strong coupling scheme proposed by Newman and co-workers [76, 77] (see also Chapter 4). We carefully checked that we are in the correlated regime at both times s and t. We also verified that both approaches yield the same exponents and scaling functions for the studied quantities [3]. The data obtained from both schemes differ by a non-universal pre-factor, as expected. Small deviations between the data sets are observed for $t \approx s$, but this is again expected as for the Lam/Shin scheme we use finite values of λ, whereas the Newman scheme works in the strong-coupling limit where

[3]Due to the very nature of the Newman algorithm, the surface tension is not a parameter that can be changed in that scheme. Therefore, we only computed with that method the global correlation function as well as the global response to a change in the noise strength.

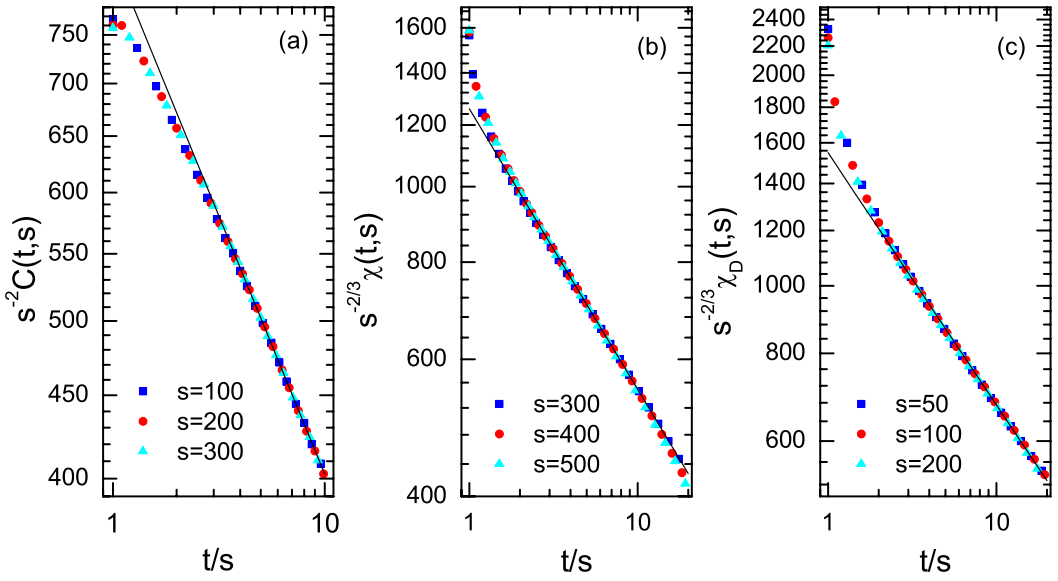

Figure 6.10: Log-log plots of global quantities as a function of t/s obtained from the one-dimensional KPZ equation in the correlated regime: (a) global correlation (b), global response to a change of the surface tension ν, and (c) global response to a change of the noise strength D. The data in (a) and (c) have been obtained with the Newman algorithm [76, 77], whereas the data in (b) result from the algorithm of Lam and Shin. We checked that both algorithms produce the same exponents and scaling functions for a given quantity. The system size is $L = 10000$, with $\lambda = 1$, $\nu = 1$, and $D = 1$. For the response shown in (b), ν has the value of 1.1 until time s at which point it is changed to the value 1, whereas for (c) D was changed from the value 1.1 to 1 at time s. The data shown have been obtained after averaging over 5×10^6 realizations for the correlation and 5×10^5 realizations for the response. The lines indicate the asymptotic power-law behavior. *J. Stat. Mech.* P08007. Used with permission of IOP Publishing Ltd and SISSA, 2010.

$\lambda \longrightarrow \infty$. Fig. 6.10 summarizes our main findings regarding the scaling behavior of global quantities in the one-dimensional KPZ universality class. For the autocorrelation (6.2) we find the scaling form

$$C(t,s) = s^2 \, f_C(t/s) \tag{6.45}$$

with $f_c(y) \sim y^{-1/3}$ for $y \gg 1$. For the response functions we note, and this is in strong contrast to the results we obtained for the linear equations, that the scaling behavior does not depend on the protocol that we use for perturbing the system [4]. Whether we change the

[4] Noting that by rescaling the height h and the time t as $h' = \lambda^{1/3} h$ and $t' = \lambda^{2/3} t$ we can rewrite the KPZ equation as

$$\frac{\partial h'(\mathbf{x},t')}{\partial t'} = \nu' \nabla^2 h'(\mathbf{x},t') + (\nabla h'(\mathbf{x},t'))^2 + \eta(\mathbf{x},t') \; ,$$

where $\nu' = \nu/(D\lambda^2)^{1/3}$ and the noise is still Gaussian with the same strength D, we only consider the same two types of perturbations as for the linear systems.

surface tension or the noise strength, we always end up with the following scaling behavior of the global response:

$$\chi(t,s) = s^{2/3}\, f_\chi(t/s) \tag{6.46}$$

with $f_\chi(y) \sim y^{-1/3}$ for $y \gg 1$. This difference between the global response in the linear and the non-linear cases is remarkable. At this stage, we can only speculate on the origin of this, but it seems that the restoring mechanism, that is responsible for the relaxation of the perturbed but still growing interface, originates in the non-linearity, thereby yielding the same scaling behavior independent of the nature of the perturbation. Further studies seem to be in order to fully clarify this point.

We can compare the scaling forms (6.45) and (6.46) with themselves as well as with the scaling forms of the local quantities. We remark that we have: $a = -2/3$ and $a_\ell = -1/3$, $b = -2$ and $b_\ell = -2/3$, $\lambda_C = \lambda_\chi = -1/3$ and $\lambda_{C_\ell} = \lambda_{\chi_\ell} = -2/3$, i.e. the global exponents always differ from their corresponding local exponents.

Finally, let us mention that also for the KPZ case one does not obtain non-trivial limits for global fluctuation-dissipation ratios. Still, one can perform a similar analysis as done in the previous section for the linear systems, thereby recovering the same three regimes, but with a different dependence on t, $X \sim t^{-4/3}$, in the correlated regime.

6.6 Summary

Our study of global quantities in growth processes has revealed some interesting results, especially in the correlated regime, and raises a range of open questions that warrant a more in-depth study in the future.

A prediction of the scaling behavior of our global quantities is far from obvious, due to the complicated nature of the mean square width that involves all Fourier components (with the exception of the zero mode) of the Fourier series representation of the surface height. We find the available results to be compatible with the scaling form

$$C(t,s) = s^{4\alpha/z+d/z}\, f_C(t/s)\ , \tag{6.47}$$

with $f_C(y) \approx y^{2\alpha/z-1}$ for $y \gg 1$, as is readily checked by recalling that for the linear equations $\alpha = \frac{z-d}{2}$ and $z = m$ whereas for the one-dimensional KPZ equation $\alpha = \frac{1}{2}$ and $z = \frac{3}{2}$. Similarly, the global response of the square of the surface width to a change in the noise strength (we need to specify this for the linear systems) is compatible with the scaling form

$$\chi(t,s) = s^{2\alpha/z}\, f_\chi(t/s)\ , \tag{6.48}$$

with $f_\chi(y) \approx y^{2\alpha/z-1}$ for $y \gg 1$. We are not able to derive these scaling forms at this stage.

In fact, the situation for the response function is rather complex. The reason is of course that for the linear systems the global response depends on how the system was perturbed,

as the different protocols lead to different scaling forms. This is different for the non-linear KPZ equation, as here the same scaling forms are found for the different perturbations. Obviously, the non-linearity provides an efficient smoothening mechanism that allows the system to relax to the state of the unperturbed system in a way that is independent on how the system has been perturbed. This mechanism is absent in the linear systems, yielding the observed dependence of the response on the protocol. A more quantitative study of this effect is left for the future.

Our study also reveals that in the correlated regime the usual limit value of the fluctuation-dissipation ratio involving global quantities only leads to trivial results. However, the ratio (6.44) at finite observation times still allows us to distinguish between the different growth regimes.

Experimentally a global response is much easier to measure than a local one. Local perturbations and local measurements are not easily achieved in a growing system. This is different for a global response that is readily observed when changing the experimental conditions, for example through a change in temperature, as this automatically affects the whole system. Another advantage of studying global quantities in the context of growth processes is seen at the upper critical dimension. Indeed, global quantities continue to display a standard dynamical scaling behavior at the critical dimension. Local quantities, however, generically display a logarithmic dependence on time in that case which makes an analysis much more demanding. For these reasons we hope that our study will motivate other groups, especially experimental ones, to use global quantities for the characterization of non-equilibrium growth processes.

Chapter 7

Global Two-time Quantities II

In the previous chapter we studied two-time quantities related to the surface width. We obtained a nice dynamic scaling behavior for the correlation and response functions both for linear and non-linear systems. However, we encountered severe limitations when discussing the fluctuation-dissipation relation for non-equilibrium growth by looking at the surface width. The Edwards-Wilkinson equation was the only case for which we were able to discuss the fluctuation-dissipation ratio to some extent. However, the different exponents for the correlation and response functions in the power-law decay regime prohibit a general result for the fluctuation-dissipation relation in the non-equilibrium state. In this chapter we discuss a quantity, denoted by G_m, which is conjugated to the diffusion constant ν for the Edwards-Wilkinson and Mullins-Herring equations through the effective Hamiltonian. We first discuss some of the properties of G_m analytically. We then study the correlation function, the response function, and the fluctuation-dissipation ratio related to G_m. A general fluctuation-dissipation relation for non-equilibrium systems based on a recent research by Baiesi, Maes and Wynants [6] can be investigated using this quantity. We show that the fluctuation-dissipation relation we derived from the linear Langevin equations satisfies the relation proposed by Baiesi et. al..

7.1 The quantity G_m

The linear Langevin equation (4.9) can be derived by inserting the effective Hamiltonian

$$H_m = \frac{\nu}{2} \int d^d x \left(\nabla^{m/2} h \right)^2 \equiv \nu G_m \tag{7.1}$$

into the equation

$$\frac{\partial h}{\partial t} = -\frac{\delta H_m}{\delta h} + \eta. \tag{7.2}$$

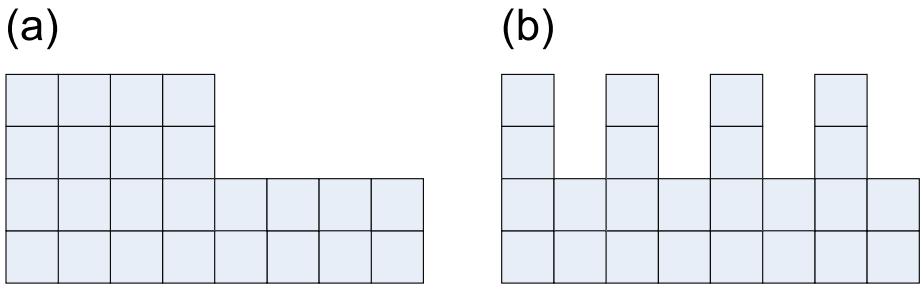

Figure 7.1: Two surfaces with same surface width but different values of G_m.

The quantity G_m, which is conjugated to ν, can be written in the case of a lattice model as

$$G_2 = \frac{1}{2}\sum_{\mathbf{x}}\sum_{i=1}^{d}\Big[h(\mathbf{x}+\mathbf{a}_i) - h(\mathbf{x})\Big]^2 \tag{7.3}$$

for $m = 2$, and

$$G_4 = \frac{1}{2}\sum_{\mathbf{x}}\left\{\sum_{i=1}^{d}\Big[h(\mathbf{x}+\mathbf{a}_i) - 2h(\mathbf{x}) + h(\mathbf{x}-\mathbf{a}_i)\Big]\right\}^2 \tag{7.4}$$

for $m = 4$, where the $\mathbf{a}_i$'s are the primitive vectors on the substrate. The vector $\mathbf{x}$ runs over all points on the Bravais lattice while the index i goes from 1 to the dimension of the substrate. For simplicity the lattice constant a is assumed to be unity. Note that G_2 is the total surface slope[1] and G_4 is the sum of the curvatures. One can use G_m to quantify the roughness of a surface which is usually expressed by the surface width. The difference is that G_m measures the local surface fluctuations whereas the surface width measure the fluctuations with respect to the average height. G_m should convey the concept of the roughness better then the surface width. To explain this claim, let us look at two surface configurations composed of the same amount of particles shown in Figure 7.1. It is easy to see that the value of G_m (for both $m = 2$ and 4) for the surface (b) should be larger then that for the surface (a). This agrees with our intuition of the roughness. However, these two surfaces have the same value for the surface width. The reason is that the surface width overestimates the roughness on the plateau and the basin which are relatively flat.

Our next goal is to derive the exact solution of G_m and discuss its asymptotic behavior for the linear Langevin equation. Using the Fourier transformation of the surface height $h(\mathbf{x})$, we obtain the following expression

$$\langle G_m\rangle = 2^{\frac{m-2}{2}} L^d \sum_{\mathbf{q}\neq 0}\Big\langle h_{\mathbf{q}} h_{-\mathbf{q}}\Big\rangle \mathcal{P}(\mathbf{q})^{m/2}, \tag{7.5}$$

[1]The generalization of this quantity, where the height difference between two columns separated by a displacement $\mathbf{r}$ is calculated, is called the second order height difference correlation function [60].

where

$$\mathcal{P}(\mathbf{q}) = \sum_{i}^{d} \Big(1 - \cos(q_i)\Big). \tag{7.6}$$

The summation of the two point correlation function weighted by the factor $\mathcal{P}(\mathbf{q})^{m/2}$ makes the quantity $\langle G_m \rangle$ significantly different to the average of the square of the surface width $\langle W^2 \rangle$. Using the two point correlation function of the surface height in q-space (Eq. (4.14)) calculated in Chapter 4, we obtain

$$\langle G_m \rangle = 2^{\frac{m-4}{2}} \frac{D}{\nu} \sum_{\mathbf{q}\neq 0} \frac{1}{q^m} \left(1 - e^{-2q^m \nu t}\right) \mathcal{P}(\mathbf{q})^{m/2}. \tag{7.7}$$

The behavior of the quantity $\langle G_m \rangle$ is therefore controlled by the length scale l_t as it is the case for the surface width.

1. For $l_t < 1/q_{max}$, the system is in the random deposition regime. The small l_t limit gives the result

$$\begin{aligned} \langle G_m \rangle &\approx 2^{\frac{m-2}{2}} Dt \sum_{\mathbf{q}\neq 0} \mathcal{P}(\mathbf{q})^{m/2} \\ &\approx 2^{\frac{m-2}{2}} Dt \left(\frac{L}{\pi}\right)^d \int_0^\pi d\mathbf{q} \mathcal{P}(\mathbf{q})^{m/2}. \end{aligned} \tag{7.8}$$

   Further evaluation shows that

$$\langle G_2 \rangle \approx dL^d Dt, \tag{7.9}$$

   and

$$\langle G_4 \rangle \approx d(2d+1)L^d Dt. \tag{7.10}$$

2. For $l_t > 1/q_{min}$, the system enters the saturation regime where $\langle G_m \rangle$ reaches the maximum value

$$\begin{aligned} \langle G_m \rangle = G_{s,m} &\approx 2^{\frac{m-4}{2}} \frac{D}{\nu} \sum_{\mathbf{q}\neq 0} \frac{1}{q^m} \mathcal{P}(\mathbf{q})^{m/2} \\ &\approx 2^{\frac{m-4}{2}} \frac{D}{\nu} \left(\frac{L}{\pi}\right)^d I(m,d), \end{aligned} \tag{7.11}$$

   with the definition $I(m,d) \equiv \int_0^\pi \mathcal{P}(\mathbf{q})^{m/2}/q^m d\mathbf{q}$. The numerically evaluated values of $I(m,d)$ for various d and m are shown in Table (7.1).

3. To calculate the asymptotic behavior in the correlated regime, we take advantage of the observation that $\mathcal{P}(\mathbf{q}) \approx q^2/2$ has hyperspherical symmetry for $q < 1$. This means that if we impose the condition $q < 1$ to the summation, $\sum_{q<1} f(\mathbf{q})$, we can simply replace the sum by the integral $L/(2\pi)^d \Omega_d \int^1 q^{d-1} f(q) dq$ with a cutoff equal to unity. Doubtless, this trick is only valid when the contributions form $f(\mathbf{q})$ with $q > 1$ can

	d=1	d=2	d=3	d=4
m=2	1.21532	3.43997	10.29687	31.53744
m=4	0.49733	1.26083	3.55376	10.51476

Table 7.1: The numerically evaluated values of $I(m,d) \equiv \int_0^\pi \mathcal{P}(\mathbf{q})^{m/2}/q^m d\mathbf{q}$

be neglected. Since the function we are going to sum over involves the factor $e^{-q^m l_t^m}$, this constraint can be implemented by requiring that $l_t \gg 1$ without imposing any additional cutoff. Therefore, after the system enters the correlated regime, we have

$$\begin{aligned} \langle G_m \rangle &\approx G_{s,m} - \frac{D}{4\nu} \sum_{\mathbf{q}\neq 0} e^{-2q^m \nu t} \\ &\approx G_{s,m} - \frac{D}{4\nu} \left(\frac{L}{2\pi}\right)^d \Omega_d \frac{\Gamma(\frac{d}{m})}{m} (2\nu t)^{-\frac{d}{m}} . \end{aligned} \tag{7.12}$$

Here we summarize the behavior of $\langle G_m \rangle$ as follows. When the system is in the random deposition regime, we find that $\langle G_m \rangle$ grows linearly with time t, without any dependence on the diffusion constant ν. However, after the system passes the first crossover point, a pre-factor that depends on the diffusion constant shows up. The system finally reaches the saturation regime where $\langle G_m \rangle$ attains its maximum value $G_{s,m}$. In the correlated regime, $\langle G_m \rangle$ approaches $G_{s,m}$ algebraically. Unlike the surface width, $\langle G_m \rangle$ is an extensive quantity proportional to the Hamiltonian and, therefore, proportional to the substrate area. This means that the curves of different system sizes can be collapsed on a common curve by dividing $\langle G_m \rangle$ by the area of the substrate. In contrast to the surface width that varies as $L^{\alpha/2}$ (or $\log(L)$ at the critical dimension), $\langle G_m \rangle / A$ shows no apparent size dependence except some small finite-size effects. We also see that $\langle G_m \rangle$ monotonically increases with the dimensionality d. We display the behavior of $\langle G_m \rangle$, both by evaluating numerically Eq. (7.7) and by analytic calculations using Eqs. (7.9), (7.10), and (7.12), see Figures 7.2, 7.3 and 7.4. Figure 7.2 shows the system of the one-dimensional EW equation for various sizes. The corresponding scaling result and the finite-size effect are plotted in Figure 7.3. Figure 7.4 shows result for both the EW and MH equations in $(1+1)$ and $(2+1)$-dimensions.

7.2 The correlation function, the response function, and the fluctuation-dissipation ratio for the quantity G_m

We next consider the two time correlation function of G_m. Starting from Eq. (7.5) we have

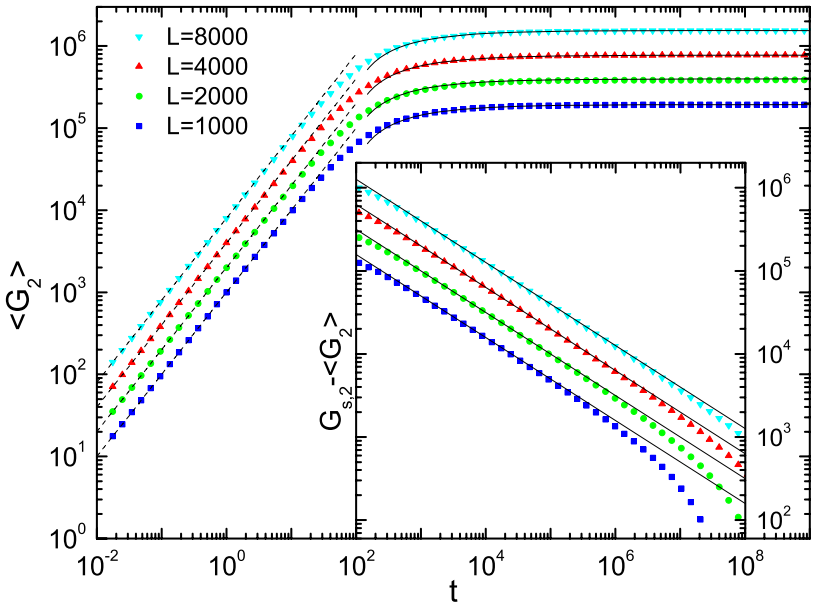

Figure 7.2: $\langle G_2 \rangle$ for various system sizes in one dimension as indicated in the figure. The inset shows the power-law decay for $G_{s,2} - \langle G_2 \rangle$ in the correlated regime. The symbols are obtained by numerically evaluating the exact expression Eq. (7.7). The dashed and solid lines are given by the asymptotic functions Eqs. (7.9) and (7.12). The parameters for the evaluations are $\nu = 0.001$ and $D = 1$

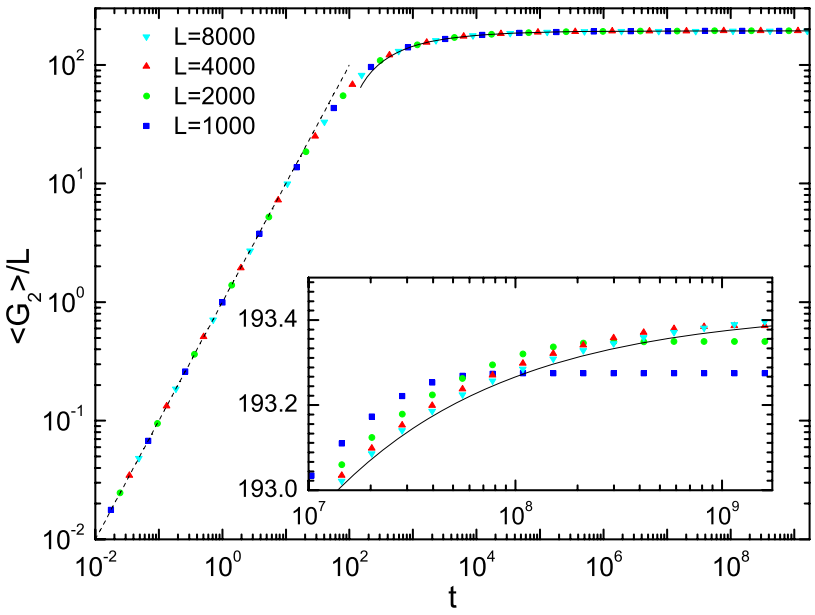

Figure 7.3: The scaled data of $\langle G_2 \rangle$ shown in Figure 7.2. The inset shows the magnified portion around the saturation regime. Deviations are due to the finite-size effects. The dashed and solid lines are given by the asymptotic functions Eqs. (7.9) and (7.12).

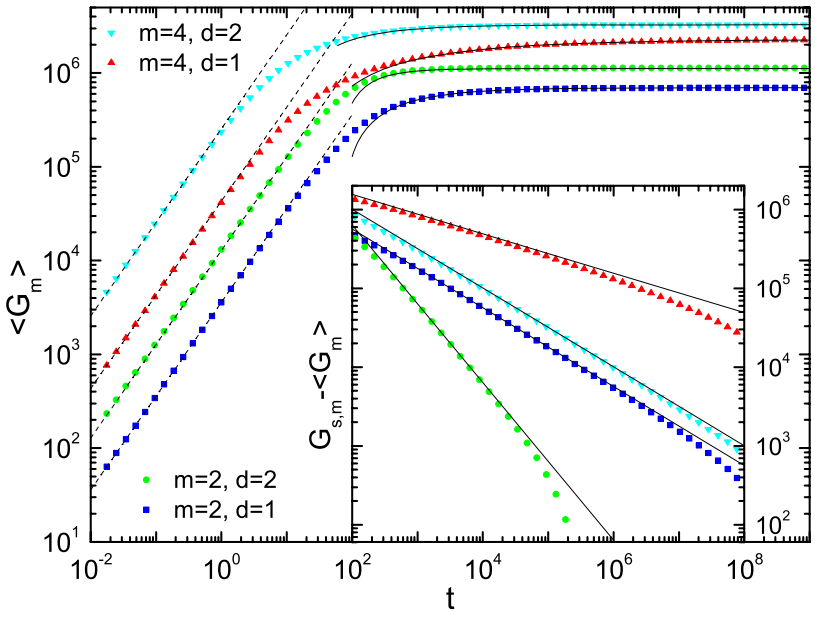

Figure 7.4: Same as Figure 7.2 but here the plots show systems with various m and d. The system size is $L = 3600$ for $m = 2$ and $d = 1$; $L^2 = 6400$ for $m = 2$ and $d = 2$; $L = 14400$ for $m = 4$ and $d = 1$; and $L^2 = 25600$ for $m = 4$ and $d = 2$

$$\begin{aligned}\langle G_m(t)G_m(s)\rangle &= 2^{m-2}L^{2d}\sum_{\mathbf{q},\mathbf{p}\neq 0}\mathcal{P}(\mathbf{q})^{m/2}\mathcal{P}(\mathbf{p})^{m/2}\\ &\Big\{\Big\langle h_{\mathbf{q}}(t)h_{-\mathbf{q}}(t)\Big\rangle\Big\langle h_{\mathbf{p}}(s)h_{-\mathbf{p}}(s)\Big\rangle\\ &+\Big\langle h_{\mathbf{q}}(t)h_{\mathbf{p}}(s)\Big\rangle\Big\langle h_{-\mathbf{q}}(t)h_{-\mathbf{p}}(s)\Big\rangle\\ &+\Big\langle h_{\mathbf{q}}(t)h_{-\mathbf{p}}(s)\Big\rangle\Big\langle h_{-\mathbf{q}}(t)h_{\mathbf{p}}(s)\Big\rangle\Big\}. \qquad (7.13)\end{aligned}$$

Here we note that the first term yields $\langle G_m(t)\rangle\langle G_m(s)\rangle$. Since $\mathcal{P}(\mathbf{q})$ is an even function, we have

$$\mathcal{P}(\mathbf{q})^{m/2}\mathcal{P}(-\mathbf{q})^{m/2} = \mathcal{P}(\mathbf{q})^{m/2}\mathcal{P}(\mathbf{q})^{m/2} = \mathcal{P}(\mathbf{q})^m. \qquad (7.14)$$

Using the Eqs. (4.14) and (7.14) we obtain the connected two-point correlation function of the quantity G_m :

$$\begin{aligned}C_G(t,s) &\equiv \langle G_m(t)G_m(s)\rangle - \langle G_m(t)\rangle\langle G_m(s)\rangle\\ &= 2^{m-3}\frac{D^2}{\nu^2}\sum_{\mathbf{q}\neq 0}\frac{1}{q^{2m}}e^{-2q^m\nu t}\left(e^{2q^m\nu s}+e^{-2q^m\nu s}-2\right)\mathcal{P}(\mathbf{q})^m. \qquad (7.15)\end{aligned}$$

We can also calculate the evolution of the average of G_m subjected to a perturbation when we suddenly change the diffusion constant ν during the growth process. In this case, the

evolution of the average of G_m is described by

$$\langle G_m \rangle_{\mu\to\nu}(t,s) = 2^{\frac{m-2}{2}} L^d \sum_{\mathbf{q}\neq 0} \left\langle h_{\mathbf{q}}^{(\mu\to\nu)} h_{-\mathbf{q}}^{(\mu\to\nu)} \right\rangle \mathcal{P}(\mathbf{q})^{m/2}, \tag{7.16}$$

where the notation "$\mu\to\nu$" shown in subscript (and/or superscript) indicates that the diffusion constant is changed from μ to ν at the waiting time s. Plugging the equation of $h_{\mathbf{q}}^{(\mu\to\nu)}$, given by Eq.(6.16), into Eq. (7.16) and comparing with Eq. (7.7), we straightforwardly obtain the response function

$$\begin{aligned} \chi_G(t,s) &\equiv \frac{\langle G_m \rangle_{\mu\to\nu}(t,s) - \langle G_m \rangle_{\nu}(t)}{\epsilon} \\ &= 2^{\frac{m-4}{2}} \frac{D}{\epsilon} \sum_{\mathbf{q}\neq 0} \frac{1}{q^m} e^{-2q^m\nu(t-s)} \left\{ \frac{1}{\mu}\left(1-e^{-2q^m\mu s}\right) - \frac{1}{\nu}\left(1-e^{-2q^m\nu s}\right) \right\} \mathcal{P}(\mathbf{q})^{\frac{m}{2}}, \end{aligned} \tag{7.17}$$

where $\epsilon = \nu - \mu$.

1. The asymptotic steady-state behavior (ie. the large νs limit) is easy to calculate for both correlation and response functions. Considering only the contribution from terms with minimum $\mathbf{q}$ in the summations, we have

$$C_G(t,s) \approx \frac{dD^2}{4\nu^2} e^{-2q_{min}^m \nu(t-s)}, \tag{7.18}$$

and

$$\chi_G(t,s) \approx \frac{dD}{2\nu^2} e^{-2q_{min}^m \nu(t-s)}. \tag{7.19}$$

We have applied the approximation

$$\mathcal{P}(\mathbf{q}_{min})/q_{min}^2 \approx 1/2 \tag{7.20}$$

to both expressions, and in addition, the limit $\epsilon \to 0$ to the response function. Therefore, we obtain the following fluctuation-dissipation ratio in the long time limit

$$X \equiv \frac{\partial_s \chi_G(t,s)}{\partial_s C_G(t,s)} = \frac{\chi_G(t,s)}{C_G(t,s)} = \frac{2}{D}. \tag{7.21}$$

If we further apply the Einstein relation $D = 2T$, we recover the fluctuation-dissipation theorem for the steady state, $X = 1/T$.

2. If we look at another limit where $l_t > 1/q_{min}$ but $l_s < 1/q_{min}$, we also have an exponential decay for both correlation and response function as follows

$$C_G(t,s) \approx dD^2 s^2 q_{min}^{2m} e^{-2q_{min}^m \nu t}, \tag{7.22}$$

and

$$\chi_G(t,s) \approx dDs^2 q_{min}^{2m} e^{-2q_{min}^m \nu(t-s)}. \tag{7.23}$$

However, the correlation function and response function are no longer time translation invariant.

3. Now we consider the case $l_s < 1/q_{max}$, and $l_t \gg 1$. In this limit, we replace the summations for both Eq. (7.15) and Eq. (7.17) by integrals and treat the integrands as hyperspherical symmetric functions (the same method that we use to derive the asymptotic equation for $\langle G_m \rangle$ in the correlated regime). We obtain power-law decay functions

$$C_G(t,s) \approx D^2 s^2 \left(\frac{L}{2\pi}\right)^d \Omega_d \frac{\Gamma\left(2+\frac{d}{m}\right)}{2m} (2\nu t)^{-2-\frac{d}{m}}, \tag{7.24}$$

and

$$\chi_G(t,s) \approx D s^2 \left(\frac{L}{2\pi}\right)^d \Omega_d \frac{\Gamma\left(2+\frac{d}{m}\right)}{2m} \left[2\nu(t-s)\right]^{-2-\frac{d}{m}}. \tag{7.25}$$

We here replaced $e^{2q^m\nu s} + e^{-2q^m\nu s} - 2$ by $(2q^m\nu s)^2$ for the correlation function and $(1-e^{-2q^m\mu s})/\mu - (1-e^{-2q^m\nu s})/\nu$ by $2(\nu-\mu)s^2q^{2m}$ for the response function before doing the integrations. These replacements correspond to retaining only the leading terms in the corresponding Taylor series. For larger waiting time s, when the condition $l_s < 1/q_{max}$ is invalid, one can expand these functions and integrate them term by term. The dominant contributions for both correlation and response functions for $t \gg s$, however, are still given by Eq. (7.24) and Eq. (7.25). In the language of aging, we can express equations (7.24) and (7.25) in the forms of (2.17) and (2.18) respectively. We thereby obtain the aging exponents $a = b = d/m$ and the autocorrelation and autoresponse exponents $\lambda_C = \lambda_R = 2 + d/m$. In this cases (where the waiting time is not in the saturation regime and the observation time is not in the random deposition regime) we have the fluctuation-dissipation ratio

$$X = \frac{1}{D} \tag{7.26}$$

provided that $t \gg s$. The correlation function and the response function for the interesting cases with $l_t < 1/q_{min}$ are shown in Figure 7.5 (here we only show the result for $m = 2$ and $d = 1$ as an example). It follows from the predictions Eqs. (7.24) and (7.25) that both the correlation and response functions can be collapsed on a single curve by dividing them by s^2 (this is also true in the regime where $l_s < 1/q_{min}$ and $l_t > 1/q_{min}$). The rescaled data sets shown by open symbols agree with the prediction. We also plot the data of χ_G v.s. C_G in the inset to demonstrate that the FDR in this regime is equal to $1/D$, as indicated by Eq. (7.26).

We summarize the fluctuation-dissipation ratio for the three regimes discussed above in the Figure 7.6. Here we calculate the FDR for one-dimensional EW equation by numerically evaluating the correlation function Eq. (7.15) and response function Eq. (7.17) for various waiting and observation times. There are two plateaus shown in the contour plot: one with $X = 2/D$ for the system in the steady state (the regime where $\log(t) > \log(t_2)$ and $\log(s) > \log(t_2)$), and one with $X = 1/D$ away from stationarity as long as $t \gg 1/2\nu$ (observed in the regime where $\log(t) \gg \log(1/2\nu)$ and $\log(s) < \log(t_2)$). The latter combines the cases 2 and 3.

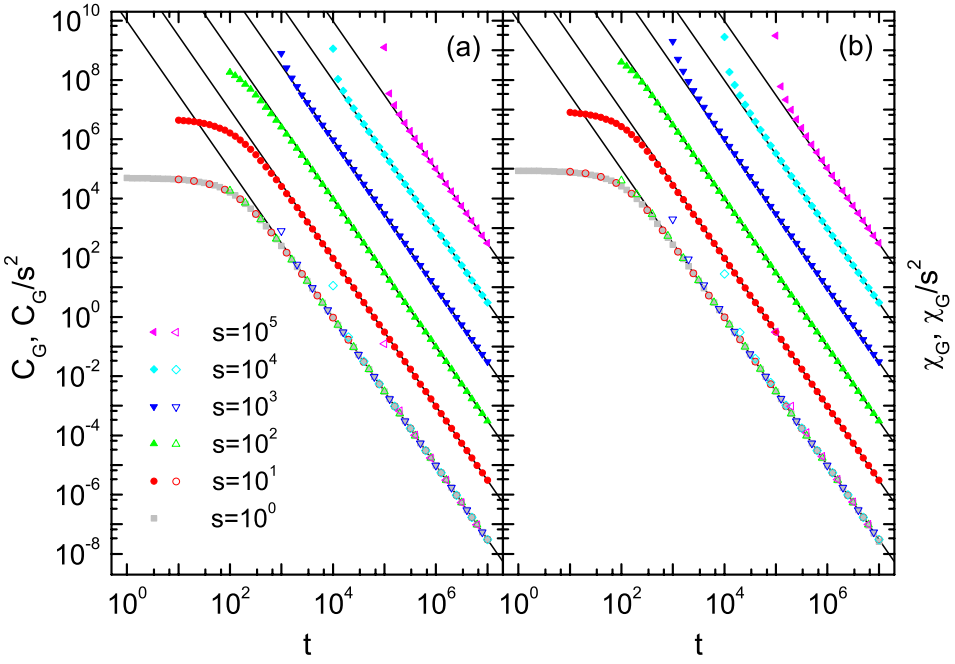

Figure 7.5: The correlation (a) and response (b) functions of G_2 in the $(1+1)$-dimensional system. The solid (open) symbols show the original (rescaled) data evaluated from Eqs. (7.15) and (7.17). The solid lines on both panels (a) and (b) are obtained from Eq. (7.24). The inset shows in log-log scale χ_G vs C_G together with a solid line given by Eq. (7.26). The parameters for the evaluations are $L = 2^{14}$, $\nu = 0.001$ and $D = 1$.

We next focus on the FDR for systems with different d and m. We study the ratio as a function of the waiting time in the limit where $t \gg s$. From Eqs. (7.21) (7.26) we have that the FDR is independent of the dimension of the substrate. Both the EW and MH equations yield the same ratios $1/D$ in case the waiting time is set before the system enters the saturation regime and $2/D$ when the waiting time is in the saturation regime. The crossover waiting time between the two regimes is given by $s_x = t_2 \sim \frac{1}{2\nu}\left(\frac{L}{2\pi}\right)^m$. We therefore have that the ratio $X(s)$ collapse on a common curve for systems with different dimension d but the same linear extension L. This result is shown in Figure 7.7.

7.3 Non-equilibrium fluctuation-dissipation theory

The non-equilibrium fluctuation-dissipation theorem proposed by Baiesi, Maes and Wynants [6] states that

$$T\frac{\partial \chi_G(t,s)}{\partial s} = \frac{1}{2}\frac{\partial}{\partial s}\Big\langle G(t)G(s)\Big\rangle - \frac{1}{2}\Big\langle G(t)\frac{\partial G(s)}{\partial s}\Big\rangle \tag{7.27}$$

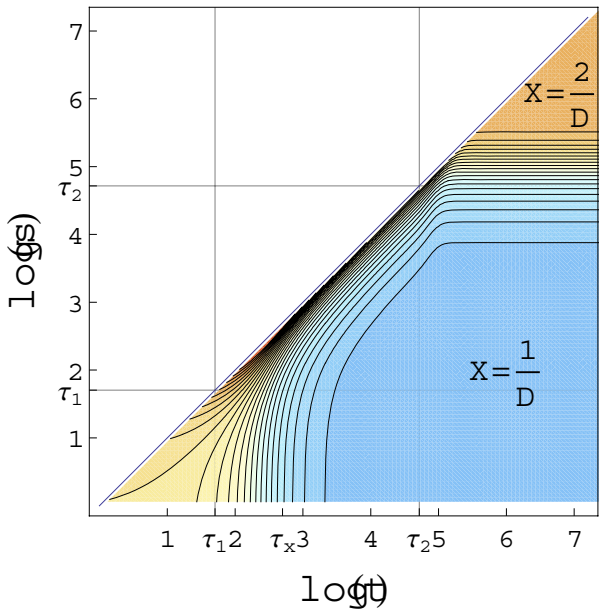

Figure 7.6: Contour plot of FDR $X(t,s)$ for the one-dimensional EW equation. The parameters for the evaluations are $L = 2^6$, $\nu = 0.001$ and $\mu = 0.99\nu$. The symbols $\tau_1 \equiv \log(t_1)$, $\tau_2 \equiv \log(t_2)$, and $\tau_x \equiv \log(1/2\nu)$ are used for simplicity.

when applied to our quantity. The first and second terms on the right-hand side of this equation come from the excess entropy flux and excess dynamical activity respectively. We drop the suffix m on the function G in the following. This equation can be expressed in terms of connected correlation functions denoted by a suffix c

$$T\frac{\partial \chi_G(t,s)}{\partial s} = \frac{1}{2}\frac{\partial}{\partial s}\Big\langle G(t)G(s)\Big\rangle_c - \frac{1}{2}\Big\langle G(t)\frac{\partial G(s)}{\partial s}\Big\rangle_c, \tag{7.28}$$

since $\partial\langle G(s)\rangle/\partial s = \langle \partial G(s)/\partial s\rangle$. We will use our exact results of the correlation and response functions derived in the previous section to test this equation. By taking the derivative of Eqs. (7.17) and (7.15), one immediately has

$$\frac{\partial \chi_G(t,s)}{\partial s} = 2^{\frac{m}{2}-1}\frac{D}{\mu}\sum_{\mathbf{q}\neq 0} e^{-2q^m\nu(t-s)}\left(1-e^{-2q^m\mu s}\right)\mathcal{P}(\mathbf{q})^{\frac{m}{2}} \tag{7.29}$$

and

$$\frac{\partial}{\partial s}\Big\langle G(t)G(s)\Big\rangle_c = 2^{m-2}\frac{D^2}{\nu}\sum_{\mathbf{q}\neq 0}\frac{1}{q^m}e^{-2q^m\nu t}\left(e^{2q^m\nu s}-e^{-2q^m\nu s}\right)\mathcal{P}(\mathbf{q})^m, \tag{7.30}$$

respectively. To derive the second term on the right-hand side of Eq. (7.28), we take the derivative of $G(s)$ with respect to s, with the help of the linear Langevin equation (4.11), and arrive at

$$\Big\langle G(t)\frac{\partial}{\partial s}G(s)\Big\rangle_c = -2^{m-2}\frac{D^2}{\nu}\sum_{\mathbf{q}\neq 0}\frac{1}{q^m}e^{-2q^m\nu t}\left(e^{2q^m\nu s}+e^{-2q^m\nu s}-2\right)\mathcal{P}(\mathbf{q})^m. \tag{7.31}$$

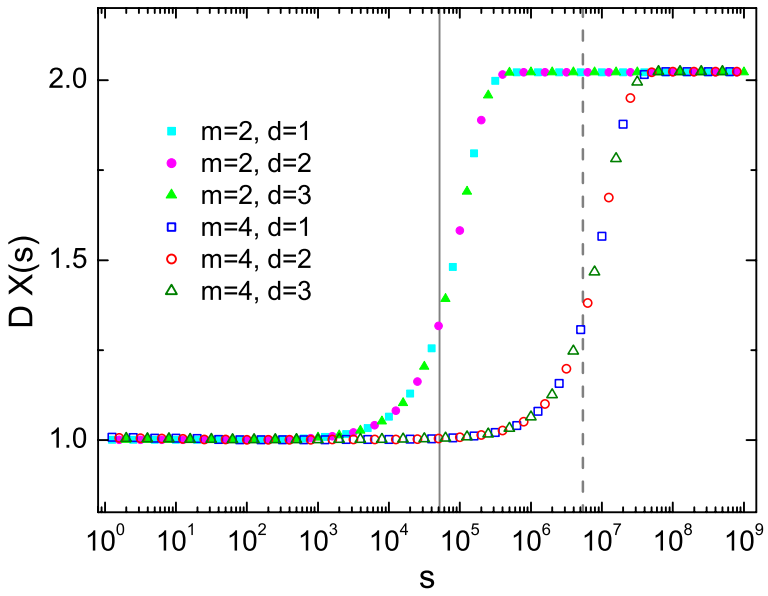

Figure 7.7: The fluctuation-dissipation ratio as a function of waiting time s. The data are by numerically evaluating the correlation function Eq. (7.15) and response function Eq. (7.17). The solid (dashed) line indicates the value of $\frac{1}{2\nu}\left(\frac{L}{2\pi}\right)^m$ for $m = 2$ ($m = 4$). The linear extension for all the systems shown in the figure is $L = 2^6$. The parameters for the evaluations are $\nu = 0.001$ and $\mu = 0.99\nu$ and $t = s + 10^7$.

The combination of Eqs. (7.30) and (7.31) yields

$$\frac{1}{2}\left\{\frac{\partial}{\partial s}\Big\langle G(t)G(s)\Big\rangle_c - \Big\langle G(t)\frac{\partial}{\partial s}G(s)\Big\rangle_c\right\} = 2^{m-2}\frac{D^2}{\nu}\sum_{\mathbf{q}\neq 0}\frac{1}{q^m}e^{-2q^m\nu(t-s)}\left(1-e^{-2q^m\nu s}\right)\mathcal{P}(\mathbf{q})^m. \tag{7.32}$$

To compare the response function Eq. (7.29) and the correlation function Eq. (7.32) a further simplification is needed. We note that the fluctuation-dissipation theory is fulfilled under the condition $t \gg s$ which implies $l^m \equiv 2\nu(t-s) \gg 1$. This allows us to use $\mathcal{P}(\mathbf{q})^n \exp\left[-(lq)^m\right] \approx q^n/2^{n/2}\exp\left[-(lq)^m\right]$ in the Eqs. (7.29) and (7.32) which yields the following simplified forms

$$\frac{\partial\chi_G(t,s)}{\partial s} = \frac{D}{2\mu}\sum_{\mathbf{q}\neq 0} q^m e^{-2q^m\nu(t-s)}\left(1-e^{-2q^m\mu s}\right), \tag{7.33}$$

and

$$\frac{1}{2}\left\{\frac{\partial}{\partial s}\Big\langle G(t)G(s)\Big\rangle_c - \Big\langle G(t)\frac{\partial}{\partial s}G(s)\Big\rangle_c\right\} = \frac{D^2}{4\nu}\sum_{\mathbf{q}\neq 0} q^m e^{-2q^m\nu(t-s)}\left(1-e^{-2q^m\nu s}\right). \tag{7.34}$$

Obviously, the fluctuation-dissipation theorem Eq. (7.28) is recovered in the limit $\mu/\nu \to 1$ by applying the Einstein relation $D = 2T$. This result is independent of the waiting time s

and the observation time t as long as $t \gg s$. In other words, we do not need to be in the steady state to have Eq. (7.28) fulfilled. For the case where μ differs from ν, however, this is different. We define the *dissipation-fluctuation* ratio as

$$Y \equiv \frac{\partial_s \Big\langle G(t)G(s) \Big\rangle - \Big\langle G(t)\partial_s G(s) \Big\rangle}{2T\partial_s \chi_G(t,s)}, \tag{7.35}$$

where ∂_s stands for $\partial/\partial s$. We study this ratio analytically in two different limits, namely for large and small νs.

1. For $l_s > 1/q_{min}$ the waiting time is in the saturation regime. Since the term with q_{min} dominates the sum, we arrive at

$$\partial_s \chi_G(t,s) \approx \frac{D}{2\mu} q_{min}^m e^{-2q_{min}^m \nu(t-s)}, \tag{7.36}$$

and

$$\frac{1}{2}\left\{\partial_s \Big\langle G(t)G(s) \Big\rangle - \Big\langle G(t)\partial_s G(s) \Big\rangle\right\} \approx \frac{D^2}{4\nu} q_{min}^m e^{-2q_{min}^m \nu(t-s)}. \tag{7.37}$$

These two equations together yield $Y = \mu/\nu$. The dissipation-fluctuation ratio is therefore identical to the ratio of perturbed and unperturbed diffusion constants.

2. Replacing the sum with an integral and expanding the term $\left(1 - e^{-2q^m \nu s}\right)$, we can rewrite equation (7.33) as

$$\partial_s \chi_G(t,s) \approx \frac{D}{2\mu m}\left(\frac{L}{2\pi}\right)^d \Omega_d \sum_{n=1}^{\infty} \frac{(-1)^{n+1}(2\mu s)^n}{n!} \Gamma\left(\frac{d}{m} + n + 1\right) [2\nu(t-s)]^{-\left(\frac{d}{m}+n+1\right)}. \tag{7.38}$$

When l_μ is small such that $2\mu s < \frac{2m}{d+2m}$, the leading term dominates[2] and we have

$$\partial_s \chi_G(t,s) \approx \frac{Ds}{m}\left(\frac{L}{2\pi}\right)^d \Omega_d \Gamma\left(\frac{d}{m} + 2\right) [2\nu(t-s)]^{-\left(\frac{d}{m}+2\right)}. \tag{7.39}$$

Using the same approach, we simplify the correlation as

$$\frac{1}{2}\left\{\partial_s \Big\langle G(t)G(s) \Big\rangle - \Big\langle G(t)\partial_s G(s) \Big\rangle\right\} \approx \frac{D^2 s}{2m}\left(\frac{L}{2\pi}\right)^d \Omega_d \Gamma\left(\frac{d}{m} + 2\right) [2\nu(t-s)]^{-\left(\frac{d}{m}+2\right)}, \tag{7.40}$$

for small $l_\nu = l_s$ such that $2\nu s < \frac{2m}{d+2m}$. Therefore, in the regime where both l_ν and l_μ are small, we have the ratio $Y = 1$. Surprisingly, the ratio is independent of the strength of the perturbation in the early time regime of surface growth. Note that in this limit the waiting time is mostly in the RD regime. However, it could also be in the early stages of the correlated regime since the waiting time can be as large as $\frac{m}{\nu(d+2m)}$ which is larger than the first crossover time $t_1 \sim \frac{1}{2\nu}\left(\frac{1}{\pi\sqrt{d}}\right)^m$. However, the condition $2\nu(t-s) \gg 1$ indicates that the observation time t must be much larger than t_1.

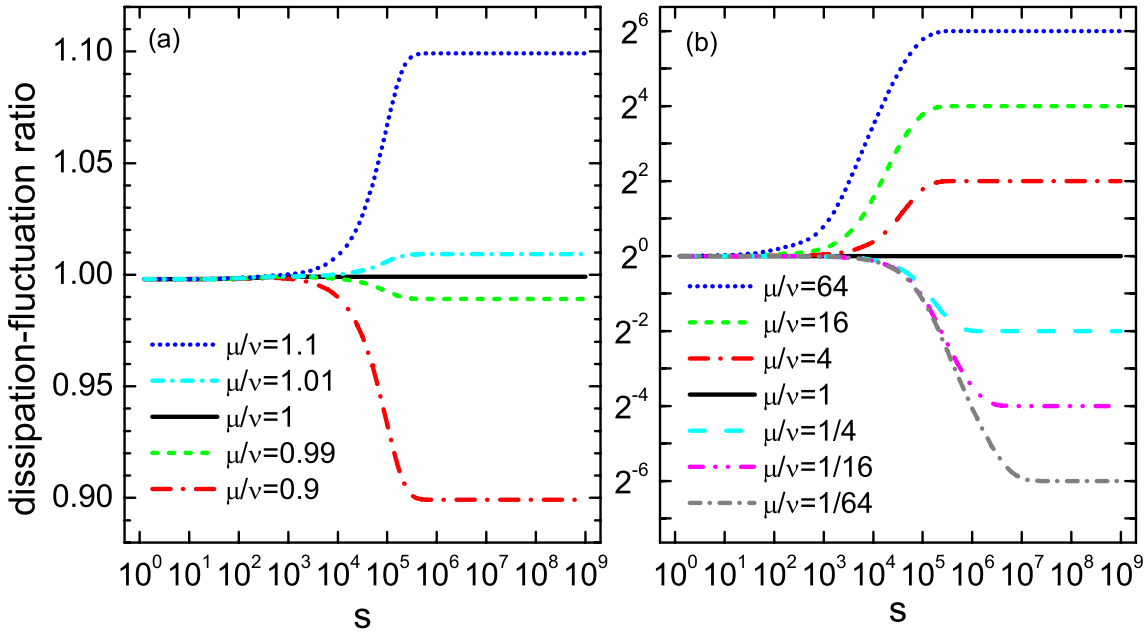

Figure 7.8: The numerical evaluation of the dissipation-fluctuation ratio Eq. (7.35) for the one dimensional EW equation. Panel (a) shows the systems with small perturbation and panel (b) shows the systems with large perturbation. The system size is $L = 2^6$, the diffusion constant for the unperturbed system is $\nu = 0.001$, and the observation time t is given by $\nu(t-s) = 100$ to ensure $2\nu(t-s) \gg 1$. Note the $Y \approx 1$ for small s and $Y \approx \mu/\nu$ for large s.

The numerically evaluation of equation (7.35) for the case $d = 1$ and $m = 2$ is shown in Figure 7.8 (a) for small perturbation (the linear response) and (b) for large perturbation (the non-linear response). Both the linear and non-linear response systems show two limits i.e. $Y \to 1$ for small s and $Y \to \mu/\nu$ for large s, which agrees with our prediction. In the non-linear response system we see that for smaller values of the ratio μ/ν the curve reaches the saturation value later. This is because when the perturbed system has already arrived at the saturation regime, the unperturbed system is still in the correlated regime. For the dissipation-fluctuation ratio Y to reach the constant μ/ν, the system needs to wait for the unperturbed system to arrive at the saturation regime. (The opposite behavior for large ratio μ/ν can be explained inversely.) In order to have a full view of the dissipation-fluctuation ratio in the different time regimes, we evaluate the ratio Y for various t and s and show the contour plot in Figure 7.9. The grid lines in Figure 7.9 show the crossover times $\tau_1 = \log(t_1)$ and $\tau_2 = \log(t_2)$. We found that the dissipation approximates the fluctuation when the observation time approaches the second crossover time and the waiting time is smaller than the second crossover time. For the waiting time larger than the second crossover time the dissipation-fluctuation ratio Y approaches μ/ν. We would like to stress that the above conclusion agrees with the non-equilibrium fluctuation-dissipation theorem Eq. (7.28) for

[2]In this limit the series converges.

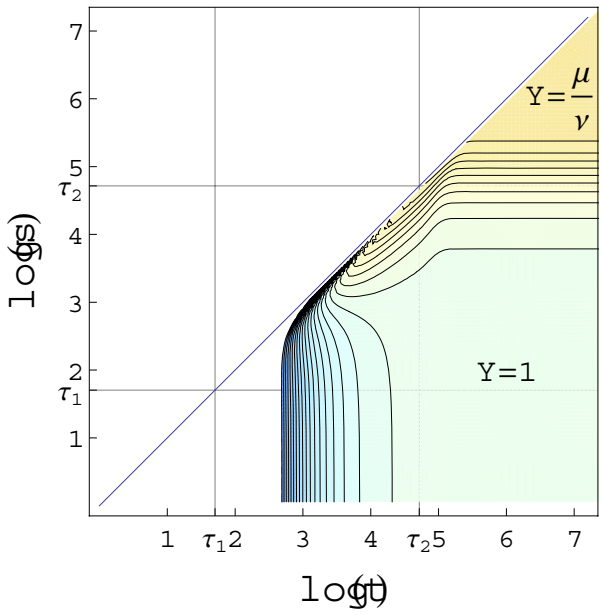

Figure 7.9: Contour plot of $Y(t,s)$. The non-equilibrium fluctuation-dissipation theorem Eq. (7.28) is valid for large observation times t and small waiting times s.

linear response systems.

We next discuss the different contributions from the correlations for large and small νs. Under the condition $t \gg s$, equations (7.30) and (7.31) can be simplified to

$$\frac{1}{2}\partial_s\Big\langle G(t)G(s)\Big\rangle = \frac{D^2}{8\nu}\sum_{\mathbf{q}\neq 0} q^m e^{-2q^m\nu t}\left(e^{2q^m\nu s} - e^{-2q^m\nu s}\right), \tag{7.41}$$

and

$$-\frac{1}{2}\Big\langle G(t)\partial_s G(s)\Big\rangle = \frac{D^2}{8\nu}\sum_{\mathbf{q}\neq 0} q^m e^{-2q^m\nu t}\left(e^{2q^m\nu s} + e^{-2q^m\nu s} - 2\right). \tag{7.42}$$

We then define that

$$Y_S \equiv \frac{\partial_s\Big\langle G(t)G(s)\Big\rangle}{2T\partial_s\chi_G(t,s)} \quad \text{and} \quad Y_T \equiv -\frac{\Big\langle G(t)\partial_s G(s)\Big\rangle}{2T\partial_s\chi_G(t,s)}, \tag{7.43}$$

where Y_S and Y_T are contributions from excess entropy flux and excess dynamical activity respectively. We discuss the two ratios in the following cases.

1. For $l_s > 1/q_{min}$, both $\left(e^{2q^m\nu s} - e^{-2q^m\nu s}\right)$ and $\left(e^{2q^m\nu s} + e^{-2q^m\nu s} - 2\right)$ approach $e^{2q^m\nu s}$, which yields $Y_S = Y_T = Y/2$. This indicates that the excess entropy flux and excess dynamical activity have equal contributions when the system is in the steady state.

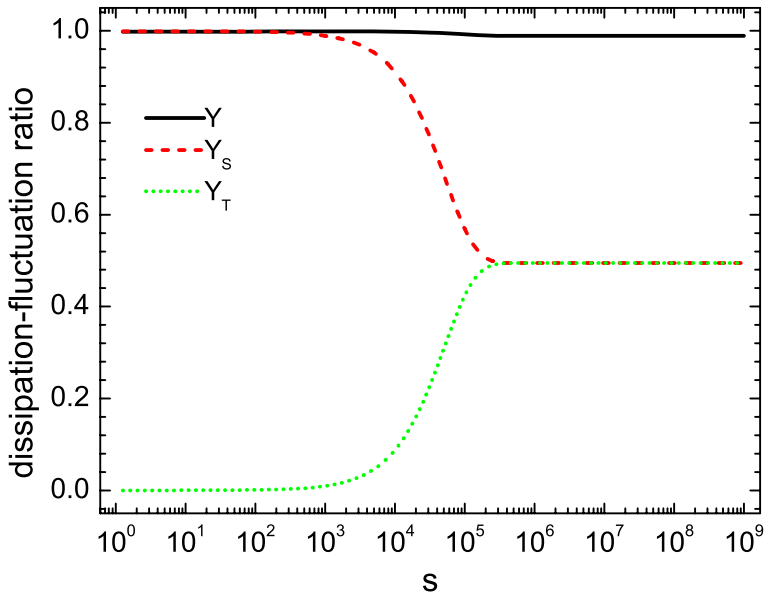

Figure 7.10: The numerical evaluation of the dissipation-fluctuation ratios Y (see Eq. (7.35)), Y_S and Y_T (see Eq. (7.43)) for the one-dimensional EW equation. The system size is $L = 2^6$, the diffusion constant for the unperturbed system is $\nu = 0.001$, the ratio of the diffusion constants is $\mu/\nu = 0.99$, and the observation time is given by $\nu(t-s) = 100$.

2. For $l_s < 1/q_{max}$, we have $\left(e^{2q^m\nu s} - e^{-2q^m\nu s}\right) = 4q^m\nu s$ and $\left(e^{2q^m\nu s} + e^{-2q^m\nu s} - 2\right) = 4(q^m\nu s)^2$. This leads to $Y_S = Y$ and $Y_T = 0$, i.e. the excess dynamical activity is absent in this regime.

As an example we numerically evaluate the ratios for the one dimensional EW equation and show the results in Figure 7.10.

Chapter 8

Conclusion

The surface width is one of the best studied quantities in the field of surface growth. By its definition as the standard deviation of surface height, it captures important aspects of the surface roughness. Hence, the time evolution of the surface width can be used to convey the idea of kinetic roughening which is widely observed in experiments. This quantity has also been used to characterize the different growth regimes. The study of finite size scaling in this quantity leads to the celebrated Family-Vicsek scaling relation which can be used to classify the universality classes. However, the Family-Vicsek scaling relation exclusively focuses on the two regimes connected by the second crossover point. Consequently it separates data which originally fell on a single curve in the random deposition regime. We propose a generalized scaling relation that yields a complete data collapse for large classes of non-equilibrium growth processes based on the Family-Vicsek scaling relation. This new scaling relation fixes the problem of data splitting that happens in the early time regime when applying the Family-Vicsek scaling relation to systems with different sizes.

We also propose a new discrete lattice model which mimics surface growth. This model is based on the famous Family model but has temperature dependent hopping rates. The model fits the Edwards-Wilkinson equation much better than the Family model. Moreover, the temperature of the model happens to be directly related to the diffusion constant of the EW equation. This model therefore allows us to study how the surface relaxes after a sudden change in temperature. Based on the Monte Carlo simulation of this model, we find two major types of relaxation processes: a power-law decay in the correlated growth regime and an exponential decay in the saturation regime. This result motivated us to investigate two-time quantities related to the surface width for more general cases such as systems described by linear or non-linear Langevin equations. The two-time quantities studied include the correlation function and different response functions (that follow when the system is subjected to different perturbations). We derived the exact form of the correlation function and the response functions for the Edwards-Wilkinson and the Mullins-Herring equations. Based on the different time regimes of the waiting time and the observation

time, we extracted various asymptotic behaviors analytically, such us linear, power-law, and exponential decay. When the surface is evolving within the correlated regime the two-time quantities display a power-law decay and perfect data collapses for different waiting times can be achieved. These properties indicate that the surface is aging. When the surface reaches the saturation regime, we observe the time-translation invariance of two-time quantities which further confirms that the surface is in the steady state regime. We also numerically study the two-time quantities for the nonlinear KPZ equation. In that system aging is also observed in the correlated growth regime. In order to be able to discuss the fluctuation-dissipation theorem the system has to be perturbed in a way such that the changed quantity is conjugated to the observable. We found that for the Edwards-Wilkinson equation the diffusion constant is conjugated to the square of the width. Therefore, we are able to discuss the fluctuation-dissipation relation for non-equilibrium growth for this case. Although the resulting fluctuation-dissipation ratio provides a way to distinguish the different growth regime, no general fluctuation-dissipation theorem can be expected in this way.

We also focused on two new quantities not previously studied in the present context: the total slope squared G_2 and the total curvature squared G_4. G_2 and G_4 measure the difference between local heights, whereas the surface width measures the difference between the local height and the average height. This makes G_m a better measure for the roughness than the surface width, since the latter overweights the roughness on plateaux and basins. Another advantage for studying G_m is that G_m is defined in the Edwards-Wilkinson equation ($m = 2$) and the Mullins-Herring equation ($m = 4$) as the effective Hamiltonian divided by the diffusion constant ν. Therefore, this quantity allows us to study the fluctuation-dissipation relation more directly than the square of the surface width. We first examined the exact results of G_m for the linear Langevin equation. Three regimes, the random deposition regime with linear growth, the correlated regime with algebraic growth, and the saturation regime, are found. Unlike the surface width, G_m per area does not noticeably depend on the system size. This is a good definition of roughness since one does not expect to measure a different roughness when a material is cut into smaller pieces. Having a basic understanding of G_m, we further investigated the two-time correlation function of G_m and the response function of G_m by changing the diffusion constant ν. We obtained the exact solutions and the asymptotic forms for both two-time quantities. Especially interesting cases are the exponential decay in the saturation regime, which preserves the time-translation invariance, and the power-law decay in the regime where $l_t \gg 1$ and $l_s < 1/q_{max}$. We found that the response function is proportional to the correlation function both for the power-law decay and the exponential decay cases (this kind of behavior is not found for the square of the width in the power-law decay regimes). This result led us to study the fluctuation-dissipation relation in more detail. The values of the fluctuation-dissipation ratio differentiate the steady state from the non-equilibrium state. This might suggest to follow the traditional approach of the fluctuation-dissipation relation for a non-equilibrium state, and to study the effective temperature. Alternatively, one can introduce the dynamical activity as a correction term to the correlation function. In this way, a generalized fluctuation-dissipation relation for systems out of equilibrium can be derived. We followed the second approach and arrived

at the result that the dissipation is equal to the corrected correlation fluctuation in the linear response regime for any waiting time as long as the observation time is large enough. For large perturbation, the generalized fluctuation-dissipation relation is valid when the system is perturbed before entering the saturation regime. If the system is perturbed in the saturation regime, the dissipation-fluctuation ratio approaches the ratio of the perturbed and unperturbed diffusion constants.

Bibliography

[1] F. D. A. Aarão Reis. Scaling in the crossover from random to correlated growth. *Phys. Rev. E*, 73(2):021605, Feb 2006.

[2] J. G. Amar and F. Family. Numerical solution of a continuum equation for interface growth in 2+1 dimensions. *Phys. Rev. A*, 41(6):3399–3402, Mar 1990.

[3] J. G. Amar and F. Family. Universality in surface growth: Scaling functions and amplitude ratios. *Phys. Rev. A*, 45(8):5378–5393, Apr 1992.

[4] J. G. Amar and F. Family. Deterministic and stochastic surface growth with generalized nonlinearity. *Phys. Rev. E*, 47(3):1595–1603, Mar 1993.

[5] A. Annibale and P. Sollich. Spin, bond and global fluctuationdissipation relations in the non-equilibrium spherical ferromagnet. *Journal of Physics A: Mathematical and General*, 39(12):2853, 2006.

[6] M. Baiesi, C. Maes, and B. Wynants. Fluctuations and response of nonequilibrium states. *Phys. Rev. Lett.*, 103(1):010602, Jul 2009.

[7] R. Baiod, D. Kessler, P. Ramanlal, L. Sander, and R. Savit. Dynamical scaling of the surface of finite-density ballistic aggregation. *Phys. Rev. A*, 38(7):3672–3679, Oct 1988.

[8] A.-L. Barabasi and H. E. Stanley. *Fractal Concepts in Surface Growth*. Cambridge University Press, Cambridge, 1995.

[9] L. Barbier, L. Masson, J. Cousty, and B. Salanon. Roughening of vicinal surfaces and step–step interactions: application to cu(1,1,11) by means of statistical analysis of stm images. *Surface Science*, 345(1-2):197 – 212, 1996.

[10] M. C. Bartelt and J. W. Evans. Temperature dependence of kinetic roughening during metal(100) homoepitaxy: transition between 'mounding' and smooth growth. *Surface Science*, 423(2-3):189 – 207, 1999.

[11] M. Beccaria and G. Curci. Numerical simulation of the kardar-parisi-zhang equation. *Phys. Rev. E*, 50(6):4560–4563, Dec 1994.

[12] O. Bondarchuk, D. B. Dougherty, M. Degawa, E. D. Williams, M. Constantin, C. Dasgupta, and S. Das Sarma. Correlation time for step structural fluctuations. *Phys. Rev. B*, 71(4):045426, Jan 2005.

[13] L. A. Braunstein and Chi-Hang Lam. Exact scaling in competitive growth models. *Phys. Rev. E*, 72(2):026128, Aug 2005.

[14] R. C. Buceta. Generalized discretization of the kardar-parisi-zhang equation. *Phys. Rev. E*, 72(1):017701, Jul 2005.

[15] S. Bustingorry. Aging dynamics of non-linear elastic interfaces: the kardarparisizhang equation. *Journal of Statistical Mechanics: Theory and Experiment*, 2007(10):P10002, 2007.

[16] S. Bustingorry, L. F. Cugliandolo, and J. L. Iguain. Out-of-equilibrium relaxation of the edwardswilkinson elastic line. *Journal of Statistical Mechanics: Theory and Experiment*, 2007(09):P09008, 2007.

[17] P. Calabrese and A. Gambassi. On the definition of a unique effective temperature for non-equilibrium critical systems. *Journal of Statistical Mechanics: Theory and Experiment*, 2004(07):P07013, 2004.

[18] P. Calabrese, A. Gambassi, and F. Krzakala. Critical ageing of ising ferromagnets relaxing from an ordered state. *Journal of Statistical Mechanics: Theory and Experiment*, 2006(06):P06016, 2006.

[19] P. M. Centres and S. Bustingorry. Effective edwards-wilkinson equation for single-file diffusion. *Phys. Rev. E*, 81(6):061101, Jun 2010.

[20] A. Chakrabarti and R. Toral. Numerical study of a model for interface growth. *Phys. Rev. B*, 40(16):11419–11421, Dec 1989.

[21] A. Chame and F. D. A. Aarão Reis. Crossover effects in a discrete deposition model with kardar-parisi-zhang scaling. *Phys. Rev. E*, 66(5):051104, Nov 2002.

[22] C.-C. Chien, N.-N. Pang, and W.-J. Tzeng. Initial-stage growth phenomena and distribution of local configurations of the restricted solid-on-solid model. *Phys. Rev. E*, 70(2):021602, Aug 2004.

[23] Y.-L. Chou and M. Pleimling. Characterization of non-equilibrium growth through global two-time quantities. *Journal of Statistical Mechanics: Theory and Experiment*, 2010(08):P08007.

[24] Y.-L. Chou and M. Pleimling. Parameter-free scaling relation for nonequilibrium growth processes. *Phys. Rev. E*, 79(5):051605, May 2009.

[25] Y.-L. Chou, M. Pleimling, and R. K. P. Zia. Changing growth conditions during surface growth. *Phys. Rev. E*, 80(6):061602, Dec 2009.

[26] S. Clarke and D. D. Vvedensky. Origin of reflection high-energy electron-diffraction intensity oscillations during molecular-beam epitaxy: A computational modeling approach. *Phys. Rev. Lett.*, 58(21):2235–2238, May 1987.

[27] A. Crisanti and F. Ritort. Violation of the fluctuationdissipation theorem in glassy systems: basic notions and the numerical evidence. *Journal of Physics A: Mathematical and General*, 36(21):R181, 2003.

[28] L. F. Cugliandolo. Dynamics of glassy systems. *ArXiv Condensed Matter e-prints*, October 2002.

[29] L. F. Cugliandolo, J. Kurchan, and L. Peliti. Energy flow, partial equilibration, and effective temperatures in systems with slow dynamics. *Phys. Rev. E*, 55(4):3898–3914, Apr 1997.

[30] G. L. Daquila and U. C. Täuber. Slow relaxation and aging kinetics for the driven lattice gas. *Phys. Rev. E*, 83(5):051107, May 2011.

[31] S. Das Sarma and S. V. Ghaisas. Solid-on-solid rules and models for nonequilibrium growth in 2+1 dimensions. *Phys. Rev. Lett.*, 69(26):3762–3765, Dec 1992.

[32] S. Das Sarma, C. J. Lanczycki, R. Kotlyar, and S. V. Ghaisas. Scale invariance and dynamical correlations in growth models of molecular beam epitaxy. *Phys. Rev. E*, 53(1):359–388, Jan 1996.

[33] S. Das Sarma and P. Tamborenea. A new universality class for kinetic growth: One-dimensional molecular-beam epitaxy. *Phys. Rev. Lett.*, 66(3):325–328, Jan 1991.

[34] D. B. Dougherty, I. Lyubinetsky, E. D. Williams, M. Constantin, C. Dasgupta, and S. Das Sarma. Experimental persistence probability for fluctuating steps. *Phys. Rev. Lett.*, 89(13):136102, Sep 2002.

[35] D. B. Dougherty, C. Tao, O. Bondarchuk, W. G. Cullen, E. D. Williams, M. Constantin, C. Dasgupta, and S. Das Sarma. Sampling-time effects for persistence and survival in step structural fluctuations. *Phys. Rev. E*, 71(2):021602, Feb 2005.

[36] S. B. Dutta, M. Henkel, and H. Park. Kinetics of a non-glauberian ising model: global observables and exact results. *Journal of Statistical Mechanics: Theory and Experiment*, 2009(03):P03023, 2009.

[37] S. F. Edwards and D. R. Wilkinson. The surface statistics of a granular aggregate. *Proceedings of the Royal Society of London. A. Mathematical and Physical Sciences*, 381(1780):17–31, 1982.

[38] F. Elsholz, E. Schöll, and A. Rosenfeld. Control of surface roughness in amorphous thin-film growth. *Applied Physics Letters*, 84(21):4167–4169, 2004.

[39] D. Ertaş and M. Kardar. Dynamic relaxation of drifting polymers: A phenomenological approach. *Phys. Rev. E*, 48(2):1228–1245, Aug 1993.

[40] F. Family. Scaling of rough surfaces: effects of surface diffusion. *Journal of Physics A: Mathematical and General*, 19(8):L441, 1986.

[41] F. Family and T. Vicsek. Scaling of the active zone in the eden process on percolation networks and the ballistic deposition model. *Journal of Physics A: Mathematical and General*, 18(2):L75, 1985.

[42] S. Fielding and P. Sollich. Observable dependence of fluctuation-dissipation relations and effective temperatures. *Phys. Rev. Lett.*, 88(5):050603, Jan 2002.

[43] A. Garriga, I. Pagonabarraga, and F. Ritort. Negative fluctuation-dissipation ratios in the backgammon model. *Phys. Rev. E*, 79(4):041122, Apr 2009.

[44] S. V. Ghaisas. $(2+1)$-dimensional stochastic growth model and its application to some experimental observations. *Phys. Rev. E*, 63(6):062601, May 2001.

[45] T. Halpin-Healy and Y.-C. Zhang. Kinetic roughening phenomena, stochastic growth, directed polymers and all that. aspects of multidisciplinary statistical mechanics. *Physics Reports*, 254(4-6):215 – 414, 1995.

[46] M. Henkel, J. D. Noh, and M. Pleimling. unpublished.

[47] M. Henkel and M. Pleimling. *Non-equilibrium phase transitions Volume 2: Ageing and dynamical scaling far from equilibrium*. Springer, 2010.

[48] C. M. Horowitz and E. V. Albano. Dynamic scaling for a competitive growth process: random deposition versus ballistic deposition. *Journal of Physics A: Mathematical and General*, 34(3):357, 2001.

[49] C. M. Horowitz and E. V. Albano. Relationships between a microscopic parameter and the stochastic equations for interface's evolution of two growth models. *The European Physical Journal B - Condensed Matter and Complex Systems*, 31:563–569, 2003. 10.1140/epjb/e2003-00066-x.

[50] C. M. Horowitz and E. V. Albano. Dynamic properties in a family of competitive growing models. *Phys. Rev. E*, 73(3):031111, Mar 2006.

[51] C. M. Horowitz, R. A. Monetti, and E. V. Albano. Competitive growth model involving random deposition and random deposition with surface relaxation. *Phys. Rev. E*, 63(6):066132, May 2001.

[52] P. Šmilauer, M. R. Wilby, and D. D. Vvedensky. Reentrant layer-by-layer growth: A numerical study. *Phys. Rev. B*, 47(7):4119–4122, Feb 1993.

[53] I. Irurzun, C. M. Horowitz, and E. V. Albano. Properties of the interfaces generated by the competition between stable and unstable growth models. *Phys. Rev. E*, 72(3):036116, Sep 2005.

[54] H. Kallabis and J. Krug. Persistence of kardar-parisi-zhang interfaces. *EPL (Europhysics Letters)*, 45(1):20, 1999.

[55] M. Kardar, G. Parisi, and Y.-C. Zhang. Dynamic scaling of growing interfaces. *Phys. Rev. Lett.*, 56(9):889–892, Mar 1986.

[56] J. M. Kim and J. M. Kosterlitz. Growth in a restricted solid-on-solid model. *Phys. Rev. Lett.*, 62(19):2289–2292, May 1989.

[57] A. Kolakowska, M. A. Novotny, and P. S. Verma. Roughening of the interfaces in (1+1) -dimensional two-component surface growth with an admixture of random deposition. *Phys. Rev. E*, 70(5):051602, Nov 2004.

[58] A. Kolakowska, M. A. Novotny, and P. S. Verma. Universal scaling in mixing correlated growth with randomness. *Phys. Rev. E*, 73(1):011603, Jan 2006.

[59] M. Kotrla, A. C. Levi, and P. milauer. Roughness and nonlinearities in (2+1)-dimensional growth models with diffusion. *EPL (Europhysics Letters)*, 20(1):25, 1992.

[60] J. Krug. Origins of scale invariance in growth processes. *Adv. Phys.*, 46:139–282, 1997.

[61] J. Krug, P. Meakin, and T. Halpin-Healy. Amplitude universality for driven interfaces and directed polymers in random media. *Phys. Rev. A*, 45(2):638–653, Jan 1992.

[62] C.-H. Lam and F. G. Shin. Anomaly in numerical integrations of the kardar-parisi-zhang equation. *Phys. Rev. E*, 57(6):6506–6511, Jun 1998.

[63] Z.-J. Liu and Y. G. Shen. Temperature effect on surface roughening of thin films. *Surface Science*, 595(1-3):20 – 29, 2005.

[64] S. Majaniemi, T. Ala-Nissila, and J. Krug. Kinetic roughening of surfaces: Derivation, solution, and application of linear growth equations. *Phys. Rev. B*, 53(12):8071–8082, Mar 1996.

[65] I. K. Marmorkos and S. Das Sarma. Atomistic numerical study of molecular-beam-epitaxial growth kinetics. *Phys. Rev. B*, 45(19):11262–11272, May 1992.

[66] P. Mayer, L. Berthier, J. P. Garrahan, and P. Sollich. Fluctuation-dissipation relations in the nonequilibrium critical dynamics of ising models. *Phys. Rev. E*, 68(1):016116, Jul 2003.

[67] P. Mayer, S. Léonard, L. Berthier, J. P. Garrahan, and P. Sollich. Activated aging dynamics and negative fluctuation-dissipation ratios. *Phys. Rev. Lett.*, 96(3):030602, Jan 2006.

[68] P. Meakin. Ballistic deposition onto inclined surfaces. *Phys. Rev. A*, 38(2):994, Jul 1988.

[69] P. Meakin, P. Ramanlal, L. M. Sander, and R. C. Ball. Ballistic deposition on surfaces. *Phys. Rev. A*, 34(6):5091–5103, Dec 1986.

[70] B. Meng and W. H. Weinberg. Dynamical monte carlo studies of molecular beam epitaxial growth models: interfacial scaling and morphology. *Surface Science*, 364(2):151 – 163, 1996.

[71] V. G. Miranda and F. D. A. Aarão Reis. Numerical study of the kardar-parisi-zhang equation. *Phys. Rev. E*, 77(3):031134, Mar 2008.

[72] K. Moser, J. Kertsz, and D. E. Wolf. Numerical solution of the kardar-parisi-zhang equation in one, two and three dimensions. *Physica A: Statistical Mechanics and its Applications*, 178(2):215 – 226, 1991.

[73] K. Moser and D. E. Wolf. Vectorized and parallel simulations of the kardar-parisi-zhang equation in 3+1 dimensions. *Journal of Physics A: Mathematical and General*, 27(12):4049, 1994.

[74] W. W. Mullins. *Metal Surfaces: Structure, Energetics, and Kinetics*. Am. Soc. Metal, Metals Park, Ohio, 1963.

[75] D. Muraca, L. A. Braunstein, and R. C. Buceta. Universal behavior of the coefficients of the continuous equation in competitive growth models. *Phys. Rev. E*, 69(6):065103, Jun 2004.

[76] T. J. Newman and A. J. Bray. Strong-coupling behaviour in discrete kardar - parisi - zhang equations. *Journal of Physics A: Mathematical and General*, 29(24):7917, 1996.

[77] T. J. Newman and M. R. Swift. Nonuniversal exponents in interface growth. *Phys. Rev. Lett.*, 79(12):2261–2264, Sep 1997.

[78] T. T. T. Nguyen, D. Bonamy, L. Phan Van, J. Cousty, and L. Barbier. Scaling and universality in the kinetic smoothening of interfaces: Application to the analysis of the relaxation of rough vicinal steps of an oxide surface. *EPL (Europhysics Letters)*, 89(6):60005, 2010.

[79] T. J. Oliveira, K. Dechoum, J. A. Redinz, and F. D. A. Aarão Reis. Universal and nonuniversal features in the crossover from linear to nonlinear interface growth. *Phys. Rev. E*, 74(1):011604, Jul 2006.

[80] S. Pal and D. P. Landau. Monte carlo simulation and dynamic scaling of surfaces in mbe growth. *Phys. Rev. B*, 49(15):10597–10606, Apr 1994.

[81] M. Pleimling and A. Gambassi. Corrections to local scale invariance in the nonequilibrium dynamics of critical systems: Numerical evidences. *Phys. Rev. B*, 71(18):180401, May 2005.

[82] J. Prost, J.-F. Joanny, and J. M. R. Parrondo. Generalized fluctuation-dissipation theorem for steady-state systems. *Phys. Rev. Lett.*, 103(9):090601, Aug 2009.

[83] A. Röthlein, F. Baumann, and M. Pleimling. Symmetry-based determination of space-time functions in nonequilibrium growth processes. *Phys. Rev. E*, 74(6):061604, Dec 2006.

[84] A. Röthlein, F. Baumann, and M. Pleimling. Erratum: Symmetry-based determination of space-time functions in nonequilibrium growth processes [phys. rev. e 74, 061604 (2006)]. *Phys. Rev. E*, 76(1):019901, Jul 2007.

[85] T. Sasamoto and H. Spohn. One-dimensional kardar-parisi-zhang equation: An exact solution and its universality. *Phys. Rev. Lett.*, 104(23):230602, Jun 2010.

[86] M. Siegert and M. Plischke. Instability in surface growth with diffusion. *Phys. Rev. Lett.*, 68(13):2035–2038, Mar 1992.

[87] P. Šmilauer and M. Kotrla. Crossover effects in the wolf-villain model of epitaxial growth in 1+1 and 2+1 dimensions. *Phys. Rev. B*, 49(8):5769–5772, Feb 1994.

[88] D. N. Sutherland. Comments on vold's simulation of floc formation. *Journal of Colloid and Interface Science*, 22(3):300 – 302, 1966.

[89] P. I. Tamborenea and S. Das Sarma. Surface-diffusion-driven kinetic growth on one-dimensional substrates. *Phys. Rev. E*, 48(4):2575–2594, Oct 1993.

[90] M. J. Vold. Computer simulation of floc formation in a colloidal suspension. *Journal of Colloid Science*, 18(7):684 – 695, 1963.

[91] H. S. Wio, J. A. Revelli, R. R. Deza, C. Escudero, and M. S. de La Lama. Discretization-related issues in the kardar-parisi-zhang equation: Consistency, galilean-invariance violation, and fluctuation-dissipation relation. *Phys. Rev. E*, 81(6):066706, Jun 2010.

[92] D. E. Wolf and J. Villain. Growth with surface diffusion. *EPL (Europhysics Letters)*, 13(5):389, 1990.